## DISCLAIMER

**This report was prepared as an account of work sponsored by an agency of the United States Government. Neither the United States Government nor any agency thereof, nor any of their employees, makes any warranty, express or implied, or assumes any legal liability or responsibility for the accuracy, completeness, or usefulness of any information, apparatus, product, or process disclosed, or represents that its use would not infringe privately owned rights. Reference herein to any specific commercial product, process, or service by trade name, trademark, manufacturer, or otherwise does not necessarily constitute or imply its endorsement, recommendation, or favoring by the United States Government or any agency thereof. The views and opinions of authors expressed herein do not necessarily state or reflect those of the United States Government or any agency thereof. Reference herein to any social initiative (including but not limited to Diversity, Equity, and Inclusion (DEI); Community Benefits Plans (CBP); Justice 40; etc.) is made by the Author independent of any current requirement by the United States Government and does not constitute or imply endorsement, recommendation, or support by the United States Government or any agency thereof.**

# Final Technical Report

## A Multi-Sensor Approach for Measuring Bird and Bat Collisions with Offshore Wind Turbines

**Prepared for:**

**Department of Energy**


**Prepared by:**

**Western EcoSystems Technology, Inc.**

415 W. 17th Street, Suite 200
Cheyenne, Wyoming 82001

**With Contributions From:**

**The Netherlands Organisation for Applied Scientific Research (TNO)**


**October 3, 2025**

WEST


1162-FTR202510-EE0008734

| | |
|---|---|
| **Federal Agency** | Department of Energy<br>Office of Energy Efficiency and Renewable Energy<br>Wind Energy Technology Office |
| **FOA Name and Number** | Advanced Wind R&D to Reduce Costs and Environmental Impact (DE-FOA-0001924) |
| **Report Type** | Research Performance Progress Report |
| **Award Number** | DE-EE0008734 |
| **Award Type** | Cooperative Agreement |
| **Prime Recipient** | Rhett Good and Jennifer H. Stucker, PhD<br>Western EcoSystems Technology, Inc.<br>415 West 17th Street, Suite 200<br>Cheyenne, Wyoming 82001<br>rgood@west-inc.com<br>jstucker@west-inc.com<br>Phone: 812.339.1756; +1.612.875.2871 |
| **Prime Recipient Type** | Private Company |
| **Project Title** | A Multi-Sensor Approach for Measuring Bird and Bat Collisions with Offshore Wind Turbines |
| **DUNS Number** | 627824261 |
| **Date of Report** | October 3, 2025 |
| **Period of Report** | November 2019 – December 31, 2024 |
| **Teaming Members** | The Netherlands Organisation for Applied Scientific Research (TNO) |
| | National Renewable Energy Lab |
| | In cooperation with St. Anthony Falls Lab, Eolos Wind Turbine team at the University of Minnesota |

**ACKNOWLEDGEMENT:**
This material is based upon work supported by the U.S. Department of Energy's Office of Energy Efficiency and Renewable Energy (EERE) under the Wind Energy Technologies Office Award Number DE-EE0008734.

**DISCLAIMER:**
This report was prepared as an account of work sponsored by an agency of the United States Government. Neither the United States Government, nor any agency thereof, nor any of their employees, makes any warranty, express or implied, or assumes any legal liability or responsibility for the accuracy, completeness, or usefulness of any information, apparatus, product, or process disclosed, or represents that its use would not infringe privately owned rights. Reference herein to any specific commercial product, process, or service by trade name, trademark, manufacturer, or otherwise does not necessarily constitute or imply its endorsement, recommendation, or favoring by the United States Government or any agency thereof. The views and opinions of authors expressed herein do not necessarily state or reflect those of the United States Government or any agency thereof.

# EXECUTIVE SUMMARY

Collision of birds and bats with wind turbines is a conservation concern for both land-based and offshore wind projects. The fatality rates of birds and bats at land-based turbines are well documented. The measurement strategies on land focus on finding carcasses following collision, estimating the number of carcasses missed through searcher efficiency, carcass persistence trials and carcass fall distributions, and modeling statistically robust fatality rates. Few technologies have been developed to monitor offshore bird and bat collisions, and many that have been developed focused on detecting collisions with large birds. The few studies that have attempted to document collisions at offshore turbines do not account for smaller bodied animals or for collisions that might be missed, which prevents the calculation of statistically robust fatality rates. The overall goal of this report, *A Multi-Sensor Approach for Measuring Bird and Bat Collisions with Offshore Wind Turbines* (Project), was to develop an effective multi-sensor system for quantifying bird and bat collision rates, specifically for offshore wind facilities. The Project goal and resulting automated collision detection system was achieved through two major technological advancements: 1) refining The Netherlands Organisation for Applied Scientific Research's (TNO's) existing WT-Bird® vibration sensing system, that had successfully detected large bird collisions during daytime, to allow for improved detection of smaller birds and bats during both daytime and nighttime hours and 2) improving image processing systems and developing and integrating machine learning algorithms to automatically detect and classify small and large bird and bat collisions with offshore turbines.

This research effort used a sequential, step-wise approach to update and validate the WT-Bird® system with advanced collision detection capabilities and sensors. During Task 1, TNO updated the WT-Bird® system, including improved fiber optic sensors for use in the turbine blades and a computing system that could better differentiate collisions from turbine operational noise—as heard through the blade— and environmental noise, including rain and hail. Additionally, cameras were updated with 20-megapixel color models suitable for capturing an adequate number of pixels near rotor hub height (80 meters [m]), such that a machine learning (computer-vision) approach could be trained to identify birds or bats involved from imagery. Following the improvements to the WT-Bird® sensor system at the TNO laboratories, the updated WT-Bird® system was shipped to the National Renewable Energy Laboratory (NREL) National Wind Technology Center's (NWTC's) Flatirons Campus in Arvada, Colorado.

For Task 2, the updated WT-Bird® system was installed in a General Electric 1.5-megawatt wind turbine by March 31, 2021. The final installation configuration of sensors in the blades included one blade with three sensors (six m from blade stem, 12 m, 18 m), and two blades with two sensors (six m, 12 m). The sensor configurations were included to evaluate the efficacy of detection recognizing increased detection may require additional sensors. The NREL used a pneumatically controlled launcher with three size classes of projectiles (balsa wood frame and food-grade gelatin, mixed with coyote urine to deter scavengers) to test the system's ability to detect collisions with objects of similar weight and size to birds and bats, referred to here as collision challenge trials. Projectile sizes included small (8 grams [g]; a small species, such as a

warbler or bat), medium (25 g; a large sparrow or flycatcher), “middle” (40 g; grosbeak or oriole) and large (250 g; a gull or small duck). Collision challenge trials (39 trials for small projectiles, 42 for medium, 37 for middle, and 28 for large) were conducted while the turbine was operational and generating electricity by NREL engineers, who shot projectiles at the blades with a pneumatic launcher. Minimum collision detection rates were 62% for small and middle sized projectiles during the trial, and greater for larger objects. Detection rates were greater for blades with three sensors, rather than two, for all projectile size classes. The detected rates of collision for the blade with three sensors ranged between 0.65 and 0.75 detections per known collision, depending on object size.

The Task 2 collision trials at the NREL’s NWTC provided substantial documentation that the WT-Bird® collision sensors detect collisions with objects as small as eight g and that detection rates exceeded the minimum rates established in the Statement of Project Objectives (SOPO) for advancing development (at least 20% detection rate for small and medium objects, at least 50% for large objects). Furthermore, the rates of false detection were low. TNO adjusted the system’s algorithms to differentiate between noise typical of operating turbines and collisions after the collision challenge test. The revised algorithms (from Algorithm 1 to Algorithm 2) increased collision detection rate while reducing the false positive rate toward zero. WT-Bird® collision detection rates were better than what might be expected during a conventional ground-based carcass search, particularly when including consideration of carcass persistence. Therefore, the decision was made to proceed to the subsequent turbine field trials with WT-Bird® (Task 4).

One of the original goals of the project was to evaluate if the monitoring system could detect collisions via the vibration sensors, and at the same time, be able to identify what collided with turbine blades using video imagery collected just prior to the collision to identify what collided with the turbine blade. Task 3 focused specifically on addressing the second advancement objective, development and testing of an image processing system and integrating machine learning algorithms to automatically detect and classify small and large bird and bat images that were collected just prior to the time collisions were detected by vibration sensors. Imagery used to train video classification algorithms to differentiate between small birds, large birds, and bats were collected at one offshore island in Maine, and two locations in Minnesota. We used auxiliary information from bat acoustic detectors and direct field observations to identify periods when bats and birds were likely to be present in the area and selected imagery collected during these periods for review and object annotation using the Computer Vision Annotation Tool Version 2.0.0. We reviewed annotations for accuracy and exported them in Common Objects in Context Version 1.0 format prior to model training. We excluded unidentified flying objects, including insects and airplanes, from model training due to poor data quality and limited sample size, respectively. WEST conducted model training using the Pytorch Version 1.9.1 library in Python Version 3.8.12. The images from the annotation dataset were split between training and validation, with 80% used for training and 20% used for validation.

WEST reviewed over 300,000 images, and annotated 1,637 birds and bats from 781 images containing flying objects. The image recognition model performed well on the validation dataset and Average Precision (AP) values for all categories, meeting or exceeding the accuracy criteria

specified in the SOPO. AP ranged from 0.71 for bats to 0.91 for large birds, and the overall model had a mean AP of 0.83. Confusion among categories was low with a majority of misclassification instances occurring between bats and bird categories. When including mis-categorized predictions, only 4% of birds and 10% of bats were not detected. Classification rates exceeded the SOPO requirements of 50% accuracy and the effort advanced to Task 4 for the in-field validation trial.

The Task 4 Validation of the WT-Bird® on a land-based turbine was initiated by July 2022 and compared how the WT-Bird® system performed against a traditional ground-based post-construction mortality survey. The goals of Task 4 included: 1) validate the comparability of a fatality estimate, developed using data from the WT-Bird® collision detection system, to a standard fatality estimate from a typical land-based carcass search study, generated using the GenEst fatality estimator (a generalized estimator of fatality; Dalthorp et al. 2018) 2) confirm whether the computer-vision system, developed by WEST, could serve as a second, independent estimate of fatality rates while reducing the amount of video data retained. The study compared how the WT-Bird® system performed against a traditional ground-based post-construction mortality survey.

Task 4 followed the approved peer-reviewed study plan (WEST 2022). We initiated field deployment of the WT-Bird® system at the University of Minnesota Eolos Wind Turbine (University of Minnesota turbine) in Rosemount, Minnesota, a Clipper Liberty 2.5-MW turbine with an 80-m hub height with 96-m rotor diameter. The WT-Bird® system was installed by early July 2022, and throughout the subsequent months, standard fatality searching occurred three times per week. The WT-Bird® system was operational from August 13 – November 3, 2022, with the period prior to September 6 focused on tuning the WT-Bird® system to the University of Minnesota turbine. The WT-Bird® system was operational 83.7% of the time. Storm-associated outages caused the system to not operate during 16.3% of the survey period. During the survey period, the blade vibration sensors documented 15 collisions, with 13 occurring during twilight or in full darkness. Concurrent land-based carcass searches by WEST detected 13 carcasses (not adjusted for searcher efficiency, carcass persistence, or carcasses that fell outside of search plots). Cameras were operational for a portion of the study period. Similarly, among the eight collisions that occurred when both color and thermal cameras were operational, seven collisions included objects observed by the thermal cameras, including six documented collisions. The color cameras documented fewer collisions (n=3) during the same time period.

Using detection probability estimates calculated during collision challenge tests of small and large projectiles at the NREL facility, while accounting for system down time, the corresponding lower and upper adjusted fatality estimates for birds and bats combined were 23.89 and 27.57 , respectively, for the study period. In comparison, the post-construction mortality field study yielded a GenEst fatality estimate of 16.8 birds and bats (90% confidence interval [CI]: 9.88–27.92 birds and bats). Thus, the estimates based on the WT-Bird® collision detections were within the 90% CI of the field estimate.

The monitoring system used to process and record video imagery during the field study at the University of Minnesota Eolos Wind Turbine failed due to overheating. The monitoring system was improved after the field study using a real-time edge image processor, and re-deployed during 2023 at the turbine for further testing. Redeployment of the real-time edge processing and monitoring system for 87 days in 2023 improved system operations as the system did not fail (overheat) or require intervention. A distinct computer vision model for the edge deployment allowed for faster data processing, saving 643 hours of video containing detected objects, which was a comparative 92.3% reduction in data storage.

The goal of Task 5 was to implement the WT-Bird® on offshore turbines, but the team encountered repeated delays and challenges with obtaining final operator agreement to test WT-Bird® at a specific offshore facility within the grant time period. This challenge, in combination with depleted funds insufficient to support the remaining testing, halted subsequent Task 5 testing. This decision was made in coordination with the Office of Energy Efficiency and Renewable Energy team during February 2024.

This research and development effort documented successful improvement of the WT-Bird® collision detection system to detect small birds and bats, and WT-Bird® is the first collision detection system to validate results compared to land-based post-construction monitoring. The collision trials provide estimates of missed targets that can be used to estimate fatality rates, a significant improvement relative to other offshore collision monitoring systems. Advances were made in developing an edge-processing solution to reduce data storage requirements, which is important if the system is deployed for long periods of time at offshore turbines. The improved WT-Bird® system also provides an important option for wind operators on land or offshore who need to document specific details about when collisions occur, particularly efforts to further research on bat impact minimization, or when standard fatality searches are impractical (e.g. offshore) or inadequate (e.g. challenging locations on land).

## TABLE OF CONTENTS

## LIST OF TABLES



## LIST OF FIGURES

## LIST OF APPENDICES

# INTRODUCTION

Collision of birds and bats with wind turbines is a conservation concern for both land-based and offshore wind projects. The fatality rates of birds and bats at land-based turbines are well documented by over 600 hundred studies over 25 years (*see* WEST 2022). The measurement strategies on land focus on finding carcasses following collision, estimating the number of carcasses missed through searcher efficiency, carcass persistence trials and carcass fall distributions, and modeling statistically robust fatality rates. Few technologies have been developed to monitor offshore bird and bat collisions, and many that have been developed, focus on detecting collisions with large birds. The few studies that have attempted to document collisions at offshore turbines (e.g. Petterrson 2005, Newton and Little 2009) do not account for collisions that might be missed, which prevents the calculation of statistically robust fatality rates, which are important for understanding the impacts of off shore wind to birds and bats.

The overall goal of this work was to document the work and findings during *A Multi-Sensor Approach for Measuring Bird and Bat Collisions with Offshore Wind Turbines* (Project). The Project goal was to develop an effective multi-sensor system for quantifying bird and bat collision rates at offshore wind facilities. The Project goal and resulting automated collision detection system was achieved through two major technological advancements: 1) refining The Netherlands Organisation for Applied Scientific Research's (TNO's) existing WT-Bird® (The Energy Research Centre of the Netherlands, Petten, Netherlands) vibration sensing system, which can successfully detect large bird collisions during daytime, to allow for improved detection of smaller birds and bats during both daytime and nighttime hours and 2) improving image processing systems and developing and integrating machine learning algorithms to automatically detect and classify small and large bird and bat collisions with offshore turbines. This Project covers work initiated in late 2019 through the end of the study in 2024.

# PROJECT OBJECTIVES

The goal of this original proposal was to develop an effective multi-sensor system for quantifying bird and bat collision rates at offshore wind facilities. This overall goal was expected to be accomplished by meeting the following specific objectives, and established within the Statement of Project Objectives (SOPO) with reference by tasks and sections, below:

1. Refine the existing WT-Bird® vibration/impact (analog-based) sensing system to allow for improved detection of small bird and bat collisions (Task 1 and 2).
2. Develop specific improvements to the image processing systems (i.e., upgrade to high-resolution cameras with night vision) to improve automated detection (via improved machine learning algorithms) to determine the species or groups of species affected (Task 3).
3. Develop, test, and validate the system based on continuous testing and optimization in the laboratory, as well as at land-based and offshore turbines (Tasks 2, 4 – 5).

4. The development target will be a system that can quantify bird and bat collisions, minimize false positives, and successfully classify collisions according to small bird, large bird, or bat to allow for calculation of separate bird and bat mortality rates (Tasks 2 and 4).
5. Utilize other sensors, for example acoustic detectors and/or marine radar, to gather additional evidence regarding the species impacted by offshore turbines (Task 5).
6. Share lessons learned to promote technologies and support offshore wind development in the U.S. (Project Output)

To meet these objectives, the Project was completed in the following tasks: 1) initial engineering tests at the TNO laboratory in the Netherlands to improve the existing WT-Bird® to detect small birds and bats, 2) installation of WT-Bird® on a utility-scale turbine and refinement of system performance at the National Wind Technology Center (NWTC), 3) field tests and refinement of the cameras, 4) validation of WT-Bird® on a land-based turbine, and 5) implementation of WT-Bird® on offshore turbines. For the study, Table I.1 summarizes locations by Task, location, and year.

**Table I.1. Study task, research locations, and year of the for the WT-Bird® system**

| Research Locations | Task 1 | Task 2 | Task 3 | Task 4 | Task 5 |
|---|---|---|---|---|---|
| TNO Laboratories, Peten, Netherlands | 2019 - 2020 | | | | |
| National Wind Technology Center, Boulder, Colorado | | 2021 - 2022 | | | |
| Private residence, Roseville, Minnesota | | | 2021 | | |
| Blazing Star Wind Farm, Hendricks, Minnesota | | | 2021 | | |
| College of the Atlantic, Mount Desert Rock, Maine | | | 2021 | | |
| U of MN, Eolos Wind Turbine, Rosemount, Minnesota | | | | 2022 - 2023 | |
| Offshore Wind Farm (US, Taiwan, UK, or Netherlands) | | | | | X |

X Indicates location was unavailable and task not completed.

## TASKS COMPLETED

In the following narrative sections, we describe how we conducted each study phase, where we met success, and how we addressed challenges for each of the completed objectives.

### Task 1. Initial Engineering Tests to Improve WT-Bird®

The goal of Task 1 was to develop and test an updated version of the WT-Bird® collision detection system, incorporating the latest vibration sensor and camera technologies. TNO completed this work, with discussions with Western EcoSystems Technology, Inc. (WEST), from TNO's research facility in the Netherlands. This work included reviewing and selecting updated hardware capable of detecting smaller objects, and engineering and testing the selected technologies using a stationary blade on the ground at TNO to meet a defined set of testing and performance criteria. This task was initiated during the early months of 2020. TNO performed system development in

the following sequential study stages:

*Study Stages*

Subtask 1.1: Technology Review and Selection

TNO completed a market and technical review of available vibration sensor and camera technologies (specifically fiber optic components) that were considered as alternatives to the existing conventional vibration sensor technology.

Subtask 1.2: Engineering and Test Plan

In coordination with the National Renewable Energy Laboratory (NREL), TNO developed an engineering and test plan that outlined the planned engineering updates and methods for testing the selected technologies.

Subtask 1.3: Engineering and Testing

TNO tested the vibration sensor and camera technologies to allow for detection of smaller collision targets. TNO completed validation tests of the updated system using stationary blades at ground level at the TNO laboratory. TNO conducted these tests to determine the most effective technologies, the expected level of sensitivity, and the criteria to be considered for successfully improving system design.

*Methods*

Subtask 1.1: Technology Review and Selection

TNO reviewed available vibration sensor and camera technologies to include in the advanced WT-Bird® system. Vibration sensor technologies evaluated for this Project included technologies for improving impact detection sensitivity of smaller objects, (e.g. two to five grams [g]), similar to small bird and bat species. TNO considered the following criteria in selecting improved vibration sensor technology: fiber optics, number of sensors and placement on turbine blades, vibration measurements, operational and impact noises, velocity of spinning turbine blades, and weight and velocity of objects colliding with turbine blades.

Additionally, the Project team compared six camera models from three manufacturers to assess resolution, day and night vision capabilities, cost, installation requirements, and ability to integrate with WT-Bird® software systems. Updated camera technology considerations included the following capabilities: ability to record video during both daytime and nighttime (e.g., night vision), weather-proofing and durability to endure harsh offshore conditions, manageable storage requirements, noise reduction, image quality sufficient for video analytics, ease of installation and maintenance, and integration with software. Consideration was given to thermal and infrared (IR) camera view (e.g., Leonardo models) to address poor visibility at night.

Subtask 1.2: Engineering and Test Plan

TNO developed a plan which outlined the engineering scheme and methods for testing the selected technologies at TNO's research facility. The goal of the testing was to determine suitable

placement for vibration sensors on the turbine blade that would be comparable to offshore turbines, and mounting and wiring techniques. The plan included testing the ability of selected vibration sensors to detect collisions with small objects, using a portion of a wind turbine blade.

Subtask 1.3: Engineering and Testing

The final step for Task 1 was to implement the engineering and test plan developed in Subtask 1.2. TNO conducted initial validation tests of the advanced WT-Bird® system using a stationary blade on the ground at TNO to determine the most effective vibration sensor technologies, expected level of sensitivity, and success criteria to be considered for the improved system design. TNO conducted tests using sample blade material, two conventional acceleration sensors (to measure vibration), and strain gauges (to measure force), installed approximately 1.0 m apart, to establish baseline measurements and allow for future comparisons. They dropped test objects weighing seven g and 250 g onto the sample blade material from 20 centimeters and 1.0 m high to measure acceleration rates and noise levels. They also conducted additional pre-tests on sample blade material under lab conditions. TNO used baseline measurements from pre-tests to identify initial sensor criteria.

*Results*

Subtask 1.1: Technology Review and Selection

TNO compared various vibration sensor and interrogator options, and cameras. TNO established selection criteria for interrogators based on maximum scan frequency, noise and resolution, and environmental properties, such as temperature range and resistance against vibration. Interrogator selection criteria are included in Table 1.1.and sensor selection criteria are included in Table 1.2.

**Table 1.1. Interrogator selection criteria identified to support equipment selection during Task 1 for the WT-Bird® system.**

| Criteria | Range and description of conditions |
|---|---|
| Scan rate | Minimum five kilohertz (kHz), preference for about 10 kHz |
| Shock and vibration | Approved or clearly sufficient |
| Interface | Transmission Control Protocol/Internet Protocol |
| Hub mount | Suitable (desktop model not preferred) |
| Mass | Maximum of five kilograms |
| Operational temperature | -20 to 60 degrees Celsius |
| Sensor count | Six to nine |
| Price/Sensor | Lower is better |

**Table 1.2. Vibration sensor selection criteria identified to support equipment selection during Task 1 for the WT-Bird® system.**

| Criteria | Range or Description of Conditions |
|---|---|
| Range | >10 Gauss |
| Frequency range | 1 to 2,500 or greater hertz (Hz) |
| Wide band noise | <10 milliGauss (mG) |
| Noise | Square root 0.14 mG (Hz; calculated with 5,000 Hz scan rate) |
| Sensitivity | Based on <1 picometer (pm) noise, 100 pm per Gauss; higher is better |

The sensors measured frequencies up to 2.5 kHz and were not sensitive to electromagnetic disturbances, unlike the analog sensors in the prior WT-Bird® system. Interrogators compared for use in this Project included two interrogator brands (i.e., Smartfibres and Fos4X) that met most of the specified criteria. Some sensors did not work well with certain interrogator models; therefore, TNO compared sensor criteria between interrogators.

In consultation with the Project team, TNO selected Fos4X as the supplier of vibration sensors and interrogators. Fos4X is an optical acceleration sensor based on fiber optics and designed to measure high frequencies (about five kilohertz [kHz]) and detect impacts from objects as small as two g, resembling a small bird or bat.

To ensure that the machine learning algorithm could accurately classify objects from imagery, sufficient image resolution would be needed, particularly between the hub and tip of blade. WEST examined test images of large birds (pigeon or gull sized) collected by TNO's WT-Bird system at the base of a wind turbine. Based on this review, we determined that a minimum of 2,048 x 2,048-pixel resolution would be needed in order to develop algorithms that could distinguish between small (8-g, bat or small bird), medium (25-g, medium-sized bird), and large (250-g, large bird) objects (Figure 1.1).

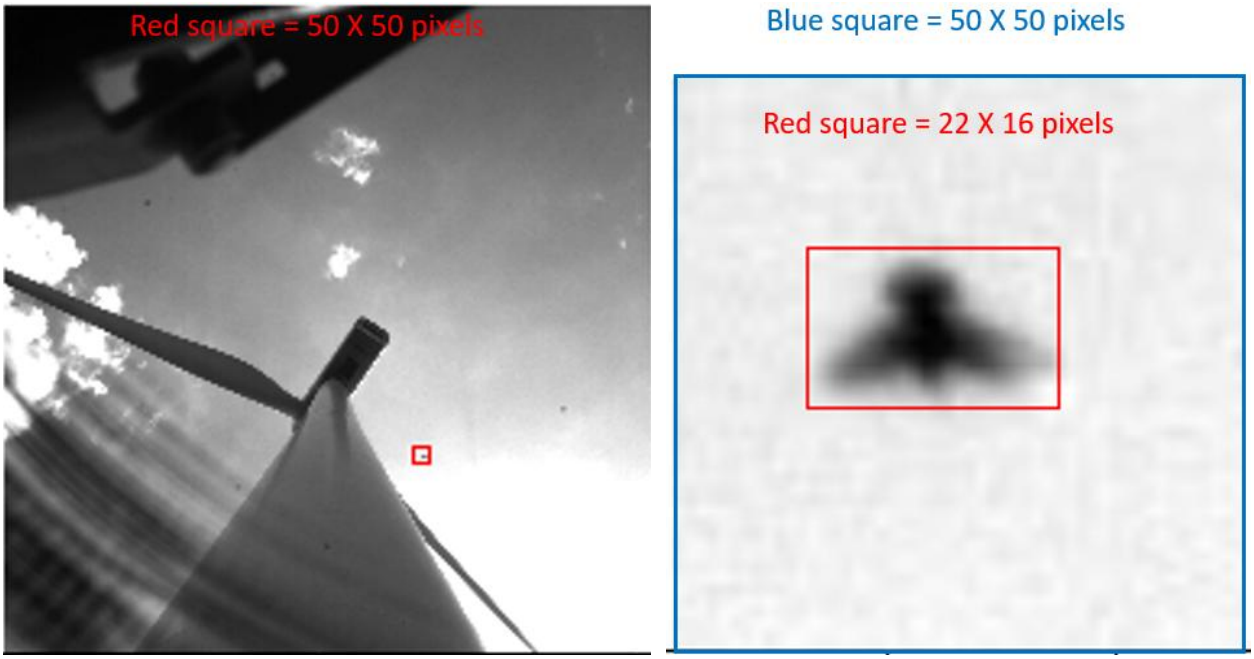


**Figure 1.1. Raw image (left) and zoomed clip (right) taken of a pigeon flying at approximately hub height using cameras in the existing WT-Bird® system.**

The final camera model selected for this Project was the Sony SNC-VM772R (Minato City, Tokyo, Japan; detailed specifications available here: https://pro.sony/en_AL/products/minidome-cameras/snc-vm772r). The Project team selected this Sony camera because it provided the highest resolution video of any outdoor camera commercially available in June 2020. This 20-megapixel (MP) camera allowed nine times optical zoom and recorded 2.5 frames per second (fps) at resolutions of 5,472 x 3,648 pixels. This resolution met our performance criteria

(approximately 50 pixels) at hub height for medium and large targets (Table 1.3). Subsequently, within two years, Sony eliminated security cameras from their product lines.

**Table 1.3. Minimum number of pixels covered by small, medium, and large targets[a].**

| Target Type | Target Width (mm) | Target Height above Camera (m) | Minimum Pixels per Target |
|---|---|---|---|
| Swallow/Bat | 440 | 80 | 30 |
| Pigeon | 700 | 80 | 47 |
| Gull | 1,500 | 80 | 102 |
| Swallow/Bat | 440 | 115 | 20 |
| Pigeon | 700 | 115 | 33 |
| Gull | 1,500 | 115 | 70 |

[a] Assuming Sony SNC-VM772R cameras mounted 3.0 meters (m) above ground level and operated with an optical zoom of approximately four times the Nacelle height of National Renewable Energy Laboratory's National Wind Technology Center turbine is 80 m with 35-m blades, hence maximum height of the rotor-swept area is 115 m.

mm = millimeters.

We predicted adequate resolution for classification of small targets at hub height (i.e., approximately 30 pixels) but also expected classification accuracy to be less for small targets than for medium and large targets due to the number of pixels available for analysis. The Project team's camera deployment plan involved mounting three cameras on the turbine's tower at approximately three meters (m) above ground level. This placement provided full coverage of the rotor-swept area (i.e., 80-m field width) plus some additional coverage outside the rotor-swept area (Figure 1.2). The Sony camera provided the same resolution at night if sufficient IR illumination was available. Table 1.4 describes the final set up for the selected sensor, interrogator, and camera technologies.

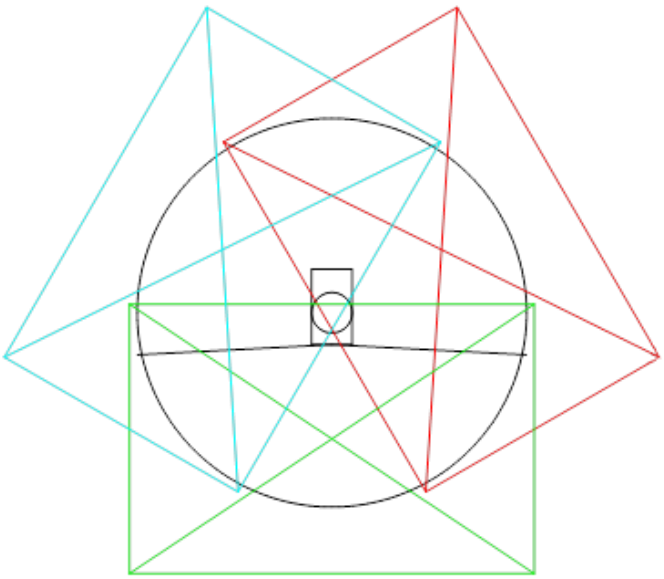

**Figure 1.2. Overhead schematic diagram of camera placement and fields of view planned during the Project[a].**

[a.] The diagram assumes three cameras mounted 3.0 meters (m) above ground on a turbine with 35-m blades and an 80-m hub height. We achieved these fields of view by optically zooming approximately four times.

Note: Red, green, and blue rectangles represent the camera fields of view at hub height. Black lines (turbine tower/nacelle, and rotor plane) and circle (rotor sweep) represent the turbine nacelle, turbine blades, and rotor-swept area at hub height.

**Table 1.4. Selected vibration sensor, interrogator, and camera specifications.**

| Name | Specification |
|---|---|
| Measurement device for fiber-optic pressure sensors | Four (4) channels for one sensor per channel<br>Sampling rate 50 kilohertz (kHz)<br>Cascading of multiple measurement devices possible<br>Web server for device configuration |
| Fabry–Pérot based vibration sensors | Noise floor: about 0.06 milliGauss/square root (hertz)<br>Eigenfrequency: about eight kHz<br>Linear range: +-20 Gauss |
| Extension cables | 20 meters (m), ZBL, two (2) E2000; 30 m, ZBL optical, two (2) E2000 |
| Sensor connection pipe LC/APC | Able to connect simplex and duplex LC/APC connectors<br>Step protection<br>IP67 protection |
| Camera | Sony SNC-VM772R<br>20 megapixels at 2.5 frames per second<br>View angle: H: 77 degrees (°) to 30°; V: 52° to 20°<br>Nine (9x) optical zoom |

Subtask 1.2: Engineering and Test Plan

The draft engineering and test plan was shared with the Project team for feedback and was finalized prior to testing.

Engineering planning and design schemes included determining suitable placement for vibration sensors on the turbine blade that would be comparable to offshore turbines and mounting and wiring techniques. Test plans outlined methods and performance criteria for completing impact tests using dummy objects on a stationary blade on the ground at TNO. Expected data to be collected during impact tests included measured vibration levels, operational and impact noise levels, and velocity and weight of dummy objects colliding with the turbine blade. Performance criteria included detection rates of the improved sensors for small objects and minimization of FPs. The improved technologies and the engineering and test plan (Figure 1.2) were finalized and made available to the Project team before testing began.

Subtask 1.3: Engineering and Testing

TNO purchased the equipment in May 2020, but due to supply chain and delivery issues, a consequence of COVID-19, the equipment arrived in late July 2020. Upon receipt, TNO initiated testing of the advanced vibration sensors on stationary blades and determined the number of sensors needed per blade and optimal placement in the turbine blade to detect vibrational measurements of smaller objects.

TNO updated the WT-Bird® collision detection system with Fabry–Pérot-based vibration sensors and a 20-MP camera operating at 2.5 fps. The typical electromagnetic interference of the turbine was considered unlikely to affect the acceleration measurements because of the fiber-optic technologies used; therefore, they expected there would be fewer false positive detections due to electromagnetic discharges or interference, as observed previously with prior analog sensors.

TNO tested the advanced vibration sensors on a stationary blade and determined the number of sensors needed per blade and optimal placement in the turbine blade to detect vibrational measurements of smaller objects. Based on the initial ground-based trials, detection rates were lower when an object's impact was from a distance greater than 12 m from the sensor or when the object weighed eight g or less. When the objects were heavier or the impacts were located nearer to the sensor, they were more likely to be detected. Following these assessments, TNO recommended spacing sensors at 12 m or less within the leading edge of the blade between the root (hub) and the mid-span. Throughout, TNO updated algorithms used to differentiate noise from collisions based on the sensitivity and frequency ranges of the new sensor

Concurrent with the camera technology assessment, WEST determined that the minimum object sizes in imagery should exceed 50 x 50 pixels to result in sufficient accuracy of automated classification rates.

*Conclusion*

TNO finalized Task 1 of the Project: *Initial Engineering Tests to Improve WT-Bird®* at TNO's facility. This phase aimed to develop and test an updated version of the WT-Bird® system using the improved vibration sensor and camera technologies (Table 1.5). It included reviewing, selecting, and integrating new hardware components to ensure the WT-Bird® system would be capable of detecting smaller objects and using a stationary blade on the ground to test the selected technologies to meet performance criteria. TNO then shipped the system to the NREL's Flatirons campus for Task 2 installation and validation testing on a production-size wind turbine.

**Table 1.5. Selected vibration sensor, interrogator, and camera specifications for the updated WT-Bird® collision detection system.**

| Name | Specification |
|---|---|
| Measurement device for fiber-optic pressure sensors | Four (4) channels for one sensor per channel<br>Sampling rate 50 kilohertz (kHz)<br>Cascading of multiple measurement devices possible<br>Web server for device configuration |
| Fabry–Pérot based vibration sensors | Noise floor: about 0.06 milliGauss/square root (hertz)<br>Eigenfrequency: about eight (8) kHz<br>Linear range: +-20 Gauss |
| Extension cables | 20 meters (m), ZBL, two (2) E2000; 30 m, ZBL, two (2) E2000 |
| Sensor connection pipe LC/APC | Able to connect simplex and duplex LC/APC connectors<br>Step protection<br>IP67 protection |
| Camera | Sony SNC-VM772R<br>20 megapixels at 2.5 frames per second<br>View angle: H: 77 degrees (°) to 30°; V: 52° to 20°<br>Nine times optical zoom |
| IR Illuminators | IR-LED Illuminators AXIS T90D40 |

Based on the test conducted at TNO, objects further than 12 m from the sensor and/or lighter than 8 g were less likely to be detected than closer and/or heavier objects.

Upon completion of this subtask, TNO shipped the updated WT-Bird® collision detection equipment to the NREL premises to initiate Task 2 testing.

*Lessons Learned*

Cameras may need to be installed on the turbine, or above the turbine base to provide adequate resolution to differentiate between small, medium, and large birds in all parts of the rotor-swept zone (RSZ; Figure 1.1). Therefore, additional cameras mounted higher on the turbine tower and utilizing optical zoom may be needed to adequately cover the full RSZ, particularly for larger turbines. Height required depends on the camera field of view.

Using commercially available equipment (e.g., cameras, sensors) is more cost-effective than manufacturing custom sensors, but it is important to specify the performance requirements needed from that equipment. Technologies change and improve over time, and manufacturers can stop producing older equipment. Future operation of the Project will eventually require

replacement of components as they age. This makes exact replacement of models impossible in some cases. As equipment fails it will need to be replaced with equipment with similar, but not exactly the same specifications. Subsequent replacements should understand performance requirements, so they can be used as a point for assessment. We anticipate that vibration sensors with similar sensitivities will be available in the future. However, if that is not the case, fatality estimates generated using the Wt-Bird® system will be conservative (eg potentially overestimate collision rates).

### Task 2. Installation of WT-Bird® on a Utility-scale Turbine at the National Wind Technology Center – National Renewable Energy Laboratory

The goal of this phase was to install the improved vibration sensors and cameras, initially developed and tested at TNO, on an operating, utility-scale test turbine at the NREL's NWTC test site in Boulder, Colorado. The improved vibration sensors and camera systems were installed on the NWTC test turbine, and a more robust set of tests were carried out to determine detection rates, with the goal of achieving overall probabilities of detection that are comparable to those documented at land-based carcass surveys. Further testing was also completed to help refine the system and determine the best placement for cameras on the turbine to optimize functionality and performance for later phases.

The requirements for accuracy of the collision detection system were also identified in the SOPO, with success defined as the following:

> *The enhanced vibration sensor's ability to detect collisions of small, medium, and large bird test objects with the following targeted levels of detection: 1) greater than 20% of small objects (approximately eight grams of weight to resemble a small bird such as a warbler or bat) and medium-sized objects (approximately 25 grams of weight to resemble a medium-sized bird such as a thrush). Objects will be detected with less than 50% false positives; and 2) greater than 50% of large object (approximately 1,000 grams of weight to resemble a large bird such as a merganser) collisions will be detected with less than 50% false positives.*

*Methods*

The NREL's NWTC was used for the installation of WT-Bird® on a utility-scale turbine and to test and refine the system's performance. The system installation requirement and plan were outlined in detail and the hardware was shipped to the NREL for installation and testing by TNO. Due to the international travel restrictions during the COVID-19 pandemic, the original plan for installation by TNO staff was cancelled and a contractor, Rope Partners, conducted the on-site installation in close cooperation with the NREL and a remote TNO team . TNO prepared installation instructions for the NREL and contractor. The NREL and contractor provided thorough installation documentation (including video) for the TNO team to review. The final configuration of sensors in the blades included one blade with three sensors (six m, 12 m, 18 m from the blade stem) and

two blades with two sensors (six m, 12 m from the blade stem). These sensor configurations were a means to evaluate the efficacy of by number of sensors, recognizing increased detection may require additional sensors. The updated WT-Bird® system was fully installed in a General Electric 1.5-megawatt (MW) wind turbine by March 31, 2021, at the NREL's NWTC Flatirons Campus in Arvada, Colorado.

The NREL staff installed the three cameras (Sony SNC-VM772R|Outdoor) just outside the base of the turbine, within 2-3 m of the tower. They placed the cameras on a stationary observation platform (concrete block), with each of the three cameras physically positioned in an equilateral triangle surrounding the turbine with 120 degrees (°) between each. The NREL staff aimed the cameras upward, ensuring that the camera views focused on the extent of the turbine hub and blades, and overlapped with the adjoining cameras to ensure birds and bats flying through the area would be captured. These visual spectrum cameras switched to gray-scale at night, supported by the addition of IR illuminators. On-site electricity powered all camera equipment, and power and data were transmitted from the cameras via Power-over-Ethernet (PoE) cables to the turbine, where they were connected to the WT-Bird® system.

The IR illuminators (AXIS Q1942-E) supported night-time image acquisition and were also fixed to the concrete blocks near the cameras. The NREL staff installed power-only electrical cables between the illuminators and a unit-specific transformer located in the turbine. Each illuminator included an internal low-light sensor, which triggered the unit to turn on during periods of low light and off as light intensified.

The NREL team completed and finalized the engineering and test plan to be carried out at the NWTC test turbine. The WEST and TNO team reviewed it internally, and subject matter experts, a WEST statistician, and TNO researcher reviewed it independently. The study team participants—NREL, WEST, and TNO—collaboratively developed a collision test matrix based on the study's objectives. Ultimately, the objective was to ensure that at least 30 projectiles of each of three size classes collided with a turbine blade while the turbine was in operation and generating electricity. The size classes of the collision projectiles were identified in the SOPO as small (eight g; a small species, such as a warbler or bat), medium (25 g; a large sparrow or a small thrush), and large (250 g; a merganser or small duck). The SOPO defined the largest size as 250 g due to constraints of the projectile air cannon (launcher) at the NREL (*see* Roadman et al 2024). A fourth projectile size, 40 g, was also included in the trials opportunistically. The NREL team launched all projectiles using the launcher, which provided consistent and repeatable collisions without damaging the turbine blades. The initial velocity was approximately 40 meters/second (m/s) with negligible speed just prior to impact with the blade. Concurrently the blade moved at 35 and 70 m/s at the midspan and tip, respectively at 18.3 rotations per minute. For the collision trials, NREL used biodegradable projectiles for the launcher that consisted of a balsa wood frame and tail, and food-grade gelatin, mixed with commercially sourced coyote (*Canis latrans*) urine, to reduce wildlife consumption of projectiles.

The NREL researchers maintained an electronic record of all launches, timed to the sub-second, during the collision trials. The NREL researchers recorded details on the size of the projectiles

launched and whether they collided with the blades following the launch, classifying collisions as solid (direct) or grazing (indirect or glancing) and identifying the relative position (percent distance) of the collision location along the blade between the hub (0%) and tip (100%). Concurrently, the WT-Bird® system recorded any signal of collisions and determined a categorical likelihood of collision using proprietary algorithms (1 and 2-c5) developed by TNO, with Algorithm 2-c5-l. WT-Bird® data provided details on which blade and sensors were triggered during each collision event. Based on time and date stamps, WEST independently reconciled the NREL launch record with the WT-Bird® tabular collision records prior to analysis.

The team counted known launches with observed (seen/heard) collisions and a collision detection by WT-Bird® as a successful detection. The team counted known launches with observed (seen/heard) collisions but no collision detection by WT-Bird® as a failed detection. A collision detection signal by WT-Bird® in the absence of a documented launch or collision was counted as a false positive (FP). Because true negatives are not recorded or quantified in the dataset, the team summarized the FP rates as the number of FPs per total number of hours during which trials were conducted. The team summarized collision data based on the size of the projectile, which sensor(s) was triggered and its position on the blade, and which WT-Bird® interpretation algorithms were involved. We defined 'signal', g, as a moment in time that was flagged by WT-Bird®, either Algorithm 1 (any confidence level) or Algorithm 2-c5. We evaluated if the type of collision (solid or grazing) and relative collision location on the blade (percent blade length) influenced detection by plotting detected and visually non-detected blade locations by object mass for visual comparison.

*Results*

There were 510 signals documented in the final reconciled dataset. Detection rates for all size classes exceeded the SOPO targets (25% for small and medium objects, 50% for large objects). Collision detection rates were greatest for the 40-g and 250-g objects, slightly lower for 25-g objects, and lowest for 8-g objects (Table 2.1).

**Table 2.1. Summary of the collisions detected (WT-Bird® Algorithm 2-c5) or not detected during collision test trials during 2021 at National Wind Technology Center, Arvada, Colorado.**

| Object size (grams) | Detected | Not Detected | Sample Size | Percent Detection |
|---|---|---|---|---|
| 8 | 20 | 19 | 39 | 51.28 |
| 25 | 26 | 16 | 42 | 61.90 |
| 40 | 26 | 11 | 37 | 70.27 |
| 250 | 19 | 9 | 28 | 67.86 |
| **Total** | **91** | **55** | **146** | **62.33** |

Increasing the number of sensors per blade from two to three increased the likelihood that a collision would be detected, particularly for objects of smaller mass (Figure 2.1). The detected rates of collision for blades with three sensors as assessed by Algorithm 2-c5 ranged between 0.65 detections per known collision to 0.75 per known collision, depending on object size.

Launching small projectiles, the sizes of birds and bats and successfully hitting moving blades was difficult. Although the launcher successfully was able to hit the blades, we were unable to

obtain an equal number of hits along the full span of the blade for each size class. The distribution of collision locations along the blade, from the hub to the tip, differed by projectile mass (Figure 2.2). Large projectiles, particularly 250 g, collided more frequently between mid-span and tip than smaller-sized projectiles. Grazing hits were observed more frequently toward the tip (Figure 2.2). This prevented us from modeling detection rates relative to distance from the turbine hub.

The performance of the WEST imagery storage system was relatively consistent, storing a large volume of imagery data from March - December, but did require several in-person restarts during the study. The reason for these failures was not determined during this Task; it was subsequently identified as system overheating during period of high graphics processing (*see* Task 4). Stable power through the inclusion of uninterruptable power sources (UPSs) with backup batteries was critical to this and subsequent testing to permit safe shutdown during power interruptions, and ensuring automatic restart once power was available.

Since the turbine was only in operation during the limited trialing periods, no wildlife fatalities were documented by WT-Bird® during the study.

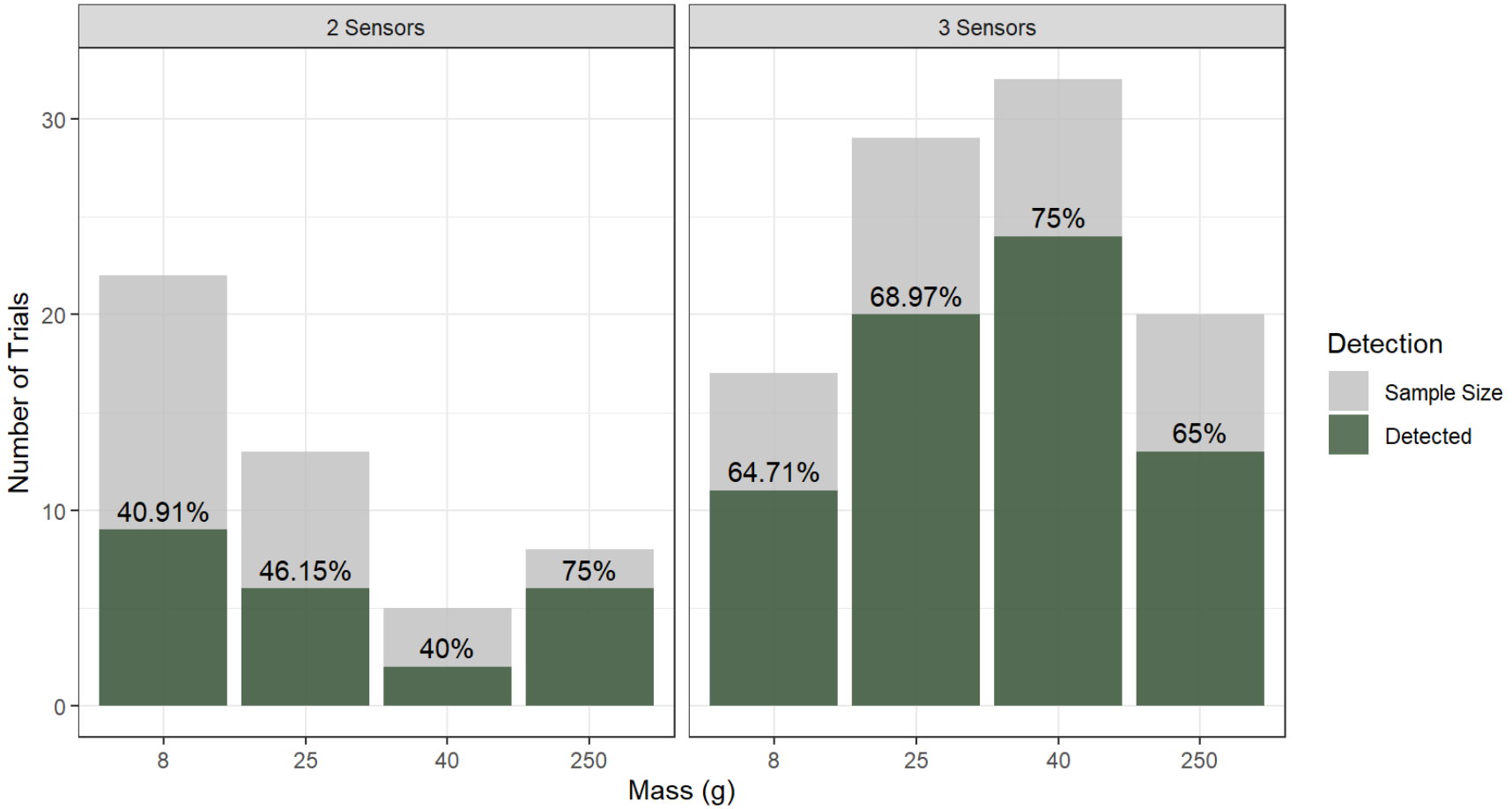


**Figure 2.1. The number of collision detections by projectile mass (grams [g]) for turbine blades with two and three sensors.**

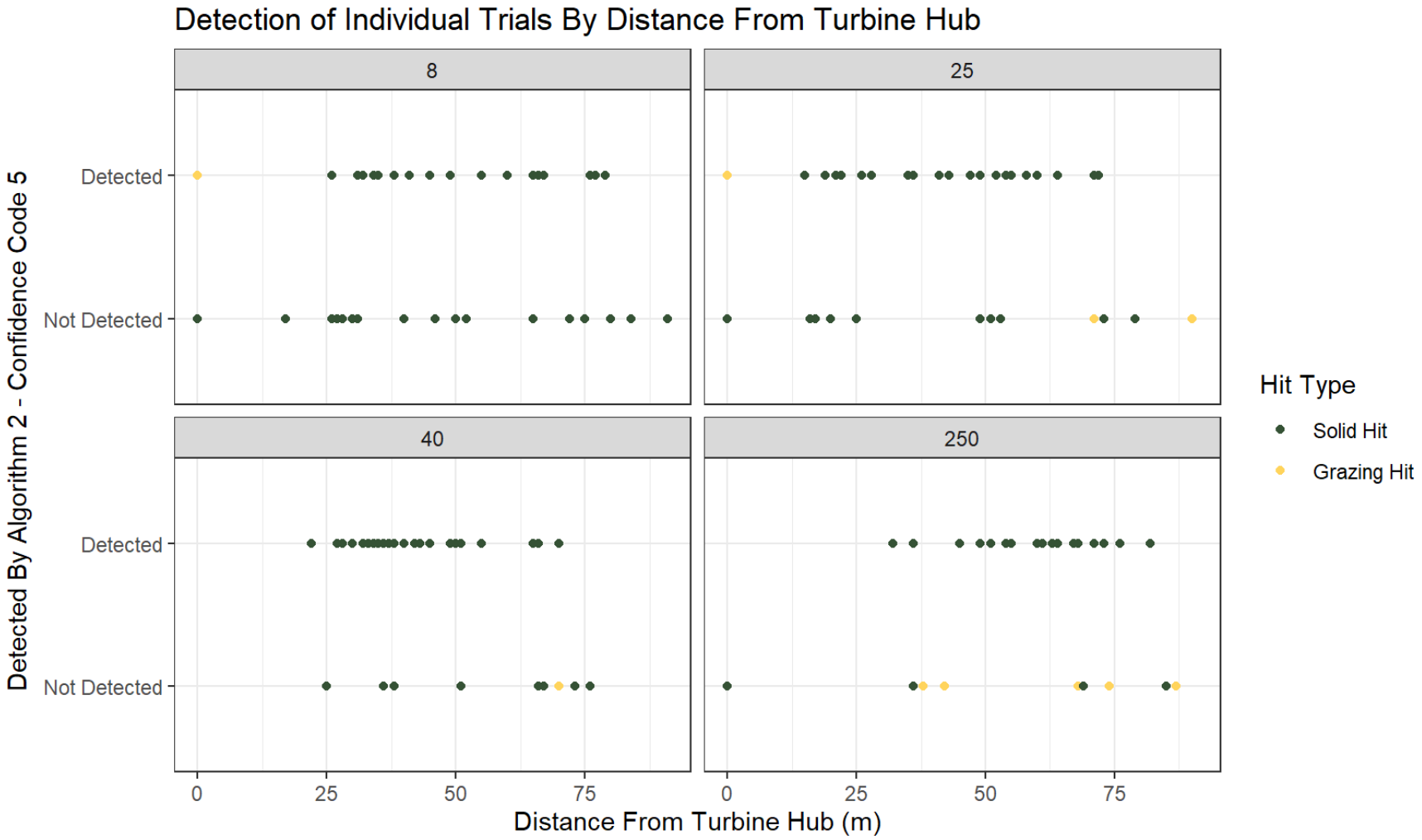


**Figure 2.2. Spatial distribution of collisions (solid and grazing), detected and undetected by WT-Bird® (Algorithm 2-c5) based on visual percent distance along blade from hub (0%) and tip (100%) by projectile mass (in grams [g]; 8 g, 25 g, 40 g, 250 g).**

Note: Spatial distribution of collisions (solid and grazing), detected and undetected by WT-Bird® (Algorithm 2-c5) based on visual percent distance along blade from hub (0%) and tip (100%) by projectile mass (g; 8 g, 25 g, 40 g, 250 g).

*Conclusion*

The Task 2 collision trials at the NREL's NWTC showed that the WT-Bird® collision sensors detect collisions, and that detection rates exceeded the minimum rates established in the SOPO for advancing development. Furthermore, the rates of false detection were low. The revised algorithms (from Algorithm 1 to Algorithm 2) further reduced the FP rate toward zero. Overall, collision detection rates were better than what might be expected from a conventional ground-ased carcass searches where detection is deprecitated by carcass persistence, a bias not present in this system. Therefore it is expected that WT-Bird® will provide the necessary precision for offshore detection rates, and potential for improved detection at land-based facilities. Blade collision detection rates also demonstrated bias patterns similar to conventional ground-based searches, with greater detection rates for larger objects. Detection percentages were better when the projectile collided with the blade with three sensors compared to the blades with two sensors. Whether the improved detection rate for three-sensor blades was due to the number of sensors per blade or their relative position on the blade was not clear. Nonetheless, careful consideration should be given to sensor location relative to span length and position within the blade span.

Despite a seemingly straightforward testing strategy, the slight differences in projectile collision distribution within the blade and across blades, compounded by difference in sensor allocation, may have influenced the estimates of detection rates across the size classes. Although unintentional, the 8-g trials more frequently collided with blades with two sensors than the blade with three sensors. This could have resulted in decreased detection levels for the 8-g trials compared to the 25-g, 40-g, or 250-g trials. Similarly, the distribution of the 250-g trials was unequal spatially and in quality of collision (direct vs. indirect), which likely reduced the overall estimates of detection for this size class. Although it was difficult to manipulate how the projectiles collided with the blade (direct vs indirect tumbling) due to the low velocities, indirect hits were detected. It is important to remember that although projectile forward velocity was approaching 0 m/s, the turbine blades were operating at 35 and 70 m/s, at the midspan and tip, respectively.

The COVID-19 pandemic caused delays in equipment shipping and delivery, which delayed full system testing. However, the most significant change was that the TNO engineering team could not travel to the NREL facility to install the WT-Bird® system. Instead, the Project consortium selected and hired a contractor to perform the installation. TNO provided on-call support during the installation at the NREL site. TNO prepared extensive instructions to ensure the system was installed as planned for operational testing.

*Lessons Learned*

- Based on this trial, sensor locations relative to span length and position within the blade span should approach 50% of blade span at 12m spacing to maximize detections.
- Winds at the NREL's Flatirons campus were not predictable or consistent. Future studies that require consistent wind for testing will want to consider their time of year carefully.

- Turbine towers accumulated heat more quickly than expected, even when outside air temperatures were less than 10° Celsius. Rather than selecting air-cooled processing components for image processing, serious consideration should include liquid-cooled options. In hindsight, this was a failure later overcome during Task 4 testing, but it took substantial time and recurrent failures during Task 2 and Task 4 to recognize the issue.
- Inclusion of stable power through the inclusion of uninterruptable power sources (UPSs) with backup batteries was critical to this and later tasks.
- Remote support of the NREL installation provided some learning aspects regarding remote third-party installation and what knowledge and expertise must be provided. Furthermore, because most of the work was completed remotely, additional discussion was needed regarding a more precise test plan. This was part of the ongoing work associated with activities at NREL.

### Task 3. Field Tests and Refinement of the Object Detection System

Task 3 directly addressed the second advancement objective, development and testing of an image processing system and integrating machine learning algorithms to automatically detect and classify video recorded just prior to the time the vibration sensors record small and large bird and bat collisions. The requirements for the accuracy of the object detection system were also identified in the SOPO, and were defined as:

> *The computer vision classifier ability to identify small, medium, and large bird guilds and bats in thermal or visual imagery with 50% accuracy when there are at least 300 independent positive samples; and 25% accuracy when there are between 75 and 300 independent positive samples.*

#### *Methods*

Field-based image acquisition occurred at four locations, with instrumentation and observation varying by location (Table 3.1). The U.S. Department of Energy (DOE) approved each of these locations via the National Environmental Policy Act EQ-1 questionnaire prior to data collection. TNO and WEST selected visual cameras during Task 1. In addition to the cameras, two additional sensor sources, acoustic bat detectors and direct human observation, were used to support efficient acquisition of targets from camera imagery. All cameras were designed and intended to record continuously, 24 hours per day, until the data collection period was complete. All trials were independent of WT-Bird® collision detection system.

**Table 3.1. Data collection locations and static survey instrumentation and observer (X) by location.**

| Observer Method (Equipment) | National Wind Technology Center, Boulder, Colorado | Roseville, Minnesota | Hendricks, Minnesota | Mount Desert Rock, Maine |
|---|---|---|---|---|
| Visual Camera (Sony SNC-VM772R\|Outdoor) | X | X | X | X |
| Infrared Illuminator (AXIS Q1942-E) | X | X | X | X |
| Thermal Camera (AXIS Q1942-E) | | X | X | X |
| Ultrasonic Bat Detector (Song Meter SM3 with SMM-U1 microphone) | | X | X | X |
| Human Observer | | | | X |

The camera setup was similar at each of the four survey locations. The team placed the cameras on stationary observation platforms (modified sawhorse) positioned in an equilateral triangle surrounding the turbine (NWTC and Hendricks) or within a smaller area (Roseville and Mount Desert Rock). The team roughly leveled and anchored the observation platforms in place to minimize movement with either bags of sand and gravel or tie-downs (Figure 3.1). In all cases, we aimed the cameras (spectral and thermal) upward, ensuring the camera views focused on the extent of the turbine hub and blades, where available, ensuring visual overlap with the adjoining cameras to make sure birds and bats that flew through the area would be captured. Visual cameras switched to gray-scale at night and were supported by IR illuminators (Figure 3.1). On-site electricity powered all camera equipment, and we transmitted power and data from the cameras via PoE cables to a network area storage device kept in a nearby building or turbine. At the NWTC, the data cables were connected to the WT-Bird® system. The team used thermal cameras as a contrasting image platform for day and night, particularly to verify bat presence during nighttime data collection. We set visual cameras to the maximum resolution and recorded 2.5 fps. Thermal cameras recorded 30 fps at their maximum resolution, but their field of view was less than 25% of the visual cameras. To summarize camera footage captured, we counted the number of days per camera with complete footage and reported that as the count of camera days.

**Figure 3.1. Stationary camera setup in Roseville, Minnesota, during an overnight snow in November 2021.**

Note: Heaters within units melted snow on contact, keeping views unobstructed and lenses relatively clear. Operating illuminators were glowing pink during the snowstorm.

A power-only cable from a transformer powered each IR illuminator, which were on an internal low-light sensor that triggered automatic power. We indicated each illuminator as a potential eye damage hazard from the IR light and alerted staff and workers at the turbine sites to the eye-hazard risk when working in the area between dusk and dawn when the illuminator was in use (e.g., Figure 3.1). We encouraged on-site staff to avoid accessing equipment during the dusk-dawn period and to use an IR-viewing mobile application (e.g., Spy Hidden Cam) to verify if the illuminators were on and a safety hazard. During each deployment, we inspected the camera equipment periodically to determine if equipment was operating and recording appropriately and to confirm that camera lenses were not fouled.

The team placed ultrasonic bat detectors (Wildlife Acoustics, Inc. [Wildlife Acoustics], Maynard, Massachusetts; Song Meter SM3 ultrasonic microphones) within or adjacent to the camera setups to provide an index of bat presence during the imagery data collection period. Rechargeable batteries powered the bat detectors, and we mounted microphones approximately three m from the ground. We programmed bat detectors to run nightly from 6:00 PM local time to 8:00 AM local time. Our team replaced data storage cards and batteries at a minimum of every two weeks. The detectors recorded sound files in full-spectrum data that were converted to zero-cross format using Kaleidoscope Pro Version 5.4.7 (Wildlife Acoustics 2022) using the Bats of North American classifier 5.4.0. One of WEST's qualified bat biologists reviewed all files in Analook (Titley Scientific) and labeled all bat calls to species when possible, or frequency group when species could not be determined. Once bats calls were verified, we used periods of abundant acoustic

occurrence data to focus image-analysis efforts on periods with a greater likelihood of detecting bats.

At the offshore Maine location, we seated observers approximately 25–30 m from the setup to verify bird and insect presence over the camera area and document observations during 2- to 3-hour periods for four to eight hours, daily, during daylight hours. Human observation hours were generally from dawn until 10:00 AM and from mid-afternoon until sunset, contingent on bird activity, which was also weather-dependent. We categorized each bird observation by type and size and documented it to the hour, minute, and second. Following observation, our team entered data into an Excel spreadsheet and the Project Manager (PM) visually checked it against the original datasheets for consistency.

We used auxiliary information from bat acoustic detectors and direct field observations to identify periods when bats and birds were likely to be present in the area and selected imagery collected during these periods for review and object annotation. For the selected imagery, we inspected each frame and drew bounding boxes around any flying objects using the Computer Vision Annotation Tool Version 2.0.0. We assigned each object to one of the following categories: bat, small bird, medium bird, large bird, aircraft, or unidentified flying object. We compared the manual classification of objects between manual annotators, or a senior staff member. The team reviewed annotations for accuracy and exported them in Common Objects in Context (COCO) Version 1.0 format prior to model training. We excluded unidentified flying objects, including insects and airplanes, from model training due to poor data quality and limited sample size, respectively.

Prior to training models, we split the image annotation dataset into training and validation sets, with 80% used for training and 20% used for validation, using the Python library Scikit-Learn, Version 0.23.2 (Pedregosa et al. 2011). To improve training efficiency, we resized all images to a width and height of 547 and 365 pixels, respectively. For model training, we used the Faster R-CNN architecture with a ResNet-50 feature pyramid network backbone (Ren et al. 2016). We obtained versions of the architecture with weights that were pre-trained on the COCO dataset (Lin et al. 2014) from torchvision Version 0.9.0 (Marcel and Rodriguez 2010). We set initial anchor box sizes at eight, 16, 32, 64, and 128, with aspect ratios of 0.5, one, and two.

We used stochastic gradient descent with momentum for the optimizer, with a momentum value of 0.9 and a weight decay rate of 0.0005. We used a plateau-based learning rate optimizer, with an initial learning rate of 0.005, and reduced the learning rate by a factor of 0.5 once the validation loss stopped improving. We evaluated validation loss in every epoch and retained model weights if the validation loss improved; otherwise, the weights were discarded and the best previous weights were loaded into the next epoch. We conducted all model training using the Pytorch Version 1.9.1 library (Paszke et al. 2019) in Python Version 3.8.12 (Python Software Foundation 2020).

We evaluated model performance by deploying the model on the 20% of images withheld from model training. For each object category in the model, we compared predicted bounding boxes

and ground-truth annotations, and calculated the amount of overlap based on Intersection over Union (IoU), where:

$$IoU = \frac{Area\ of\ bounding\ box\ overlap\ between\ ground{-}truth\ and\ prediction}{Area\ of\ bounding\ box\ union\ between\ ground{-}truth\ and\ prediction}$$

For this study, we defined a true positive (TP) detection as a predicted bounding box that overlaps a ground-truth annotation with an IoU of 0.25 or greater. Many studies set a higher IoU threshold of 0.5. However, for this study we deemed the lower threshold of 0.25 acceptable given the objects (birds and bats) were small relative to the camera field of view. Thus, IoU values of 0.25 were sufficient to achieve our goals with respect to identifying the position of objects in each image. All predicted bounding boxes that had an IoU less than 0.25 with a ground-truth annotation were considered an FP. Additionally, all ground-truth bounding boxes that did not have a matching predicted bounding box with an IoU of 0.25 or greater were considered a false negative (FN). Next, we calculated recall and precision for each category, where:

$$Recall = \frac{TP}{TP+FN}$$

and

$$Precision = \frac{TP}{TP+FP}$$

For each category, we calculated the average precision (AP), which was a measure of the area under the precision-recall curve following standard methods for evaluating object detection algorithms (Girshick et al. 2016). We then calculated a mean AP (mAP) across all categories, which summarizes overall model fit. Lastly, we calculated a confusion matrix comparing predicted and ground-truth categories when deploying the model using a confidence value that balanced precision and recall (value of 0.1 used).

*Results*

System stability and reliability increased as electrical power availability was managed such that operation was 100% during the final Roseville data collection period between September and November (Table 3.2). Incomplete data retention was primarily a consequence of power loss at both turbine sites, followed by an error in initial camera programming during camera setup. Power loss was ameliorated through the use of an UPS in addition to a programming shutdown during power loss and an auto restart once power returned. Imagery of birds and bats at turbine and non-turbine sites collected data with increasing success under a variety of power and weather conditions.

During the period of observation in terrestrial and marine environments, the visual cameras provided excellent performance. WEST noted no instances of cameras fogging or moisture intrusion. One camera was externally fouled by bird feces at the NWTC and was cleaned manually prior to the start of the trial; the NWTC sees very little rain that would wash off the dome cover of this camera. No cameras were externally fouled during the other WEST deployments, although

the system did accumulate salt spray while on Mount Desert Rock in the Gulf of Maine. The Maine deployment did not experience rain during the observation period, so we could not determine if rain would remove salt from the cameras. Following the deployment in Maine, the equipment was rinsed with fresh water, which removed the accumulated salt from the equipment. Snow briefly accumulated on the cameras in November during a period of sub-freezing temperatures (Figure 3.1) but melted quickly due to internal heaters.

**Table 3.2. Data collection dates, camera days of visual imagery, and comments on data loss.**

| Location | Data Collection Period | Count of Camera Days (% success) | Comment on Data Loss |
|---|---|---|---|
| National Wind Technology Center, Boulder, Colorado | Mar – Dec 2021 | >500[a] (% unknown) | Periodic power failure, equipment failed to restart.<br>Turbine not consistently operational until late September |
| Roseville, Minnesota | Jul 22–27, 2021 | 16 (88%) | Camera programming error on night one for one camera. |
| Hendricks, Minnesota | Jul 28 – Aug 25, 2021 | 45 (54%) | Two power failures, equipment failed to restart as intended and uninterruptible power source failed to restart after power drain. |
| Mount Desert Rock, Maine | Sep 14–21, 2021 | 21 (96%) | First eight hours failed to store; 100% following system reset. |
| Roseville, Minnesota | Sep 28 – Nov 15, 2022 | 150 (100%) | None documented. |

[a] Total days of operation unconfirmed but exceeded 500 camera days.

Of the visual imagery inspected to date, we reviewed over 300,000 images (approximately 100 hours of field monitoring), identified 781 images containing flying objects, and annotated 1,637 birds and bats (Table 3.3). The companion bat call data and the human observers were valuable additions in targeting time periods when animals were likely to be captured in the imagery.

Our image-recognition model performed well on the validation dataset and AP values for all categories met the accuracy criteria specified in the SOPO. Average precision ranged from 0.71 for bats to 0.91 for large birds (Table 3.3). For the overall model, mAP was 0.83. In general, confusion among categories was low with most misclassification instances occurring between bats and small birds (Table 3.4). When including mis-categorized predictions, only 4% of birds and 10% of bats were not detected.

**Table 3.3. Sample sizes (N) and average precision estimates for birds and bat categories used for training and validation of the model.**

| Category | N (training) | N (validation) | Average Precision |
|---|---|---|---|
| Large bird | 527 | 136 | 0.91 |
| Medium bird | 331 | 74 | 0.81 |
| Small bird | 333 | 84 | 0.88 |
| Bat | 122 | 30 | 0.71 |
| **mean Average Precision** | | | **0.83** |

N indicates the number of object annotations used for model training and validation. Average Precision indicates the area under the precision-recall curve for each category.

**Table 3.4. Confusion matrix comparing predicted object categories and ground-truth annotations.**

| | Predicted | | | | |
|---|---|---|---|---|---|
| **Ground-truth** | **Large Bird** | **Medium Bird** | **Small Bird** | **Bat** | **None** |
| Large bird | 124 | 0 | 0 | 0 | 13 |
| Medium bird | 0 | 78 | 0 | 0 | 0 |
| Small bird | 1 | 0 | 77 | 5 | 1 |
| Bat | 2 | 1 | 0 | 23 | 4 |
| None | 4 | 2 | 5 | 20 | 0 |

Values along the diagonal (shaded blue) represent true positive detections with an Intersection over Union (IoU) greater than 0.25. Values in the ground-truth “none” row indicate instances where no ground-truth annotation overlapped the predicted bounding box with an IoU greater than 0.25. Values in the predicted “none” column indicate instances where a ground-truth annotation existed, but no bounding box overlapped with an IoU greater than 0.25.

*Conclusion*

The objective for Task 3 was to develop and test an image recognition system to automatically detect and classify four categories of animal from visual or thermal imagery: small birds, medium birds, large birds, and bats. The WEST computer vision system exceeded SOPO minimum requirements (50% accuracy if more than 300 samples, 25% accuracy if 75-300 samples), classifying objects correctly with a mAP of 83% (Table 3.3). Despite small sample sizes, the models were developed with imagery from three very different areas (prairie/crop, suburban lawn/woodland, and offshore rocky island) featuring a diversity of bird taxa. The models performed better than expected. The primary constraint on model development for bats was identifying the very few bats captured within the large volume of imagery. The team initiated data collection in July, thus covering most of the active bat period for the region (June – September), but bats were observed on only on a few nights.

The interpretation of these model results was straightforward, but there were physical challenges of the research and development effort that limited image data collection. Six cameras were deployed for more than 16 months, with only one instance of a lens being externally fouled by a bird. None of the cameras, visual or thermal, appeared to be attractive as perches for birds, which is positive as perching could lead to physical obstruction by birds or more frequent fouling from bird feces. None of the cameras had condensation or water intrusion. While the NWTC had few rain events that might have washed away debris, cameras in Minnesota were exposed to dew, rain, and snow. Inclement weather (severe rain and snow) only impeded clear image acquisition

for less than 1% of the survey period, and even during snow the lenses of the cameras remained clear because of internal heating units. It was not known if rain would have washed away accumulating salt on the cameras in Maine. Overall, the cameras performed well under a variety of field conditions.

*Lessons Learned*

Although image constraints were known when the cameras were selected during Task 1, the image file size from the true-color (color) cameras was large. While this size and resolution was needed to identify a bird or bat flying at greater than 150 m from the camera (in the rotor-swept area), the digital size of these images, in combination with the Sony data file storage approach, required additional processing steps and slowed efficient transfer and processing of the large volumes of data. Camera image resolution was reduced at night, despite the use of powerful infrared illuminators, and animals captured with thermal cameras (primarily bats) were not captured with the color cameras. Consequently, thermal cameras with the color cameras were jointly deployed in Task 4.

Maintaining continuous power to support the cameras, illuminators, and data storage device was a requirement that proved more challenging than expected. Maintaining power through the inclusion of multiple UPS units in the data collection system was vital for data collection continuity, but even battery backup was not adequate for periods of prolonged power outage (more than three hours) that drained backup batteries on the UPSs. At the NWTC, inclusion of an automatic notification on power/Ethernet loss was helpful. However, automatic restart options on the UPS were not feasible due to limitations in physical access (COVID-19), initially, and information technology security concerns, later, which were recently exposed (Kovacs 2022). When the UPSs did not restart automatically, the programmed auto restart on the cameras and storage could not engage. For two of the WEST deployments (Hendricks, MN and Mount Desert Rock), remote access for monitoring via Ethernet was not possible; and therefore physical system checks were necessary to ensure the system was operating as expected, and for periodic data retrieval. The Maine deployment was an interesting test case as the field station's electricity was generated almost exclusively by solar power and stored in a large bank of batteries; power was extremely stable at this site. The expected 2022 deployment included Ethernet-based power monitoring and remote data retrieval options. Maintaining consistent power and data with automatic system restarts was a vital part of future system deployments.

### Task 4. Validation of WT-Bird® on a Land-based Turbine

The goals of Task 4 included: *1) validate the comparability of a fatality estimate, developed using data from the WT-Bird® collision detection system, to a standard a fatality estimate from a typical land-based carcass search study, generated using the GenEst fatality estimator (a generalized estimator of fatality; Dalthorp et al. 2018) 2) confirm whether the computer-vision system, developed by WEST, could serve as a second, independent estimate of fatality rates while reducing the amount of video data retained.*

*Methods*

Task 4 followed the approved peer-reviewed study plan (WEST 2022). We initiated field deployment of the WT-Bird® system at the University of Minnesota Eolos Wind Turbine (University of Minnesota turbine) in Rosemount, Minnesota, a Clipper Liberty 2.5-MW turbine with an 80-m hub height with 96-m rotor diameter. The turbine has been in operation since 2011. We deployed cameras in June 2022, followed by TNO engineers installing the complete WT-Bird® system, in-blade sensors, and fiberoptic cables by July 1, 2022. Networking among the blade sensors, hub, nacelle, and tower base was completed with system tuning in early August 2022. Concurrently with the camera installation, traditional ground-based fatality monitoring was initiated in June 2022, and conducted three times per week. The monitoring report and fatality estimate from the ground-based fatality monitoring are provided as a supporting report and included as Appendix A. Throughout the Task 4 study, TNO staff remained blind to when and if carcasses were found by WEST personnel to ensure independence of WT-Bird® system observations. WEST field personnel also did not know when or if the WT-Bird® system detected collisions. Due to unrecognized overheating issues during high volumes of image processing, a second WEST camera-only deployment occurred between March – June 2023, to better assess the edge-processing computer system. Details on the components and deployments are provided below.

WT-Bird® System

TNO engineers installed the WT-Bird® vibration sensors in the turbine blades, with support from University of Minnesota turbine engineers during June 30 – July 1, 2022. Additional details are included in the TNO installation report (Kaandorp 2022). Engineers installed three sensors in each of the three blades, placing one each at 8 m, 16 m, and 24 m from the hub. Sensors one and two on each blade were installed on the leading edge of the blade, but because of blade architecture, sensor three was installed further back on the blade within a box-beam compartment. Following installation and networking, the system underwent a 4-week tuning period, allowing the WT-Bird® system to “listen” to the sounds of turbine operation and refine the collision detection algorithm. The tuning period ended by early September 2022, and the trial began thereafter.

TNO monitored the performance of the WT-Bird® system throughout this study period. Following the end of the monitoring, TNO prepared a detailed report of likely collisions observed with the WT-Bird® system for use by WEST in evaluating a fatality estimate (Appendix B).

Video Camera Systems

The 2022 camera monitoring system consisted of camera stations located approximately one to two m from the turbine base, at a location similar to the turbine platform railing where deployment of the system on offshore turbines is expected. We installed cameras and illuminators on a modified adjustable-height sawhorse, stabilized with 50-pound bags of gravel (Figure 4.1). During 2022, we spaced the three paired camera stations equidistantly around the turbine tower, with the cameras facing upwards and the field of view centered on the turbine nacelle. Each camera station included a Sony ( SNC-VM772R) color camera with an 8.8-millimeter (mm) focal length and 5,472 x 3,648 resolution. We had previously used the Sony cameras during the WT-Bird® deployment at the NREL, for data collection in Task 2, and during WEST’s computer vision

model development (Task 3). The second camera at each station was an Axis (Q1942-E) thermal camera equipped with 35-mm lenses; we had also previously used this camera during Task 3 deployments. This thermal camera recorded video in 640 x 480 resolution and 30 fps. The thermal cameras were set to record continuously, and the Sony color cameras were programmed to save one image per second at night and 2.5 images per second during the day. Our team used the thermal camera data specifically for development of the computer vision algorithm and detection of birds and bats, while the Sony color cameras provided better resolution data during the daytime. The three Sony color cameras were supported at night by an Axis IR illuminator (T90D40 IR-LED) at each camera station. The IR illuminators automatically initiated operations in low-level visible light conditions based on the integrated low-light sensor; low-light sensor was set as sensor default and observed to activate after sunset and prior to civil twilight, and other periods of low-level visible light. The WT-Bird® system received constant video feed from the Sony color cameras via PoE cables, which provided power and transmitted data from cameras to in-turbine computer components (WT-Bird® or WEST storage). Similarly, the Axis thermal cameras received power via a PoE cable and transmitted data back to WEST data storage. The illuminators were powered by a dedicated electrical cable from the turbine.

**Figure 4.1. The camera stations at the University of Minnesota Eolos Wind Turbine, Dakota County, Minnesota.**

Note: On the left was the Axis infrared illuminator (Axis T90D40 IR-LED), paired with a Sony (SNC--VM772R) true-color camera feeding the WT-Bird® system. On the board to the right and behind is another Sony (SNC-VM772R) true-color camera with an Axis thermal camera (Q1942-E). In the background, at 120 degrees counterclockwise from the foreground setup is the next camera station.

In 2023, to support testing of the real-time capacity of WEST's edge processing and video target-identification system, the WEST cameras were redeployed to capture spring migration without the WT-Bird® collision sensors. The team's goal for 2023 monitoring was to evaluate whether the updated edge target-identification system could reduce footage while retaining videos of potential collision events. The edge processing system was intended to reduce the need for storing large quantities of video footage offshore. The camera-only deployment took place between March 21 – June 15, 2023. In this phase of the study, the camera monitoring system consisted of four camera stations that were located approximately one to two m from the turbine base, spaced equidistantly around the turbine tower, and faced upwards with the field of view centered on the turbine nacelle. We used four stations in anticipation of the greater field of view of larger offshore wind turbines. We used one additional camera model in this deployment, and each station had either an Axis (Q1942-E) thermal camera equipped with a 35-mm lens or an Axis (Q1952-E) thermal camera equipped with a 19-mm lens. Each model recorded 10-second video clips, in 640 x 480 resolution, at 30 fps. In addition, the two camera stations with 19-mm lenses were equipped with the same Sony (SNC-VM772R) color camera with an 8.8-mm focal length and 5,472 x 3,648 resolution as had been deployed during 2022. Figure 4.2 shows the approximate field of view of the cameras around the turbine tower, depicted in blue, with the 35-mm thermal cameras in red, the 19-mm thermal cameras in green, and the color cameras in purple, relative to the spherical RSZ in yellow.

Computer Vision Methods

In Task 4, we used data collected from thermal videos in conjunction with a computer vision model to aid in detection of birds and bats flying through the field of view. The primary goal of the computer vision effort was to support the identification of birds and bats during operation of the WT-Bird® system. A secondary goal for the system was to serve as a second collision observer.In order to identify potential collisions using only camera data, we developed an object detection, computer-vision model to detect flying objects, including birds and bats, in thermal videos and implemented a tracking algorithm to identify flight paths of unique flying objects in each video. Then, we deployed the computer-vision model on both a random stratified portion of videos collected during the study period and portions of video coinciding with detections from the vibration sensors to identify portions of video that contained potential collisions. Then, biologists reviewed videos containing potential collisions to determine if a collision occurred and classify the species and size class (e.g., small or large bird, bat). In some cases, reviewers disagreed if a collision occurred and if the object in the imagery was a bird or bat. Therefore, we designated two levels of confidence regarding collision events:

*High:* Two reviewers classified the event as a collision and the object was classified by an expert as a bat or bird.
*Medium:* One reviewer classified the video clip as a collision (and one disagreed) and the object was classified by an expert as a bat or bird.

We then used the collisions detected under the two confidence levels to produce separate fatality estimates in the double-observer statistical analysis described below.

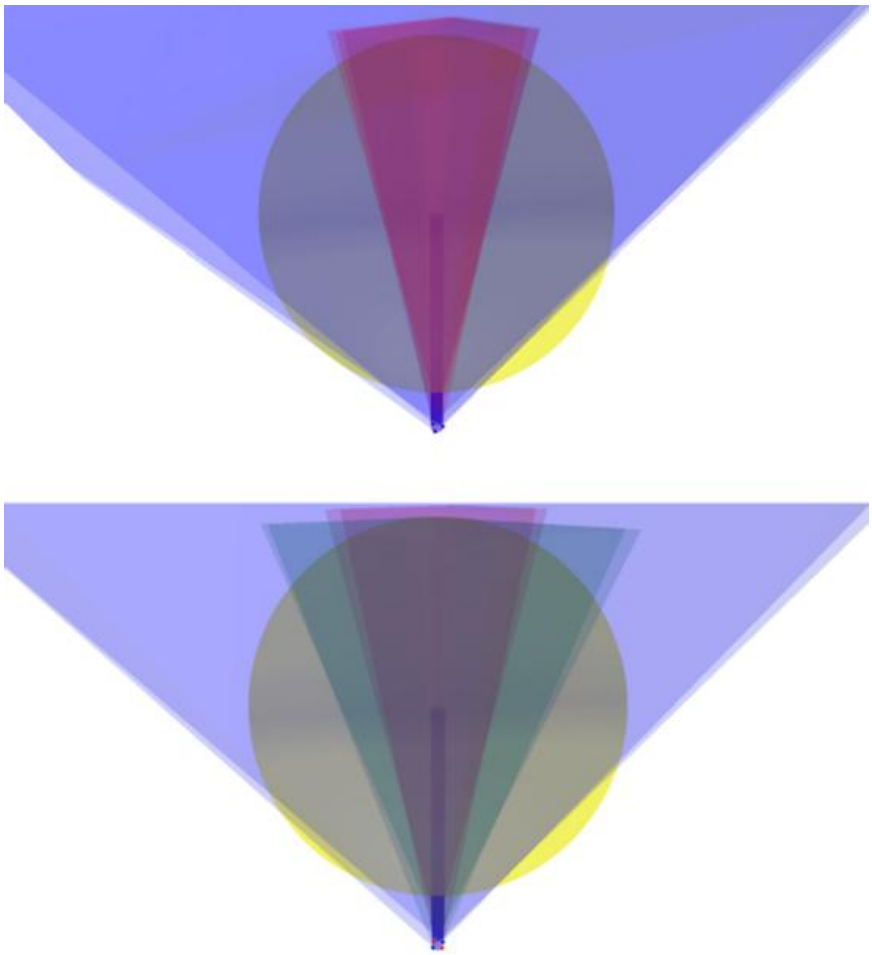

**Figure 4.2. The field of view of the cameras relative to the rotor-swept zone (RSZ) of the turbine for the 2022 deployment (above) and 2023 deployment (below).**

Note: The yellow sphere shows the entirety of the RSZ. The red and green pyramids represent the approximate field of view (35-millimeter [mm] and 19-mm cameras, respectively), which have significant overlap with each other, allowing for multiple frames of reference to activity in the RSZ, but full visual coverage did not extend to the outer edges of the RSZ. The purple pyramids depict the approximate field of view of the true-color cameras, which have greater coverage of the RSZ.

For the Spring 2023 camera-only deployment, we developed and tested an edge computing deployment system for real-time video processing. The system included a liquid cooling system to reduce the likelihood of heat buildup observed in 2022. During edge-processing, when a flying object was detected in a thermal video, that video, the detected object's locations per frame, and the Sony images from that 10-second period were saved on a local Network Area Storage device for further review. Additionally, we programmed the system to retain a random sample of videos and their accompanying color imagery when no detections were found for the purpose of later evaluation of false negative rates of the real-time detection system.

The videos saved from the edge deployment underwent several stages of post-processing. We developed a segmentation computer-vision model to find the pixel-level boundaries of the turbine in each frame of video. These segmentations, in conjunction with the object detections, were used in a filtering algorithm to further narrow down videos when a collision was possible. The collision

classifier considered whether the object ever approached the turbine and whether it abruptly changed direction and velocity upon approaching the turbine, which describes a collision. We tested the collision classifier on known collision videos from the previous deployment. We applied modelling techniques post-deployment to further filter out videos that did not contain collisions.

Among videos flagged by the collision classifier, we reviewed those that were contemporary with the possible time of death based on carcasses discovered during the traditional ground-based carcass searching.

Statistical Methods

The primary goal of Task 4 was to evaluate if the fatality estimate developed from WT-Bird® collision data was comparable to an estimate developed using traditional ground-based carcass searches.

*Fatality Estimation using WT-Bird® System Data*

We investigated two approaches to account for detection probability and to estimate fatalities using the vibration sensor and video monitoring components of the WT-Bird® system. In the first approach, we utilized previous detection probability estimates obtained from the 2021 trials of the WT-Bird® vibration sensors at the NREL, in which vibration sensor detection rates ranged from 0.65–0.75 detections per known collision (i.e., Task 2). In this approach, we used these lower and upper bounds of detection rates from the NREL trials as plausible range of detection rates for the WT-Bird® system at the University of Minnesota turbine.

In the second fatality estimation approach, we expected to treat the vibration sensors and the video monitoring components as separate independent observers, using double-observer estimation techniques to estimate a separate detection probability for the WT-Bird® system. Generally, double observer efforts aim to improve overall population approximations and tend to assume that each observer records detections independently. Examples of double-observer surveys include wild horses by aircraft (Graham and Bell 1989), polar bears by transect (Manly et al. 1996), river birds by canoe (Fletcher and Hutto 2006), and avian point counts (Nichols et al. 2000). In this study, we anticipated treating the vibration sensors and video monitoring components as separate observers, including the following assumptions in our double-observer analysis:

- The vibration sensors and video monitoring systems operated independently with respect to collision detection.
- There were no false positive collision detections; a time-stamped detection from either observer implied a fatal collision.

The rate of collisions during system downtime was assumed to be the same as when the system was operating normally.

*Results*

Field Monitoring A single staff member, trained to conduct standardized carcass searches systematically searched the ground beneath the turbine between June 24 – November 9, 2022.

The observer conducted searches three times each week on a 120-m radius circular plot centered on the turbine and cleared by regular mowing. The observer also measured searcher efficiency and carcass persistence through bias trials. Eight bird carcasses composed of three identifiable bird species were found and left in place, and 15 bat carcasses composed of four identifiable bat species were found and collected during the study (permit 19204). One bald eagle (*Haliaeetus leucocephalus*) carcass was found during surveys. Three of the bird carcasses included in the analysis were found in the summer (June 24 – August 17) and five carcasses in the fall (August 18 – November 9). Seven bat carcasses were found in the summer and eight carcasses in the fall. Further details on the fatality monitoring and estimation are provided in Appendix A.

The WT-Bird® system was operational from August 13 – November 3, 2022, with the period prior to September 6 focused on tuning the system to the University of Minnesota turbine. Except for storm-associated power outages, the turbine and the WT-Bird® system was operational 83.7% of the time, although one of the 24-m sensors within the box beam (Blade 3, Sensor 3) was not operational for much of the trial due to a failure following installation. Of 15 collisions documented by the blade vibration sensors during the survey period, 13 occurred during twilight or in full darkness. Concurrent land-based carcass searches by WEST detected 13 carcasses (not adjusted for searcher efficiency, carcass persistence, or carcasses that fell outside of search plots).

Cameras operated correctly throughout the study. The WT-Bird® color imagery did not document 11 of the 15 collisions; these collisions primarily occurred at night when the IR illuminators were operating. Due to loss of a portion of the thermal camera imagery data due to a hard drive failure, corroborating thermal imagery was available for only a portion of the study. Similarly, among the eight collisions that occurred when both color and thermal cameras were operational, seven detections included objects observed by the thermal cameras, including six documented collisions, but the color cameras only saw three collisions. Only one collision occurred during daylight, a bald eagle, and the color imagery clearly captured this collision with the blade tip. We identified the remaining 14 collisions as bats based on observed carcasses. Bat collisions were detected most strongly at the sensor 16 m from the root, with visual confirmation also indicating that most collisions occurred within the blade midspan.

*Fatality Rate Estimation*

Using the lower and upper detection rates from the Task 2 NREL study (0.65 and 0.75, respectively), multiplied by the proportion of vibration system uptime, and 15 detections classified as collision by the WT-Bird® system, we calculated lower and upper overall detection probability estimates of 0.54 and 0.63, respectively, for the WT-Bird® system. Using these *assumed* detection probability estimates, the corresponding lower and upper adjusted fatality estimates while accounting for proportion of time sensors were operational were 23.89 and 27.57, respectively, for the study period (Table 4.1). In comparison, the post-construction mortality field study yielded a GenEst fatality estimate of 16.8 birds and bats (90% confidence interval [CI]: 9.88–27.92 birds and bats). Thus, the WT-Bird® collision-based estimates were within the 90% CI of the field estimate but were higher than the mean (Appendix A; Stucker et al. 2024).

**Table 4.1. Fatality rates per turbine derived from the WT-Bird® collision detection monitoring at the University of Minnesota Eolos Turbine in Rosemount, Minnesota, from August 18 – November 3, 2022.**

| Assumed Collision Detection Probability[a] | Uptime Proportion | Overall DetectionProbability | Detected Collisions | Adjusted Fatality Estimate[b] |
|---|---|---|---|---|
| 0.75 | 0.84 | 0.63 | 15 | 23.89 |
| 0.65 | 0.84 | 0.54 | 15 | 27.57 |

[a.] Collision detection probability based on detection trials at the National Renewable Energy Laboratory (Stucker et al 2022).
[b.] Adjusted Fatality Estimates account for Uptime Proportion, to account for when WT-Bird® and turbine were operational.

Due to insufficient collision data, neither the double observer approach to fatality estimation, nor verifying the WT-Bird® detection rates at the University of Minnesota Turbine using video data were possible.

*Results Spring 2023 Edge Deployment and Post-processing*

In the spring of 2023, we deployed the real-time edge monitoring system for 87 days, or approximately 2,088 hours of monitoring and 8,352 video hours, across the four thermal cameras. During that 87-day period, the system did not fail or require intervention. We developed the distinct computer vision model for the edge deployment to allow for faster data processing. Using the real-time computer vision model for edge processing at the turbine, we saved 643 hours of video containing detected objects, which is a 92.3% reduction in data storage.

During deployment, we retained a random sample of 100 videos where no image detections were made to evaluate if the edge monitoring systems missed objects. We determined that the edge detection system generated no false negatives or missed detections of objects.

In testing, the post-processing turbine segmentation model had precision and recall of 0.98 and 1.00, respectively (where precision measures the proportion of predictions that were correct and recall measures the proportion of known TPs that the model correctly identified). Errors in precision are FPs, while errors in recall are FNs. When the system flagged a video for review, all IR videos available from the four cameras were merged into a mosaic for review so that the reviewer could see the most complete view of the flying object's trajectory. We tested the criteria used to filter videos against known collision clips, all of which were flagged under this algorithm.

During the edge deployment, we found five fatalities during ground searches. We assumed that all collisions occurred between the previous search and the search on which the fatalities were found, which aligned with the estimated time of death of the fatalities based on their physical condition. We ran the collision detection algorithm on all possible dates of collision events for the five fatalities, resulting in 15 days. Out of the 34,928 videos, or 97.12 hours, of footage collected across these days, we reviewed 4,482 videos, or 12.40 hours, flagged by the algorithm as having a high likelihood of a bird or a bat collision and found four out of the five known collisions based

on observed 2023 carcasses. As simultaneous videos from different cameras were reviewed at the same time, the actual time to review this footage was less than 12.40 hours.

In three of the four cases when a collision was found during Spring 2023, the system only saved one camera's video footage. In the fourth case, the system saved footage from two cameras, but the collision was not visible from one of the camera angles. Only thermal cameras were able to document turbine collisions during Spring 2023 deployment; none of the collision events or the animals associated with the events could be seen in the accompanying color images. If the study had progressed to the Task 5 offshore turbine testing, the system would have been updated to save all views from all cameras for each collision preceding and following collisions, and incorporated thermal cameras more formally into the monitoring system.

*Conclusion*

The goal of Task 4 was to: 1) validate the comparability of a fatality estimate, developed using data from the WT-Bird® collision detection system, to a standard, land-based GenEst fatality estimate and 2) confirm whether the computer-vision system, developed by WEST, could serve as an independent second observer in a subsequent offshore trial (Task 5) while reducing the amount of video data retained. Each of these goals were achieved and substantial improvements were made to enable the operations to work independently.

**Did the WT-Bird® system provide comparable fatality estimates to standard, land-based GenEst fatality estimates?**

Observers have completed hundreds of post-construction monitoring studies on land in the U.S., most of which estimated the number of bird and bat collisions through standardized searches under turbines, within an area that was typically equal to that of a circle with a radius equal to the length of a turbine blade. Observers then adjusted the number of carcasses found for known biases that affect the number of carcasses detected, such as searcher efficiency, carcass persistence, and the number of carcasses that fell outside of the search area (Dalthorp et al. 2018). Monitoring for and estimating the number of collisions of birds and bats offshore presents unique challenges, including the inability to regularly search areas where carcasses could fall using humans or dog teams. The ultimate goal of this Project was to determine if improvements to the WT-Bird® system could be used to generate bird and bat fatality estimates that were comparable to estimates collected using traditional methods employed at land-based wind turbines. Our results showed that the system produced bird and bat fatality estimates similar to those obtained from traditional land-based wind energy carcass survey and thus can be employed to answer questions regarding the rate of fatalities at offshore wind projects. Future applications of the WT-Bird® that desire to generate fatality rates will need an estimate detection probabilities. The detection rates we generated during our challenge tests at NREL may provide a rough estimate of detection probabilities, however, we recommend detection rates for future applications offshore be verified and further quantified using double-observe techniques and camera technology.

The WT-Bird® system was reliable, operated without interruption, and appeared to detect collisions at rates greater than those recorded by traditional ground-based monitoring, despite the need, due to blade design, to place the third sensor within the turbine blade's box beam. Due to data losses on the video cameras, we were unable to identify the species or species groups for most collisions from imagery. This was a problem that can easily be solved in the future with regular back-ups of video data and improved camera technologies that can detect birds and bats at greater distances.

Despite the issues with thermal camera data loss, the deployment of the WT-Bird® system benefited from the inclusion of thermal cameras. While the color imagery was helpful during the day, identifying objects from color cameras supported with illuminators during night was generally not possible. The thermal cameras are more robust in their ability to filter non-target objects from the analysis, but the reduced resolution introduces additional uncertainty.

During the 2022 trials, the WT-Bird® system was able to detect what were primarily bat collisions for most of the deployment. Furthermore, most of these objects, when observable in cameras, appeared to be colliding with the turbine blade within the mid-span, and not necessarily at the blade tip, where the collision would result in a greater vibration. While the second sensors at 16 m were triggered most frequently, the configuration of the blade prevented installation of the sensor on the leading edge. This may have resulted in the third sensor at 24 m not triggering as much as expected.

The fatality point estimate derived from the WT-Bird® system was near the upper end of the 90% CI of the fatality estimate generated by traditional land-based survey techniques, suggesting that estimates calculated from the WT-Bird® might have been slightly conservative (i.e., estimates were slightly higher than land-based estimates). There were possible explanations, including:

- 2021 NREL detection rates reused at the University of Minnesota may have underestimated WT-Bird® detection rates for this turbine installation and study period.
- The collision rate was not constant (e.g., seasonal) during the period of sensor downtime.
- Although unlikely based on observing zero FP vibrations classified as collisions during 2021 (Appendix A), there is a potential that an FP "collision" could occur.

Overall, a system that provided a fatality estimate for offshore turbines that fell within the CI of the estimates calculated using modern land-based techniques would meet the primary objectives of most wildlife resource agencies, which is to determine how many bird and bat fatalities are occurring.

**Did the computer-vision system developed by WEST serve as an independent second observer in a subsequent offshore trial (Task 5) while reducing the amount of video data retained?**

We estimated the detection rate of the WT-Bird® system at the NREL testing facility, by launching objects at turbine blades. This was relatively labor intensive and expensive and there may be need in the future to estimate the detection rates for the WT-Bird® system in an offshore environment, as the system was applied to new turbines that may require differing spacing of sensors or numbers of vibration sensors. The use of a camera-based system could serve as a double observer and be used to estimate detection rates offshore, which would allow future deployments of WT-Bird® to report the number of collisions detected and generate fatality rates that account for detection bias and are thus more defensible. Our ability to empirically test if our computer-vision system could serve as a second observer was hindered by a data loss incident. Only 20–30% of the vibration-based collisions had a corresponding video-based detection using the color cameras with illuminators. The machine-learning training results from thermal camera imagery indicated the computer vision algorithms successfully detected 72% of bats and over 90% of birds present in the footage, but that a smaller percentage of collisions were visible due to the limited field of view of the cameras. This is a relatively high detection rate, when compared to standard post-construction monitoring (e.g., Stucker et al 2024), which suggests that a computer-vision system could be used in an offshore setting to serve as a second observer. Collision detection rates for the computer vision system could be improved by increasing the field of view with additional cameras. Adding additional cameras should increase the likelihood of detection and identification of observed objects, within limits. For example with high resolution color imagery, a larger bird may be identified to species, particularly during the daytime. This can support assessments of collision risk for sensitive species which are easily identified. Unfortunately, nocturnal cryptic species, like bats, may not be identifiable beyond “bat” using camera sensors alone, or even with inclusion of acoustic sensors. The number and types of cameras or other technologies used should depend on the goal of monitoring. Is the goal to determine if the overall bird and bat fatality rate is similar to land-based wind-energy facilities? Is the goal to determine if a rare species collides with turbines with great certainty and precision? The amount of effort, including the number of turbines sampled, and the technologies employed, will differ between these two example goals. It is important to remember that monitoring collisions in the offshore environment requires high investments in technology, and adding additional cameras or other sensors can result in a system that is more logistically complex to implement if the monitoring goals are not well defined.

The post-deployment computer vision system significantly reduced the burden of post-deployment review time by filtering out 87.17% of the saved videos while still retaining good recall; we located four out of the five known collision events during deployment.

In future deployments, we could implement several changes to the system to further improve the monitoring system and reduce the burden of review time, including:

1. Adding the post-deployment computer vision model into the real-time system to reduce the necessity of data storage and post-processing labor.
2. Changing the monitoring system to automatically save all camera videos when any of the videos have a potential collision detected to ensure more data when a collision is possible and more certainty in collision classification.

3. Using 3-dimensional triangulation to estimate the position and size of flying objects and exclude objects outside the RSZ that are very close to the camera and airplanes that are very far away.
4. Altering the tilt and/or positioning of the cameras to cover a greater portion of the RSZ with less overlap among the fields of view.
5. Increasing the sample size of training data for each portion of the machine learning algorithms.

*Lessons Learned*

Installation of the system required less than 16 hours of turbine down-time over a two-day period. Prior to the Task 4 deployment we noted that coating loss on some of the plastic domes on the color camera lens covers compromised clarity in the video; cameras were mounted to minimize lens view through those areas, and one of the camera's plastic domes was replaced. Likewise, one of the color cameras trapped water within the housing rather than allowing it to drain. Silicon sealant was placed over exposed fasteners to ensure water shedding from the camera housing, and silica drying packets were included within the camera dome to absorb any remaining moisture. For the thermal cameras, water occasionally pooled on the flat lens surface (see Fig 4.1, center back Axis thermal camera), but quickly evaporated within an hour with internal heat. Importantly, for installations where nighttime (bat) collisions are the primary concern, use of multiple thermal cameras was critical to confirm the presence of an object, given their inherent reduced resolution and field of view, when compared to the color imagery camera. For offshore deployments a combination of color and thermal cameras would be most suitable, but mounting placement would be best split between platform and nacelle to ensure the upper rotor sweep is sampled or monitored; thermal cameras are hampered by limitations in field of view and resolution at distance. Use of infrared illuminators was a challenge near the reflective tower surface, and even use of multiple illuminators failed to provide adequate light for appropriate resolution for image analysis during night, when the majority of collisions occurred.

WEST's advances in deploying an automated edge-processing system for evaluating incoming imagery prior to storage was critical for efficient data retention in situ. Edge-based image processing produced substantial heat that resulted in overheating computers despite low ambient temperatures (less than 10°C) within the turbine. Once a liquid-cooled system was implemented, the edge processing system worked continuously and without failure. The "containerized" approach using Docker containers to implement rapid redeployment was an important development for future efforts.

Technologies designed to record wildlife occurence, or collisions near turbines in the land-based or offshore environment require physical space, stable mounting systems, power, and digital storage. The specifics of space requirements and mounting mechanisms will differ among the technologies selected, and the turbine design, but particularly offshore, many components need to be marine grade, or in marine grade housing. Based on this study, and implementation planning for Task 5, deployment of the equipment should consider the following:

- Including wildlife, IT, and engineering experts in the front-end engineering design (FEED) process, or as early as possible to plan for all aspects of wildlife sensing equipment.

- Consistent power sources from turbine need to be available, potentially with temporary battery backup for highly sensitive computer components.
- Cable runs and access ports to permit power and data cables pass through from inside to outside of turbine.
- Access to an internet or satellite provider for managing processes and equipment. Download capability may not be needed, but access to monitor equipment is necessary.
- Intra-turbine networks, including Wi-Fi, may be required, but can be separate from those used operationally.
- Expect multiple internet protocol (IP) addressing systems, IPv4 and IPv6.
- Multiple storage cabinets (e.g. industrial control panel enclosure) often ~ 60 x 66 x 40 cm in size may be needed in the turbine nacelle and lower in tower near base or platform, relatively close to sensing equipment.
- Computers/servers if needed may need to be internally liquid cooled particularly if graphics processing capabilities are needed (i.e. edge processing).
- Data storage and data backup capabilities, in the 50 -100 Terabyte range for storage of multiple streams of imagery data, but size is dependent on duration of deployment, internal processing, and advances in data compression.
- Use of a mounting bracket system on the safety railing or at multiple designated spaces (>3) for multiple cameras or sensors and other observational equipment on turbine platform and on nacelle. Attachment may be requested via magnets on tower exterior.

### Task 5. Implementation of WT-Bird® on an Offshore Turbine

Although the team had initiated substantial planning and documentation to support an offshore deployment (Task 5) during Task 4, we encountered repeated delays and challenges with obtaining final operator agreement to test WT-Bird® at a specific offshore facility within the grant time period. Inclusion of this type of equipment requires years of preparation and negotiation among the developers (operators), and financial investors, for developing plans for logistics, and legal concerns, including turbine and equipment liability. This challenge, in combination with depleted funds insufficient to support the remaining testing, halted subsequent Task 5 testing. This decision was made in coordination with the Office of Energy Efficiency and Renewable Energy team during February 2024.

## ISSUES, RISKS, AND MITIGATION

Two long-standing issues were an operational challenge throughout this Project: 1) changes in Project partners, turbine facilities, and the loss of associated cost-share funding compromised planning and delayed implementation, and 2) the COVID-19 pandemic halted in-person collaboration, and the subsequent supply chain issues and rising inflation were recurring problems for the duration of the research and development effort. In combination, these two challenges led to serial delays, unanticipated and unavoidable expenses, increased costs, and necessary

changes in data collection strategies. While the research and development effort succeeded in accomplishing its goals, doing so required expending substantial effort.

# PROJECT OUTPUT

## Publications

To date, we have not published the results of the study in a peer-reviewed journal.

To support information exchange and following Objective 6: *share lessons learned to promote technologies and support offshore wind development in the U.S.* (see *Project Objectives*), the Project team presented updates on the Project status at appropriate wind energy conferences or symposiums, particularly when WEST staff were already going to be in attendance (no added cost). Below are the formal venues where presentation was made.

- WEST presented an overview of the Project to the wind-wildlife community during the National Wind Coordinating Collaborative webinar, titled *New Research on Wildlife Monitoring at Offshore Wind Energy Facilities Supported by the U.S. Department of Energy*, on January 16, 2020.
- WEST presented at American Wind Energy Association Offshore from October 13–14, 2020.
- WEST presented at the National Wind Coordinating Collaborative meeting from December 2–4, 2020.
- WEST (Jennifer Stucker) served on a live panel discussion, *Offshore Wind-Wildlife Technologies and Challenges*, on December 3, 2020.
- WEST-NREL-TNO presented an update on the status of the research and development effort for the American Clean Power Siting and Environmental Compliance Virtual Summit in 2021.
- WEST-NREL-TNO presented an update on the status of the research and development effort at the American Clean Power Offshore Windpower Conference in October 2021.
- WEST-NREL-TNO presented an update on the status of the research and development effort for the Conference on Wind and Wildlife (CWW) in April 2022.
- WEST-NREL-TNO presented an update on the status of the research and development effort for a poster session for the American Clean Power Offshore Windpower Conference in October 2022.
- WEST-NREL-TNO presented an update on the status of the research and development effort during a live oral presentation and panel discussion at the biennial Renewable Energy Wildlife Institute Wind Wildlife Research Meeting from November 15–17, 2022.
- WEST-NREL-TNO presented an update on the status of this research and development effort for the CWW in September 2023.
- WEST-NREL-TNO presented an update on the status of this research and development effort to the Waterbird Society in Fort Lauderdale in October 2023.

- WEST presented to the North American Wind Energy Academy on the WEST Computer Vision system and approach in 2023.
- WEST presented at DockerCon, sharing how WEST innovatively used Docker containers to provide for a swift deployment of edge computing and object detection in the industrial turbine environment, in 2023.

### Technologies/Techniques, Inventions/Patent Applications, and Licensing Agreements

There are no new technologies or techniques at the time of this report.

There are no new inventions/patent applications or licensing agreements at the time of this report.

### Other Products

There are no other products, such as data or databases, physical collections, audio or video, software or netware, models, educational aids or curricula, instruments, or equipment, developed to date.

## ACKNOWLEDGEMENTS

WEST wishes to acknowledge the support of the following organizations and individuals during this research and development effort.

- The original idea for this research was supported by LEEDCo (Dave Karpinski), and TNO (Hans Verhoef)
- Funding was provided by a grant from the U.S. Department of Energy's Office of Energy Efficiency and Renewable Energy (EERE) under the Wind Energy Technologies Office Award Number DE-EE0008734. Additional funding was provided by the following: Western EcoSystems Technology, and through grants from Vineyard Wind, the Dutch Innovation Fund awarded through TNO, and Diamond Offshore Wind.
- In-kind contributions were provided by Ørsted North America, Xcel Energy's Blazing Star Wind Farm, University of Minnesota's St. Anthony Falls Laboratory, College of the Atlantic, LEEDCo, and the Stucker family.
- Additionally, the authors would like to thank the following individuals who contributed to this collaborative effort
    - TNO – Hans Verhoef, Frank Kaandorp, Catherine Eeckels, Pi Danzl, and Novita Saraswati
    - National Renewable Energy Lab: Jason Roadman, Chris Ivanov, Samantha Rooney, and Cris Hein
    - Xcel Energy: Kate Schindler and Tim Sanderson
    - College of the Atlantic: Prof. John Anderson, Prof. Dan DenDanto, Olivia Jolley, Nathan Dubrow, Captain Toby Stephenson
    - St. Anthony Falls Laboratory, particularly Chris Feist, Christopher Milliren, Matt Lueker, and Dick Christopher
    - Peer-reviewers for this report from DOE, USFWS, and USGS.

- WEST's support was enormous, and included numerous staff over five years: Wally Erickson, Rebecca Schmitt, Trent McDonald, Sam Rankl, Josh Walrath, Chris Roberts, Kevin Heist, Karsten Dahlberg, Lauren Schell, Nick O'Neil, Aaron Suehring, Molly Tuma, Hayley Ellingsen, Mikey Tabak, Tom Prebyl, Riley Knoedler, Andrew Telander, Paul Rabie, Julie Bushey, Simon Weller, Andrew Tredennick, Fawn Hornsby, Jacob Morris, Grant Glouser, Lewis Hein, John Lloyd, editors and WEST's Document Assistance Group, and so many others sharing their intellectual and technical expertise to support this research and development effort.

## LITERATURE CITED

Cook, R. D. and J. O. Jacobson. 1979. A Design for Estimating Visibility Bias in Aerial Surveys. Biometrics 35(4): 735-742. doi: 10.2307/2530104.

Dalthorp, D. H., L. Madsen, M. M. Huso, P. Rabie, R. Wolpert, J. Studyvin, J. Simonis, and J. M. Mintz. 2018. Genest Statistical Models—a Generalized Estimator of Mortality. U.S. Geological Survey Techniques and Methods, Volume 7, Chapter A2. 13 pp. doi: 10.3133/tm7A2. Avalable online: https://pubs.usgs.gov/tm/7a2/tm7a2.pdf

Fletcher, R. J. and R. L. Hutto. 2006. Estimating Detection Probabilities of River Birds Using Double Surveys. Biological Sciences Faculty Publications 123(3): doi: 10.1642/0004-8038(2006)123[695:EDPORB]2.0.CO;2.

Girshick, R., D. J., T. Darrell, and J. Malik. 2016. Region-Based Convolutional Networks for Accurate Object Detection and Segmentation. IEEE Transactions on Pattern Analysis and Machine Intelligence 38(1): 142-158. doi: 10.1109/TPAMI.2015.2437384.

Graham, A. and R. Bell. 1989. Investigating Observer Bias in Aerial Survey by Simultaneous Double-Counts. Journal of Wildlife Management 53(4): 1009-1016.

Kaandorp, F. 2022. WT-Bird Installation Report University of Minnesota. TNO R11392. Submitted to Western EcoSystems Technology, Inc. (WEST). 2023. 18 pp.

Kovacs, E. 2022. Millions of APC Smart Ups Devices Can Be Remotely Hacked, Damaged. Security Week: Cybersecurity News, Insights and Analysis, IOT Security. Published March 8, 2022. Accessed April 2025. Available online: https://www.securityweek.com/millions-apc-smart-ups-devices-can-be-remotely-hacked-damaged/

Lin, T.-Y., M. Maire, S. Belongie, L. Bourdev, R. Girshick, J. Hays, P. Perona, D. Ramanan, C. L. Zitnick, and P. Dollar. 2014. Microsoft COCO: Common Objects in Context. Version 3. *In*: Computer Vision–Eccv 2014: 13th European Conference. Zurich, Switzerland. doi: 10.48550/arXiv. 1405.0312.

Manly, B. F. J., L. L. McDonald, and G. W. Garner. 1996. Maximum Likelihood Estimation for the Double-Count Method with Independent Observers. Journal of Agricultural, Biological, and Environmental Statistics 1: 170-189.

Marcel, S. and Y. Rodriguez. 2010. Torchvision the Machine-Vision Package of Torch. Pp. 1485-1488. *In*: Proceedings of the 18th Association for Computing Machinery International Conference on Multimedia. New York, New York. doi: 10.1145/1873951.1874254.

Newton, I, and B. Little. 2009. Assessment of wind-farm and other bird casualties from carcasses found on a Northumbrian beach over an 11-year period. Bird Study 56:158-167 Accessed online https://www.tandfonline.com/doi/pdf/10.1080/00063650902787767

Nichols, J. D., J. E. Hines, J. R. Sauer, F. W. Fallon, J. E. Fallon, and P. J. Heglund. 2000. A Double-Observer Approach for Estimating Detection Probability and Abundance from Point Counts. The Auk 117: 393-408.

Paszke, A., S. Gross, F. Massa, A. Lerer, J. Bradbury, G. Chanan, T. Killeen, Z. Lin, N. Gimelshein, L. Antiga, A. Desmaison, A. Kopf, E. Yang, Z. DeVito, M. Raison, A. Tejani, S. Chilamkurthy, B. Steiner, L. Fang, J. Bai, and S. Chintala. 2019. PyTorch: An Imperative Style, High-Performance Deep Learning Library. Pages 8026–8037 in H. Wallach, H. Larochelle, A. Beygelzimer, F. Alché-Buc, E. Fox, and R. Garnett, editors. Advances in Neural Information Processing Systems 32. Curran Associates, Inc.

Pedregosa, F., G. Varoquaux, A. Gramfort, V. Michel, B. Thirion, O. Grisel, M. Blondel, P. Prettenhofer, R. Weiss, V. Dubourg, J. Vanderplas, A. Passos, D. Cournapeau, M. Brucher, M. Perrot, and É. Duchesnay. 2011. Scikit-Learn: Machine Learning in Python. Journal of Machine Learning Research 12: 2825-2830.

Petterson, J. 2005. The Impact of Offshore Wind Farms on Bird Life in Southern Kalmar Sound, Sweden - A Final Report to Studies 1999-2003 to the Swedish Energy Agency. Accessed online via Tethys https://tethys.pnnl.gov/sites/default/files/publications/The_Impact_of_Offshore_Wind_Farms_on_Bird_Life.pdf

Python Software Foundation (PSF). 2020. Python. PSF, Beaverton, Oregon. Accessed April 2025. Available online: https://www.python.org/

Ren, S., K. He, R. Girshick, and J. Sun. 2016. Faster R-CNN: Towards Real-Time Object Detection with Region Proposal Networks. Computer Vision and Pattern Recognition. Cornell University, Ithaca, New York. January 6, 2016. Accessed April 2024. arXiv:1506.01497.

Roadman, J., R. Goldhor, C. Hein, C. Ivanov, and S. Rooney. 2024. Design of a Launcher for Wildlife Collision Simulation on Wind Turbines to Validate Strike Detection Systems. National Renewable Energy Laboratory (NREL). Presented at the North American Wind Energy Academy (NAWEA)/WindTech 2024 Conference, 30 October - 1 November 2024, New Brunswick, New Jersey. Available online: https://www.nrel.gov/docs/fy25osti/91582.pdf

Western EcoSystems Technology, Inc. (WEST). 2022. Milestone 4.2: Approved Study Plan for a Multi-Sensor Approach for Measuring Bird and Bat Collisions with Offshore Wind Turbines. U.S. Department of Energy, Office of Energy Efficiency and Renewable Energy Wind Energy Technology Office Advanced Wind R&D to Reduce Costs and Environmental Impact (DE-FOA-0001924) DE-EE0008734. Finalized April 2022. 16 pp.

Western EcoSystems Technology, Inc. (WEST). 2023. Regional Summaries of Wildlife Fatalities at Wind Facilities in the United States and Canada, 2022 Report from the Renew Database. Cheyenne, Wyoming. July 1, 2023. Available online: connect.west-inc.com/Renew/RenewReport2022.html

Wildlife Acoustics, Inc. 2022. Kaleidoscope Pro® Version 5.4.7 (Acoustic Analysis Computer Software) and Bats of North America Version 5.4.0 (Bat Pass Classifier Computer Software). Wildlife Acoustics, Maynard, Massachusetts. February 1, 2022. Available online: www.wildlifeacoustics.com

# Appendix A. A Multi-Sensor Approach for Measuring Bird and Bat Collisions with Offshore Wind Turbines Task 4: Land-Based Validation Trial Results

# Research Performance Report

## A Multi-Sensor Approach for Measuring Bird and Bat Collisions with Offshore Wind Turbines

## Task 4: Land-Based Validation Trial Results

**Prepared for:**

**US Department of Energy**

Office of Energy Efficiency and Renewable Energy Wind Energy Technology Office Advanced Wind R&D to Reduce Costs and Environmental Impact (DE-FOA-0001924) DE-EE0008734.

**Prepared by:**

**Western EcoSystems Technology, Inc.**

7575 Golden Valley Road, Suite 300
Golden Valley, Minnesota 55427

**With Contributions From:**

The Netherlands Organisation for Applied Scientific Research (TNO)
National Renewable Energy Laboratory (NREL)

**February 2, 2025**

WEST

| | |
|---|---|
| **Federal Agency** | Department of Energy<br>Office of Energy Efficiency and Renewable Energy<br>Wind Energy Technology Office |
| **FOA Name and Number** | Advanced Wind R&D to Reduce Costs and Environmental Impact (DE-FOA-0001924) |
| **Report Type** | Research Performance Progress Report |
| **Award Number** | DE-EE0008734 |
| **Award Type** | Cooperative Agreement |
| **Prime Recipient** | Jennifer H. Stucker, PhD and Rhett E. Good, CWB®<br>Western EcoSystems Technology, Inc.<br>400 West 7th Street, Suite 200<br>Bloomington, Indiana 47404<br>jstucker@west-inc.com<br>rgood@west-inc.com<br>Phone: 812.339.1756 |
| **Prime Recipient Type** | Private Company |
| **Project Title** | A Multi-Sensor Approach for Measuring Bird and Bat Collisions with Offshore Wind Turbines |
| **DUNS Number** | 627824261 |
| **Date of Report** | January 8, 2025; February 2, 2025 |
| **Period of Report** | March 2022 – December 2024 |



**NOT FOR DISTRIBUTION**

## REPORT PARTICIPANTS

| | |
|---|---|
| Jennifer Stucker, Ph.D. | Project Manager |
| Rhett Good | Prime Recipient, Senior Report Reviewer |
| John Lloyd | Report Reviewer |
| Thomas Prebyl | Machine Learning Lead |
| Riley Knoedler | Machine Learning Lead, Writer |
| Molly Tuma | Field Biologist |
| Nick O'Neil | Report Compiler, Field Biologist |
| Christine Kuykendall | Editor |

## REPORT REFERENCE

Stucker, J., R. Knoedler, and Tom Prebyl. 2025. Research Performance Report. A Multi-Sensor Approach for Measuring Bird and Bat Collisions with Offshore Wind Turbines, Task 4: Land-Based Validation Trial Results. Prepared for the US Department of Energy. Prepared by Western EcoSystems Technology, Inc. (WEST), Golden Valley, Minnesota, with contributions from The Netherlands Organisation for Applied Scientific Research (TNO) and the National Renewable Energy Laboratory (NREL). February 2, 2025. 17 pages + appedices



**NOT FOR DISTRIBUTION**

## TABLE OF CONTENTS



## LIST OF TABLES

## LIST OF FIGURES



## LIST OF APPENDICES

# INTRODUCTION

The overall goal of "*A Multi-Sensor Approach for Measuring Bird and Bat Collisions with Offshore Wind Turbines*" (Project) was to develop an effective multi-sensor system for quantifying bird and bat collision rates at offshore wind facilities. The Project aimed to create an automated collision detection system with two major technological advancements: 1) a refined The Netherlands Organisation for Applied Scientific Research- (TNO-) improved WT-Bird® vibration-sensing system, capable of detecting small bird and bat collisions during daytime and nighttime hours, and 2) improved image-processing systems and computer-vision algorithms (Western EcoSystems Technology, Inc.'s [WEST's]) to automatically detect and classify small and large bird and bat collisions with offshore turbines. This report documents work completed in support of validation testing of the WT-Bird® collision detection system at a land-based wind turbine from June 2022 – June 2023 (Task 4). The goal of Task 4 was to 1) validate the comparability of a fatality estimate developed using data from the WT-Bird® collision detection system to a standard GenEst (a generalized estimator of fatality) fatality estimate and 2) confirm whether the computer-vision system developed by WEST could serve as an independent second observer in a subsequent offshore trial (Task 5) while reducing the amount of video data retained.

# METHODS

Task 4 followed the approved peer-reviewed study plan (WEST 2022). Field deployment of the WT-Bird® system was initiated at the University of Minnesota Eolos Wind Turbine (University of Minnesota turbine) in Rosemount, Minnesota. The turbine was a Clipper Liberty 2.5-megawatt turbine with an 80-meter (m) hub height and 60-m blades that had been in operation since 2011. Cameras were deployed in June 2022, followed by installation of the complete WT-Bird® system, in-blade sensors, and fiberoptic cables by July 2, 2022. Networking among the blade sensors, hub, nacelle, and tower base was completed with system tuning in early August 2022. Concurrent with the camera installation, traditional ground-based fatality monitoring was initiated in June 2022 and conducted three times weekly. The monitoring report and fatality estimate from the ground-based fatality monitoring are provided as a supporting report and included as Appendix A. Throughout the Task 4 study, TNO staff remained blind to when and if carcasses were found by WEST personnel to ensure independence of the WT-Bird® system observations. WEST field personnel also did not know when or if the WT-Bird® system detected collisions. Due to technical issues with the WEST system, a second camera-only deployment occurred between March – June 2023 to better assess WEST's edge computer system. Details on the components and deployments are provided below.

### WT-Bird® System

The WT-Bird® vibration sensors were installed in the turbine blades by TNO engineers, with support from University of Minnesota turbine engineers during June 30 – July 1, 2022. Additional details are included in the TNO installation report (Kaandorp 2022). Each of the three blades had three sensors installed, one each at eight m, 16 m, and 24 m from the hub. Sensors at eight m

and 16 m from the hub were installed on the leading edge of the blade. The 24-m sensors were installed in a separate compartment within the blade (within the box beam, off the leading edge due to the turbine's blade architecture). Following installation and networking, the system underwent a 4-week tuning period, allowing the WT-Bird® system to "listen" to the sounds of turbine operation and refine the collision detection algorithm. Tuning of the system started with the approach that had been used previously during collision testing (Task 2) at the National Renewable Energy Laboratory (NREL), which is documented in the Task 2 report (Stucker et al. 2022). The tuning period ended by early September 2022 and the trial began thereafter.

TNO monitored the performance of the WT-Bird® system throughout this study period. Following the end of the monitoring, TNO prepared a detailed report of likely collisions observed with the WT-Bird® system for use by WEST in evaluating a fatality estimate (Appendix B).

**Video Camera Systems**

Camera selection was detailed previously by WEST and TNO in earlier progress reports. True-color (color) cameras were intended to provide auxiliary data to the collision sensors and aid both manual review of collisions and object size-class determinations.

The 2022 camera monitoring system consisted of camera stations located approximately one to two m from the turbine base at a location similar to the expected turbine platform railing location on an offshore turbine. Cameras and illuminators were installed on a modified adjustable-height sawhorse, stabilized with 50-pound bags of gravel (Figure 1). During 2022, the three paired camera stations were spaced equidistantly around the turbine tower with the cameras facing upwards and the field of view centered on the turbine nacelle. Each camera station included a Sony SNC-VM772R color camera with an 8.8-millimeter (mm) focal length and 5,472x3,648 resolution; the Sony cameras were used previously in the WT-Bird® deployment at NREL and for data collection in Task 2 and during WEST's computer vision model development (Task 3). The second camera at each station was an Axis Q1942-E thermal camera equipped with 35-mm lenses; this camera was also previously used during Task 3 deployments. This thermal camera recorded video in 640x480 resolution and 30 frames per second. The thermal cameras were set to record continuously, and the Sony color cameras were programmed to save 1 image per second at night, and 2.5 images per second during the day. The thermal camera data was used specifically for development of the computer vision algorithm and detection of birds and bats, while the Sony color cameras provided better resolution data during the daytime. The three Sony color cameras were supported at night by an Axis infrared (IR) illuminator (T90D40 IR-LED) at each camera station. The IR illuminators automatically initiated operations in low-level visible light conditions based on the integrated low-light sensor. The WT-Bird® system received constant video feed from the Sony color cameras via power-over-ethernet (PoE) cables, which provided power and transmitted data from cameras to in-turbine computer components (WT-Bird® or WEST storage). Similarly, the Axis thermal cameras received power via a PoE cable and transmitted data back to WEST data storage. The illuminators were powered by a dedicated electrical cable from the turbine.

**Figure 1. The camera stations at the University of Minnesota Eolos Wind Turbine, Dakota County, Minnesota.**

Note: On the left is the Axis infrared illuminator (Axis T90D40 IR-LED), paired with a Sony (SNC--VM772R) true-color camera feeding the WT-Bird® system. On the board to the right and behind is another Sony (SNC-VM772R) true-color camera with an Axis thermal camera (Q1942-E). In the background, at 120 degrees counterclockwise from the foreground setup is the next camera station.

In 2023, to support testing of the real-time capacity of WEST's edge processing, video target -identification system, the WEST cameras were redeployed to capture spring migration without the WT-Bird® collision sensors. The goal of 2023 monitoring was to evaluate whether the updated edge target-identification system could reduce footage while retaining videos of potential collision events. The aim of this edge processing system was to reduce the need for storing large quantities of video footage offshore. The camera-only deployment took place between March 21 – June 15, 2023. In this phase of the study, the camera monitoring system consisted of four camera stations that were located approximately one to two m from the turbine base, spaced equidistantly around the turbine tower, and faced upwards with the field of view centered on the turbine nacelle. Four stations were used in anticipation of the greater field of view of larger offshore wind turbines. One additional camera model was used in this deployment and each station had either an Axis Q1942-E thermal camera equipped with a 35-mm lens, or an Axis Q1952-E thermal camera equipped with a 19-mm lens. Each model recorded 10-second video clips, in 640x480 resolution, at 30 frames per second. In addition, the two camera stations with

19-mm lenses were equipped with the same Sony SNC-VM772R color camera with an 8.8-mm focal length and 5,472x3,648 resolution, as had been deployed during 2022. Figure 2 shows the approximate field of view of the cameras around the turbine tower, depicted in blue, with the 35-mm thermal cameras in red, the 19-mm thermal cameras in green, and the color cameras in purple, relative to the spherical rotor swept zone (RSZ) in yellow.

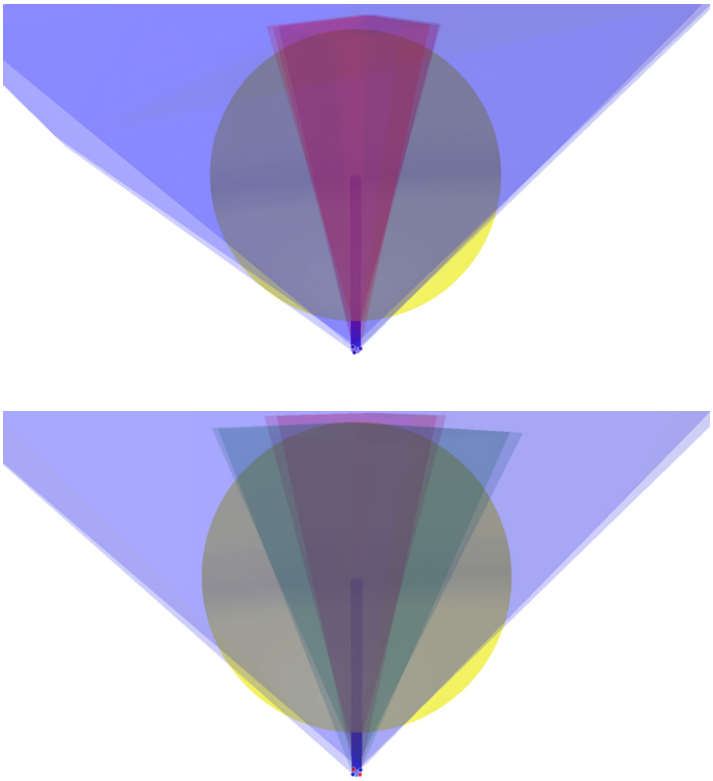

**Figure 2. The field of view of the cameras relative to the rotor swept zone (RSZ) of the turbine for the 2022 deployment (above) and 2023 deployment (below).**

Note: The yellow sphere shows the entirety of the RSZ. The red and green pyramids represent the approximate field of view (35-millimeter [mm] and 19-mm cameras, respectively), which have significant overlap with each other, allowing for multiple frames of reference to activity in the RSZ, but full visual coverage did not extend to the outer edges of the RSZ. The purple pyramids depict the approximate field of view of the color cameras, which have greater coverage of the rotor RSZ.

## Computer Vision Methods

In Task 4, we used data collected from thermal videos in conjunction with a computer vision model to aid in detection of birds and bats flying through the field of view. The primary goal of the computer vision effort was to support the identification of objects during the operation of the WT-Bird® system. A secondary goal for the system was to serve as a second collision observer during the anticipated Task 5 offshore deployment. The thermal video collected during Task 4 was of improved quality but differed from prior video data collection to the extent that it was necessary to train a new computer vision model for the detection of birds and bats. Detailed methods on the training procedure and performance of the computer vision model are provided

in Appendix B. Briefly, we selected a portion of videos containing birds and bats for annotation (drawing bounding boxes and assigning size-class labels to birds and bats) by human reviewers. We then developed an object detection, computer-vision model to detect flying objects, including birds and bats, in thermal videos and implemented a tracking algorithm to identify flight paths of unique flying objects in each video. Then, we deployed the computer vision model on both a random stratified portion of videos collected during the study period and portions of video coinciding with detections from the vibration sensors to identify portions of video that contained potential collisions. Time and budgetary constraints prevented processing of all videos collected. Videos containing potential collisions were then reviewed by biologists to determine if a collision occurred and classification of the species and size class (e.g., small or large bird, bat). In some cases, reviewers disagreed if a collision occurred and if the object in the imagery was a bird or bat. Therefore, we designated two levels of confidence regarding collision events:

*High:* Two reviewers classified the event as a collision and the object was classified by an expert as a bat or bird.

*Medium:* One reviewer classified the video clip as a collision (and one disagreed) and the object was classified by an expert as a bat or bird

We then used the collisions detected under the two confidence levels to produce separate fatality estimates in the double-observer statistical analysis described below.

For the Spring 2023 camera-only deployment, we developed and tested an edge computing deployment system for real-time video processing. The system included a liquid cooling system to reduce the likelihood of heat buildup observed in 2022. During edge-processing, when a flying object was detected in a thermal video, that video, the detected object's locations per frame, and the Sony images from that 10-second period were saved on a local Network Area Storage device for further review. Additionally, the system was programmed to retain a random sample of videos and their accompanying color imagery when no detections were found for the purpose of later evaluation of false negative rates of the real-time detection system. As in 2022, WEST conducted traditional systematic carcass searches to support the camera data collected.

The videos saved from the edge deployment underwent several stages of post-processing. We developed a segmentation computer vision model to find the pixel-level boundaries of the turbine in each frame of video. These segmentations, in conjunction with the object detections, were used in a filtering algorithm to further narrow down videos when a collision was possible. The collision classifier considered whether the object ever approached the turbine and whether it abruptly changed direction and velocity upon approaching the turbine, which describes a collision. We tested the collision classifier on known collision videos from the previous deployment. We applied modelling techniques post-deployment to further filter out videos that did not contain collisions.

Among videos flagged by the collision classifier, we reviewed those that were contemporary with the possible time of death based on carcasses discovered during the traditional ground-based carcass searching.

## Statistical Methods

The primary goal of Task 4 was to evaluate if the fatality estimate developed from WT-Bird® collision data was comparable to an estimate developed using traditional ground-based carcass searches.

*Fatality Estimation using WT-Bird® System Data*

We investigated two approaches to account for detection probability and to estimate fatalities using the vibration sensor and video monitoring components of the WT-Bird® system. In the first approach, we utilized previous detection probability estimates obtained from the 2021 trials of the WT-Bird® vibration sensors at NREL in which vibration sensor detection rates ranged from 0.65 – 0.75 detections per known collision (Stucker et al. 2022). In this approach, we use these lower and upper bounds of detection rates from the NREL trials as a plausible range of detection rates for the WT-Bird® system at the University of Minnesota turbine. In the second fatality estimation approach, we treated the vibration sensors and the video monitoring components as separate independent observers, using double-observer estimation techniques to estimate a separate detection probability for the WT-Bird® system.

There is robust literature for modeling and estimating detections, populations, and species identification when two observers are applied under various study designs. Generally, double-observer efforts aim to improve overall population approximations and tend to assume that each observer records detections independently. Examples of double-observer surveys include wild horses by aircraft (Graham and Bell 1989), polar bears by transect (Manly et al. 1996), river birds by canoe (Fletcher and Hutto 2006), and avian point counts (Nichols et al. 2000). In this study, we treated the vibration sensors and video monitoring components as separate observers.

We made the following assumptions in our double-observer analysis:

- The vibration sensors and video monitoring systems operated independently with respect to collision detection.
- There were no false positive collision detections; a time-stamped detection from either observer implied a fatal collision.
- The rate of collisions during system downtime was assumed to be the same as when the system was operating normally.

Given these assumptions, point estimates and variance estimates can be found numerically from derivations using properties of multinomial functions. There are multiple ways to find estimates numerically as considered by the ecological studies listed above. We largely use notation and methods as outlined by Cook and Jacobson (1979) and further used by Graham and Bell (1989). To establish nomenclature, we assume the first observer was a vibration detection, as indicated by subscript “1.” The second observer was a video detection and was indicated by subscript “2.” Consider an observation made by the first observer but missed by the second as $x_{12}$ and,

accordingly, $x_{21}$ as a video detection not observed by vibration sensors. Then total observations seen by one detection method and not the other are:

$$S_1 = \sum x_{12}$$
$$S_2 = \sum x_{21}$$

Define the sum of observations that were detected by both with $B$. Then we estimate the detection probabilities of each observer $P_1$ and $P_2$, as well as the overall detection probability $P$.

$$\widehat{P_1} = \frac{B}{(S_2 + B)}$$
$$\widehat{P_2} = \frac{B}{(S_1 + B)}$$

With the independence assumption, and using basic properties of probability, the overall detection estimate is:

$$\hat{P} = \widehat{P_1} + \widehat{P_2} - \widehat{P_1}\widehat{P_2}$$

The estimated variance for each detection probability is found numerically by the following:

$$\widehat{Var_1} = \frac{S_2 * \widehat{P_1}}{(S_2 + B)^2}$$
$$\widehat{Var_2} = \frac{S_1 * \widehat{P_2}}{(S_1 + B)^2}$$
$$\widehat{Var} = \frac{S_1 S_2 (S_1 + S_2)\hat{P}}{(S_1 + B)^2 (S_2 + B)^2}$$

Typically, when two independent observers are used, the overall estimated detection probability provides greater precision. From above, the overall variance estimate has a comparatively smaller ratio by accounting for the relative observation totals in the numerator versus that of the denominator. However, this outcome requires that detection probability estimates are sufficiently large (greater than 0.5).

To arrive at fatality estimates, observation counts were divided by the appropriate detection probability and then adjusted by the proportion of observer uptime (i.e., when the system was operating normally). Note that the number of observations from each observer and overall divided by the respective detection rate gives the same estimated number of fatalities. The uncertainty of each fatality estimate provides insight into observer accuracy used for fatality estimation (*Fats*).

$$\widehat{Fats}^* = \frac{x}{\hat{P}},$$

where *x* is the number of observations for detection probability *P*

Next, if there are noted times when an observer was not functioning, then dividing the $\widehat{Fats}^*$ by proportion of uptime (*up,* where 0 < *up* < 1) gives an overall $\widehat{Fats}$. The assumption for applying continuous time through the study period is that fatalities arrive uniformly. Therefore, confidence bounds for fatalities are also linear and found by adjusting variance estimates by the appropriate confidence level and uptime.

$$\widehat{Fats} = \frac{\widehat{Fats}^*}{up}$$

Proportion of uptime requires that both observers are functioning properly, otherwise detections made by any single observer do not apply to a double-observer analysis and must be excluded or applied to a simple single-observer study.

Given the limited sample size of collisions detected by the WT-Bird® system, we conducted a simulation-modeling analysis to investigate the influence of sample size on the accuracy of estimated fatality rates obtained using the double-observer methodology (Appendix C).

## RESULTS

### WT-Bird® System

As summarized by TNO (Kaandorp 2023; Appendix D) WT-Bird® system was operational from August 13 – November 3, 2022, with the period prior to September 6 focused on tuning the system to the University of Minnesota turbine. Except for storm-associated power outages, the WT-Bird® system was operational 83.7% of the time, although one of the 24-m sensors within the box beam (Blade 3, Sensor 3) was not operational for much of the trial. During the survey period, a total of 15 collisions were documented by the blade vibration sensors (Table 1), with 13 occurring during twilight or in full darkness. Concurrent land-based carcass searches by WEST detected 13 carcasses (not adjusted for searcher efficiency, carcass persistence, or carcasses that fell outside of search plots).

Eleven of the 15 collisions were not documented by the WT-Bird® color imagery; these collisions primarily occurred at night when the IR illuminators were operating. Similarly, among the eight collisions occurring when both color and thermal cameras were operational, seven detections included objects observed by the thermal cameras, including six documented collisions, but only three collisions were observed by the color cameras. Only one collision occurred during daylight, a bald eagle (*Haliaeetus leucocephalus*), and the color imagery clearly captured this collision with the blade tip (Figure 3). Of the 15 collisions, besides the eagle, the remaining 14 collisions were identified as bats based on observed carcasses, detected most strongly at the second sensor from the root at 16 m, with most collisions, based visual confirmation, occurring within the midspan.

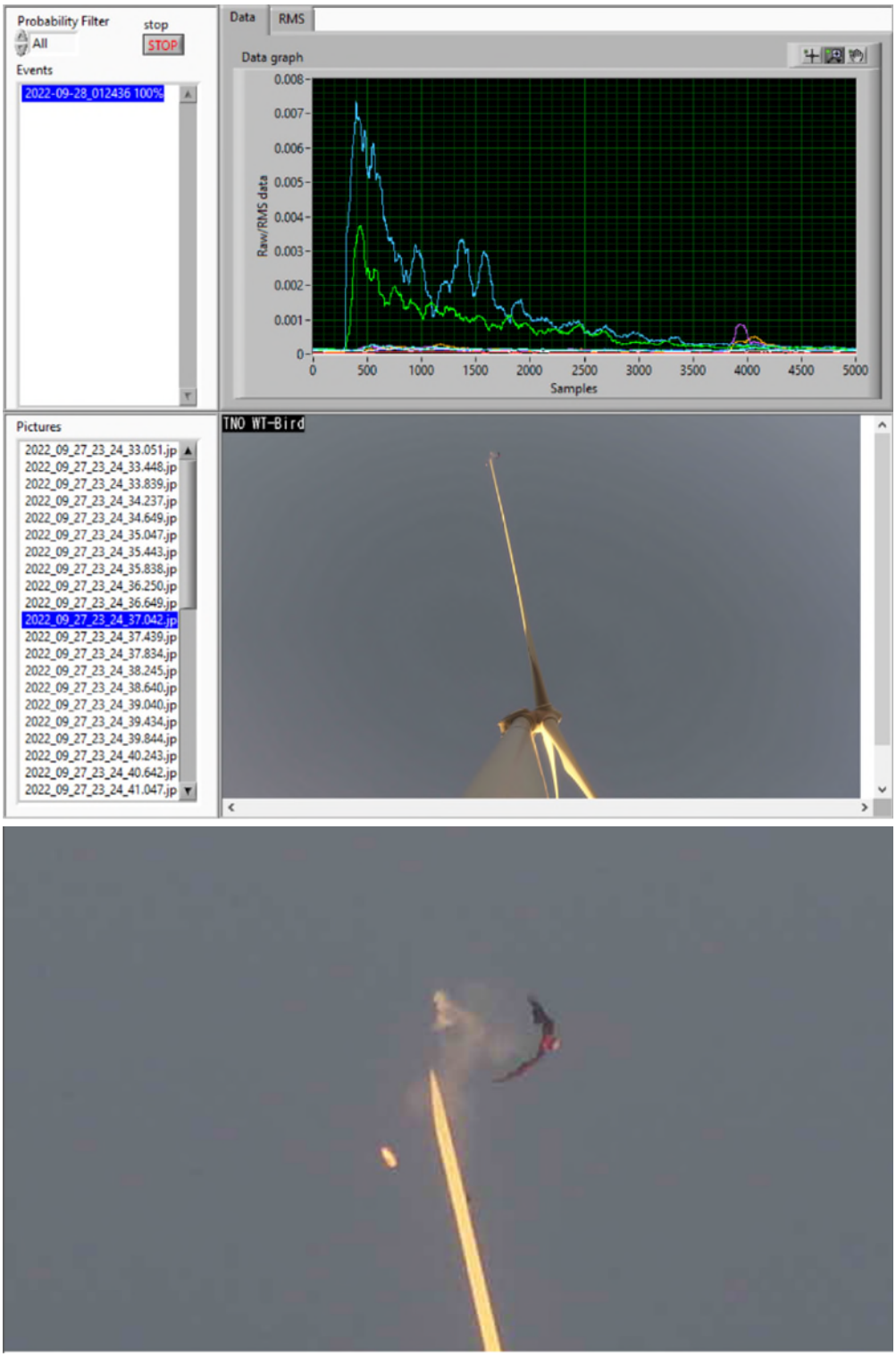


**Figure 3. WT-Bird® detected bald eagle collision on September 27, 2022, at the University of Minnesota Eolos Turbine in Dakota County, Minnesota, with imagery from the Sony true-color camera.**

Note: At the top is the output from collision and the view of the collision at the blade tip. At the bottom is an enlargement of the collision detailing the fatality's three parts.

**Table 1. Collisions detected by the WT-Bird® system, indicating turbine blade and primary sensor where collision was detected, and sources of imagery confirmation by image source during the 2022 evaluation period at the University of Minnesota Eolos Turbine in Rosemount, Minnesota.**

| Date | | | | Primary Visual Sensor | |
|---|---|---|---|---|---|
| | Time (UTC) | Light | Blade | Color | Thermal |
| 8/21/2022 | 08:29:35 | Night | 1 | 3 | no |
| 8/25/2022 | 05:59:31 | Night | 2 | 2 | yes |
| 8/25/2022 | 09:46:40 | Night | 3 | 2 | yes |
| 8/26/2022 | 01:39:28 | Dusk | 2 | 2 | no |
| 8/26/2022 | 08:45:20 | Night | 2 | 2 | no |
| 8/31/2022 | 05:36:55 | Night | 3 | 2 | no |
| 9/2/2022 | 01:20:53 | Dusk | 2 | 2 | no |
| 9/2/2022 | 02:04:58 | Dusk | 1 | 2 | yes |
| 9/11/2022 | 01:07:14 | Dusk | 2 | 2 | NA |
| 9/21/2022 | 07:23:28 | Night | 2 | 2 | no |
| 9/21/2022 | 17:42:07 | Day | 3 | 2 | NA |
| 9/23/2022 | 05:57:42 | Night | 3 | 2 | NA |
| 9/27/2022 | 23:24:36 | Day | 2 | 2 | NA |
| 10/6/2022 | 03:46:05 | Night | 3 | 2 | NA |
| 10/22/2022 | 03:47:40 | Night | 2 | 2 | no |

Note: All times are Coordinated Universal Time (UTC). “NA” indicates that thermal imagery was not available

* Reviewers disagreed on whether this detection could be classified as collision.

**Table 2. Detail on collisions detected by the WT-Bird® system and thermal video monitoring components by date and time during the 2022 evaluation period at the University of Minnesota Eolos Turbine in Rosemount, Minnesota.**

| | | | | Thermal Video – ID confidence | |
|---|---|---|---|---|---|
| Date | Time (UTC) | Size Class[a] | WT-Bird® vibration | High[b] | Medium[c] |
| 8/21/2022 | 8:29:35 | NA | yes | no | no |
| 8/25/2022 | 5:59:31 | bat | yes | yes | yes |
| 8/25/2022 | 9:46:43 | bat | yes | no | yes |
| 8/26/2022 | 1:39:28 | NA | yes | no | no |
| 8/26/2022 | 8:45:20 | NA | yes | no | no |
| 8/31/2022 | 5:36:55 | NA | yes | no | no |
| 9/2/2022 | 1:20:53 | NA | yes | no | no |
| 9/2/2022 | 2:04:58 | bird | yes | yes | yes |
| 9/11/2022 | 1:07:14 | NA | yes | NA | NA |
| 9/21/2022 | 7:23:28 | NA | yes | no | no |
| 9/21/2022 | 17:42:07 | NA | yes | NA | NA |
| 9/23/2022 | 5:57:42 | NA | yes | NA | NA |
| 9/27/2022 | 23:24:36 | bird | yes | NA | NA |
| 10/6/2022 | 3:46:05 | NA | yes | NA | NA |
| 10/22/2022 | 3:47:40 | NA | yes | no | no |

[a.] Size Class determination from expert review of thermal and true-color imagery. The “NA” values indicated instances when thermal video sensor data was not available for analysis.

[b.] High identification (ID) confidence: Two reviewers classified the event as a collision, and the object was classified by an expert as a bat or bird.

[c.] Medium ID confidence: One reviewer classified the video clip as a collision (and one disagreed), and the object was classified by an expert as a bat or bird.

Note: All times are Coordinated Universal Time (UTC).

## Fatality Rate Estimation

Given the limited availability of data from the video-monitoring system and limited sample size of video-based detections, this dataset was not appropriate for the planned double-observer methodology. Therefore, we present fatality estimates developed using the detection rates observed during 2021 at the Task 2 study at the NREL turbine (Stucker et al. 2022).

Using the lower and upper detection rates from the 2021 NREL study (0.65 and 0.75, respectively), multiplied by the proportion of vibration system uptime, and 15 total detections classified as collision by the WT-Bird system®, we calculated lower and upper overall detection probability estimates of 0.54 and 0.63 for the WT-Bird® system. Using these *assumed* detection probability estimates, the corresponding lower and upper adjusted fatality estimates are 23.89 and 27.57 for the study period (Table 3). In comparison, the post-construction mortality field study yielded a GenEst fatality estimate of 16.8 birds and bats (90% confidence interval [CI] = 9.88–27.92 birds and bats). Thus, the WT-Bird® program estimates are within the 90% CI of the field estimate but are higher than the mean (Appendix A [Stucker et al. 2024]).

**Table 3. Fatality rates per turbine derived from the WT-Bird® collision detection monitoring at the University of Minnesota Eolos Turbine in Rosemount, Minnesota, from August 18 – November 3, 2022.**

| Assumed Collision Detection Probability[a] | Uptime Proportion | Overall Detection Probability | Detected Collisions | Adjusted Fatality Estimate |
|---|---|---|---|---|
| 0.75 | 0.84 | 0.63 | 15 | 23.89 |
| 0.65 | 0.84 | 0.54 | 15 | 27.57 |

[a.] Detection probabilities from detection trials at the National Renewable Energy Laboratory (Stucker et al 2022).

## Results for Spring 2023 Edge Deployment and Post-processing

In the spring of 2023, the real-time edge monitoring system was deployed for 87 days, or approximately 2,088 hours of monitoring and 8,352 total video hours across the four thermal cameras. During that 87-day period, the system did not fail or require intervention. The distinct computer vision model was developed for the edge deployment to allow for faster data processing. Using the real-time computer vision model for edge processing at the turbine, 643 hours of video containing detected objects were saved which is a 92.3% reduction in data storage.

During deployment, a random sample of videos were retained where no image detections were made to evaluate if the edge monitoring systems missed objects. We reviewed a random selection of 100 videos retained and the edge detection system generated no false negatives nor missed detections of objects.

In testing, the post-processing turbine segmentation model had precision and recall of 0.98 and 1.00, respectively (where precision measures the proportion of predictions that were correct and recall measures the proportion of known true positives that the model correctly identified). Errors in precision are false positives, while errors in recall are false negatives. When a video was flagged for review, all IR videos available from the four cameras were merged into a mosaic for

review so that the reviewer could see the most complete view of the flying object's trajectory. The criteria used to filter videos were tested against known collision clips, all of which were flagged under this algorithm.

During the edge deployment, five fatalities were found during ground searches. We assumed that all collisions occurred between the previous search and the search on which the fatalities were found, which aligned with the estimated time of death of the fatalities, based on their physical condition. We ran the collision detection algorithm on all possible dates of collision events for the five fatalities, totaling 15 days. Out of the 34,928 videos, or 97.12 hours of footage collected across these days, we reviewed 4,482 videos, totaling 12.40 hours flagged by the algorithm as having a high likelihood of a collision, and found four out of the five known collisions based on observed 2023 carcasses. As simultaneous videos from different cameras were merged, the actual time to review this footage was less than 12.40 hours.

Four of the five ground fatalities were found in the thermal videos. In three of the four cases when a collision was found, only one camera's video was saved during deployment. In the fourth case, footage was saved from two cameras, but the collision was not visible from one of the camera angles. None of the collision events or the animals associated with the events could be seen in the accompanying color images.

## DISCUSSION

The goal of Task 4 was to 1) validate the comparability of a fatality estimate developed using data from the WT-Bird® collision detection system to a standard, land-based GenEst fatality estimate and 2) confirm whether the computer-vision system developed by WEST could serve as an independent second observer in a subsequent offshore trial (Task 5) while reducing the amount of video data retained. Each of these goals was achieved and substantial improvements were made to enable the operations to work independently.

### Does the WT-Bird® system provide comparable fatality estimates to standard, land-based GenEst fatality estimates?

Hundreds of post-construction monitoring studies have been completed on land in the U.S., most of which estimate the number of bird and bat collisions through standardized searches under turbines, within an area that is typically equal to the length of a turbine blade. The number of carcasses found are then adjusted for known biases that affect the number of carcasses detected, such as searcher efficiency, carcass persistence, and the number of carcasses that fell outside of the search area (Dalthorp et al. 2018). Monitoring for and estimating the number collisions of birds and bats offshore presents unique challenges, including the inability to regularly search areas where carcasses could fall using humans or dog teams. The ultimate goal of this project was to determine if improvements to the WT-Bird® system could be used to generate small bird and bat fatality estimates that were comparable to estimates collected using traditional methods employed at land-based wind turbines. Our results clearly show the system detected a similar

number of collisions to the number of bat and bird carcasses found during standardized carcass searches, and produced comparable bird and bat fatality estimates that occur within the confidence interval of a traditional land-based wind energy carcass survey and can be employed to answer questions regarding the rate of fatalities at offshore wind projects.

The WT-Bird® system was reliable, operated without interruption, and appeared to detect collisions at rates greater than those recorded by traditional ground-based monitoring, despite the need to place the third sensor within the turbine blade's box beam. Due to data losses on the video cameras, we were unable to identify the species or species groups for most collisions. This was a problem that can easily be solved in the future with regular back-ups of video data, and improved camera technologies that can detect birds and bats at greater distances.

Despite the issues with thermal camera data loss, the deployment of the WT-Bird® system benefited from the inclusion of thermal cameras. While the color imagery was helpful during the day, identifying objects from color cameras supported with illuminators during night was generally not possible. The thermal cameras are more robust in their ability to filter non-target objects from the analysis, but the reduced resolution introduces additional uncertainty.

During the 2022 trials, the WT-Bird® system was able to detect what were primarily bat collisions for most of the deployment. Furthermore, most of these objects, when observable in cameras, appeared to be colliding with the turbine blade within the mid-span, and not necessarily at the blade tip, where the collision would result in a greater vibration. While the second sensors at 16 m were triggered most frequently, the configuration of the blade prevented installation of the sensor on the leading edge. This may have resulted in the third sensor at 24 m not Triggering as much as expected.

The fatality point estimate derived from the WT-Bird® system was near the upper end of the 90% confidential interval surrounding the bat fatality estimate based on traditional land-based survey techniques. For management purposes, a system that provides a fatality estimate for offshore turbines within the typical confidence interval of an estimate calculated using modern land-based techniques will meet the primary objectives of most wildlife resource agencies, that is, how many bird and bat fatalities are occurring, and how do they compare to land-based fatality estimates. This also suggests that estimates calculated from the WT-Bird® may be slightly conservative (i.e. estimates are slightly higher than land-based estimates). There are possible explanations, including:

- 2021 NREL detection rates may have underestimated WT-Bird® detection rates for this turbine installation and study period
- Collision rate was not constant (e.g. seasonal) during period of sensor downtime
- Although unlikely based on observing zero false-positive vibrations classified as collisions during 2021 (Stucker et al 2022), there is a potential that a false positive "collision" could occur.

Our study was the first that we were aware to quantify detection bias any offshore collision monitoring system. Two decades of research and monitoring in the U.S. has focused on

accurately quantify and adjust for detection bias at land-based carcass studies in the U.S, and is considered essential for developing defensible fatality estimates (Dalthorp et al. 2018). Past work on this project has also shown how difficult it can be to empirically measure detection bias for offshore systems tested on land (Cite Task 2). While our estimate of detection bias for the WT-Bird® system is the first to attempt to quantify detection bias, it may have resulted in an underestimate of true detection rates.

A second factor that may have led to error in the WT-Bird® fatality estimate is the assumption that the collision rate was constant with respect to sensor uptime/downtime. We note some evidence that this assumption was violated in that fatalities tended to occur earlier in the study period, consistent with migration, whereas sensor downtime was generally uniform and later periods of downtime, which may have unnecessarily inflated fatality estimates. Correction factors for detection may need to be applied seasonally, as they often are with GenEst (Dahlthorp et al 2018).

A third possible explanation is the WT-Bird® system falsely detected vibrations as fatalities. During the 2021 trials at NREL, no false positive collisions were classified, and the false positive rate was determined to be zero (Stucker et al 2022). It is unlikely that this had a significant impact on the estimated fatality rate because the system detected 13 of the 15 carcasses that were found during land-based monitoring, and the system is designed to identify other sources of noise that could be misclassified as a collision.

**Can the computer-vision system developed by WEST serve as an independent second observer in a subsequent offshore trial (Task 5) while reducing the amount of video data retained?**

We estimated the detection rate of the WT-Bird system at the NREL testing facility. This was relatively labor intensive and expensive, and there may be need in the future to estimate the detection rates for the WT-Bird system in an offshore environment, as the system is applied to new turbines that may require differing spacing of sensors or numbers of vibration sensors. The use of a camera-based system could serve as a double observer, and be used to estimate detection rates offshore, which would allow future deployments of WT-Bird to not only report the number of collisions detected, but also generate fatality rates that account for detection bias, and are more defensible. Our ability to empirically test if our computer-vision system could serve as a second observer was hindered by a data loss incident. Only 20–30% of the vibration-based collisions had a corresponding video-based detection using the color cameras with illuminators. The machine-learning training results from thermal camera imagery indicated the computer vision algorithms successfully detected 72% of bats and over 90% of birds present in the footage, but that a smaller percentage of collisions were visible due to the limited field of view of the cameras. This is a relatively high detection rate when compared to standard post-construction monitoring (e.g. Stucker et al 2024), that suggests that a computer-vision system could be used in offshore setting to serve as a second observer. Collision detection rates for the computer vision system could be improved with an increased field of view by the additional use of cameras. It is important to consider that adding additional cameras may gain an increase of the rotor swept volume, but

the logistics associated with positioning and deploying multiple extra cameras, including ones at height, may result in a system that is too costly or logistically complex to implement.

For this study we were unable to utilize the proposed double-observer detection estimation approach due to limited fatalities within the observation period. However, in our subsequent simulation, the double-observer approach yielded accurate fatality estimates with as few as 20 collisions, although larger sample sizes yield greater precision. Further, it should be noted that this approach could be naturally extended to pooled data from multiple turbines within a facility, allowing more precise estimates of detection probability and temporal variability in fatality rates.

The 2023 real-time system was able to process four thermal video streams in real time with minimal system downtime and data loss. Only one instance of downtime occurred, due to heat-related hardware breakdown in the processing computer located inside the turbine. The implementation of real-time analysis on a liquid-cooled computer led to a 92.3% reduction in required data storage, not including the random sample for validation purposes of videos saved that had no object detections.

The post-deployment computer vision system significantly reduced the burden of post-deployment - review time by filtering out 87.17% of the saved videos. Furthermore, using the collision classification algorithm, we were able to locate four out of the five known collision events during deployment.

The one missed known collision in 2023 can be attributed to several potential causes. The bird, found during carcass searches, could have been missed by the real-time computer vision algorithm or the post-deployment algorithm. It is also likely that the missed collision occurred outside the field of view of the thermal camera. Although the system of four thermal cameras (2023) covers a larger field of view than the three thermal cameras (2022), they do not monitor the entirety of the RSZ.

In future deployments, we could implement several changes to the system to further improve the monitoring system and reduce the burden of review time, including:

1. Add the post-deployment computer vision model into the real-time system to reduce the necessity of data storage and post-processing labor.
2. Change the monitoring system to automatically save all camera videos when any of the videos have a potential collision detected to ensure more data when a collision is possible and more certainty in collision classification.
3. Use 3-dimensional triangulation to estimate the position and size of flying objects and exclude objects outside the RSZ that are very close to the camera and airplanes that are very far away.
4. Alter the tilt and/or positioning of the cameras to cover a greater portion of the RSZ with less overlap among the fields of view.
5. Increase the sample size of training data for each portion of the ML algorithms.

In an offshore setting, we would not have the ability to narrow our review based on presence of a carcass from a carcass search, as we did in 2023. In this case, the system would be most effective if it had a processing feature to flag all the videos where a collision was most likely each day and have those reviewed on a rolling basis. In this deployment, review time ranged from about one minute of video to 2.6 hours of video for a given day, but, with improvements to the system, that post-processing review burden could be reduced.

# REFERENCES

Cook, R. D. and J. O. Jacobson. 1979. A Design for Estimating Visibility Bias in Aerial Surveys. Biometrics 35(4): 735-742. doi: 10.2307/2530104.

Dalthorp, D. H., L. Madsen, M. M. Huso, P. Rabie, R. Wolpert, J. Studyvin, J. Simonis, and J. M. Mintz. 2018. GenEst Statistical Models—a Generalized Estimator of Mortality. US Geological Survey Techniques and Methods, Volume 7, Chapter A2. 13 pp. doi: 10.3133/tm7A2. Available online: https://pubs.usgs.gov/tm/7a2/tm7a2.pdf

Fletcher, R. J. and R. L. Hutto. 2006. Estimating Detection Probabilities of River Birds Using Double Surveys. Biological Sciences Faculty Publications 123(3): doi: 10.1642/0004-8038(2006)123 [695:EDPORB]2.0.CO;2.

Graham, A. and R. Bell. 1989. Investigating Observer Bias in Aerial Survey by Simultaneous Double-Counts. Journal of Wildlife Management 53(4): 1009-1016.

Kaandorp, F. 2022. WT-Bird Installation Report University of Minnesota. The Netherlands Organisation for Applied Scientific Research (TNO) R11392. Submitted to Western EcoSystems Technology, Inc. (WEST). 2023. 18 pp.

Kaandorp, F. 2023. Test results of TNO WT-Bird® trial at the University of Minnesota. The Netherlands Organisation for Applied Scientific Research (TNO) R10376. Submitted to Western EcoSystems Technology, Inc. (WEST). April 12, 2023. 33 pp.

Manly, B. F. J., L. L. McDonald, and G. W. Garner. 1996. Maximum Likelihood Estimation for the Double-Count Method with Independent Observers. Journal of Agricultural, Biological, and Environmental Statistics 1: 170-189.

Nichols, J. D., Hines, J. E., Sauer, J. R., Frederick W. Fallon, Fallon, J. E., & Heglund, P. J. (2000). A Double-Observer Approach for Estimating Detection Probability and Abundance from Point Counts. *The Auk*, *117*(2), 393–408.

Stucker, J., A. Suehring, N. O'Neil, and T. Prebyl. Western EcoSystems Technology, Inc. (WEST). 2024. Post-construction Fatality Monitoring Study, DOE Wind Project, Dakota County, Minnesota. June 24 – November 9, 2022. Prepared for Department of Energy, Office of Energy Efficiency and Renewable Energy Wind Energy Technology Office Advanced Wind R&D to Reduce Costs and Environmental Impact (DE-FOA-0001924) DE-EE0008734. Prepared by Western EcoSystems Technology, Inc. (WEST), Golden Valley, Minnesota. May 2023.

Stucker, J., J. Bushey, and R. Good. 2022. Milestone 2.3 Preliminary Report on Collision Testing of the WT-Bird® system. Prepared for the US Department of Energy. Prepared by Western EcoSystems Technology, Inc. (WEST), Golden Valley, Minnesota, with contributions from The Netherlands Organisation for Applied Scientific Research (TNO) and the National Renewable Energy Laboratory (NREL).April 28, 2022. pp 14.

Western EcoSystems Technology, Inc. (WEST). 2022. Milestone 4.2: Approved Study Plan for a Multi-Sensor Approach for Measuring Bird and Bat Collisions with Offshore Wind Turbines. US Department of Energy, Office of Energy Efficiency and Renewable Energy Wind Energy Technology Office Advanced Wind R&D to Reduce Costs and Environmental Impact (DE-FOA-0001924) DE-EE0008734. Finalized April 2022. 16 pp.

# Appendix A. A Multi-Sensor Approach for Measuring Bird and Bat Collisions with Offshore Wind Turbines, Supporting Task 4: Post-Construction Mortality Study, Dakota County, Minnesota, June – November 2022

# A Multi-Sensor Approach for Measuring Bird and Bat Collisions with Offshore Wind Turbines

# Supporting Task 4: Post-construction Mortality Study

# Dakota County, Minnesota

---

## June – November 2022

*University of Minnesota 2.5-megawatt Clipper Wind Turbine - Photo: Patrick O'Leary*

**Prepared for:**

**US Department of Energy**

Office of Energy Efficiency and Renewable Energy Wind Energy Technology Office Advanced Wind R&D to Reduce Costs and Environmental Impact (DE-FOA-0001924) DE-EE0008734.

---


**Prepared by:**

**Jennifer Stucker, Aaron Suehring, Nick O'Neil, and Simon Weller**

Western EcoSystems Technology, Inc.
7575 Golden Valley Road, Suite 300
Golden Valley, Minnesota 55427


**January 8, 2025**

WEST


*Confidential Business Information*

| | |
|---|---|
| **Federal Agency** | Department of Energy<br>Office of Energy Efficiency and Renewable Energy<br>Wind Energy Technology Office |
| **FOA Name and Number** | Advanced Wind R&D to Reduce Costs and Environmental Impact (DE-FOA-0001924) |
| **Report Type** | Milestone 4.3 *Preliminary Report on Validation Testing of the WT-Bird® system* |
| **Award Number** | DE-EE0008734 |
| **Award Type** | Cooperative Agreement |
| **Prime Recipient** | Rhett Good and Jennifer H. Stucker, PhD<br>Western EcoSystems Technology, Inc.<br>400 West 7th Street, Suite 200<br>Bloomington, Indiana 47404<br>rgood@west-inc.com<br>jstucker@west-inc.com<br>Phone: 812.339.1756 |
| **Prime Recipient Type** | Private Company |
| **Project Title** | A Multi-Sensor Approach for Measuring Bird and Bat Collisions with Offshore Wind Turbines |
| **DUNS Number** | 627824261 |
| **Date of Report** | January 8, 2025 |

## EXECUTIVE SUMMARY

Western EcoSystems Technology, Inc. (WEST), received funding from the US Department of Energy to develop and validate an effective multi-sensor system for quantifying bird and bat collision rates at offshore wind turbines. WEST partnered with The Netherlands Organisation for Applied Scientific Research (TNO) to test an improved version of TNO's existing collision monitoring system for offshore wind turbines known as WT-Bird® for detecting collisions of bats and small birds. The objective of the study was to compare how the WT-Bird® system performed against a traditional ground-based post-construction mortality survey. The study was completed at the University of Minnesota, which owns and operates a single 2.5-megawatt (MW) Clipper Liberty turbine (80-meter [m] hub height and 96-m rotor diameter).

Standardized carcass searches were conducted to systematically search the ground beneath the turbine between June 24 – November 9, 2022. Searches were conducted on a 120-m radius circular plot centered on the turbine and cleared by regular mowing. Searcher efficiency and carcass persistence were also measured through bias trials. Eight bird carcasses composed of three identifiable bird species were documented as fatalities during the study. Fifteen bat carcasses composed of four identifiable bat species were documented as fatalities during the study. One bald eagle was documented during surveys. Three of the bird carcasses included in analysis were observed in the summer (June 24 – August 17) and five carcasses were observed in the fall (August 18 – November 9). Seven bat carcasses included in the analysis were observed in the summer and eight carcasses were observed in the fall.

The WT-Bird® system operated between August 18 – November 3, 2022. The estimated fatality rate during this period using GenEst, a generalized estimator of fatality, was 8.68 birds and bats (90% confidence interval [CI] 5.65–13.33) per MW, 2.44 birds (90% CI 1.73–3.02) per MW, and 6.27 bats (90% CI 3.47–10.55) per MW. Four feather spots were found that were suspected to have perished due to reasons other than colliding with a wind turbine. The estimated fatality rate during this period, after removing feather spots from the GenEst analysis was 6.75 (90% CI 3.95–11.17) birds and bats per MW.

## REPORT PARTICIPANTS

| | |
|---|---|
| Jennifer Stucker, Ph.D. | Project Manager |
| Rhett Good | Report Reviewer |
| Thomas Prebyl | Lead Client Analyst |
| Simon Weller | Data Analyst |
| Aaron Suehring | Field Coordinator and Writer |
| Molly Tuma | Field Biologist |
| Hayley Ellingsen | Field Biologist |
| Nick O'Neil | Report Compiler, Field Biologist |
| Christine Kuykendall | Technical Editor |

## REPORT REFERENCE

Stucker, J., A. Suehring, N. O'Neil, and S. Weller. 2025. A Multi-Sensor Approach for Measuring Bird and Bat Collisions with Offshore Wind Turbines, Supporting Task 4: Post-construction Mortality Study, Dakota County, Minnesota. June – November 2022. Prepared for the US Department of Energy, Office of Energy Efficiency and Renewable Energy Wind Energy Technology Office Advanced Wind R&D to Reduce Costs and Environmental Impact (DE-FOA-0001924) DE-EE0008734. Prepared by Western EcoSystems Technology, Inc. (WEST), Golden Valley, Minnesota. January 8, 2025.

## TABLE OF CONTENTS

## LIST OF TABLES



## LIST OF FIGURES

## LIST OF APPENDICES

# ACRONYMS AND ABBREVIATIONS

| | |
|---|---|
| AICc | corrected Akaike Information Criterion |
| carcass search | standardized carcass search |
| CI | confidence interval |
| cm | centimeter |
| CPT | carcass persistence trial |
| g | gram |
| GenEst | generalized estimator of fatality |
| *k* | detection reduction factor |
| m | meter |
| MET | meteorological tower |
| MNDNR | Minnesota Department of Natural Resources |
| MW | megawatt |
| plot | search area |
| Project | University of Minnesota Eolos Turbine at the Rosemount Research Station, Dakota County, Minnesota |
| QA/QC | quality assurance and quality control |
| SEEF | searcher efficiency |
| SGCN | Species of Greatest Conservation Need |
| TNO | The Netherlands Organisation for Applied Scientific Research |
| USFWS | US Fish and Wildlife Service |
| WEST | Western EcoSystems Technology, Inc. |

## INTRODUCTION

Western EcoSystems Technology, Inc. (WEST), received a grant from the US Department of Energy to develop and validate an effective multi-sensor system for quantifying bird and bat collision rates at offshore wind turbines. WEST partnered with The Netherlands Organisation for Applied Scientific Research (TNO) to test an improved version of TNO's existing collision monitoring system for offshore wind turbines known as WT-Bird®. The WT-Bird® system was modified during earlier phases of this project to improve the system's ability to detect collisions of bats and small birds. The objective of the study was to calculate bird and bat fatality rates using standard techniques typically employed at other land-based wind facilities, for comparison to fatalities recorded by the WT-Bird® system (Stucker et al. 2024).

## LOCATION

The University of Minnesota, through the Eolos Wind Research Consortium, operates a 2.5-megawatt (MW) Clipper Liberty turbine for research to benefit the wind industry. The Eolos wind turbine (80-meter [m] hub height and 96-m rotor diameter) and meteorological tower (MET; 130-m; the Project) are located in Rosemount, Minnesota, at the University's Rosemount Research Station (Figure 1, Appendix A). This turbine was chosen because of its status as a research turbine, and its proximity—five kilometers—to the Mississippi River. It is a larger-scale turbine than the 1.5 MW turbine used in prior collision testing at National Renewable Labs (Stucker et al. 2022), and it offered a flexible and internet wired facility for validation and refining operations.

## METHODS

The study consisted of three primary components: 1) standardized carcass searches (carcass searches), 2) searcher efficiency (SEEF) trials to estimate the probability that searchers found a carcass, and 3) carcass persistence trials (CPTs) to estimate the average length of time that a carcass remained in the field for possible detection. Additionally, an area adjustment was calculated to account for carcasses that fell outside of the search area (plot). The methods for these components and associated analysis are described below, and included in Appendix A.

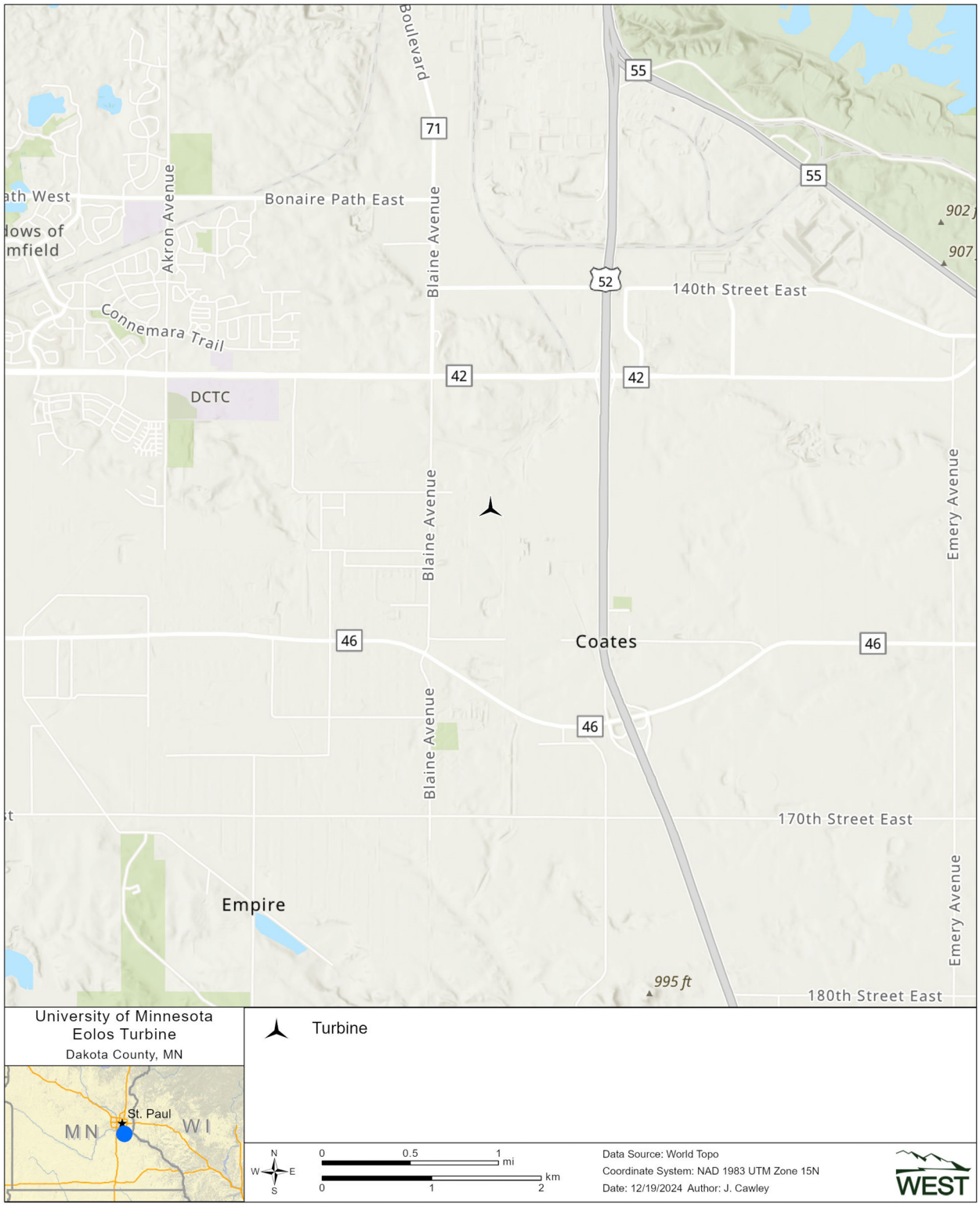


**Figure 1. Location of the University of Minnesota Eolos Turbine at the Rosemount Research Station, Dakota County, Minnesota.**

## Definitions

WEST classified bird sizes by body length and wingspan: large birds (length greater than 26 centimeters [cm], wingspan greater than 70 cm, and greater than 100 grams [g] weight); medium birds (length between 16 and 26 cm, wingspan between 20 and 70 cm, and a weight between 20 and 100 g); small birds (length between nine and 16 cm, wingspan less than 20 cm, and a weight less than 20 g); and bats (length between eight and 14 cm, wingspan between 24 and 45 cm and a weight between seven and 15 g). Species of concern were defined as species afforded protection under the Endangered Species Act (1973) and Bald and Golden Eagle Protection Act (1940), or state-listed as endangered, threatened, or species of Special Concern (Minnesota Administrative Rules Chapter 6134). Additionally, species identified by the state as Species of Greatest Conservation Need (SGCN; Minnesota Department of Natural Resources [MNDNR] 2015) were included as species of concern for the Project.

### *Standardized Carcass Searches*

Carcass searches consisted of personnel, trained in proper search techniques, visually searching for bird and bat carcasses while walking transects between June 24 – November 9, 2022. A clearance search was conducted prior to the start of the study, and any carcasses found during this search were excluded from analyses. Searches were conducted across two seasons: summer (June 24 – August 17) and fall (August 18 – November 9).

### *Search Areas and Search Frequency*

#### Search Area

The search area consisted of a 120-m radius circle plot centered on the turbine (Figure 2; Appendix A). The cleared plot was regularly mowed to keep vegetation height below 30 cm, providing relatively uniform searching conditions for the duration of the study. The plot contained some areas dominated by shrub and tree cover, which were not searched. These areas were delineated prior to starting the study. Cropped areas were searched following late summer grain harvest in the southern portion of the plot. Changes in the searched area were documented by the searcher.

#### Search Frequency

Searches were conducted approximately three times per week from June 24 – November 9, 2022, totaling 60 visits during the study period.

## Field Surveys

Searchers walked transects six m apart at a pace of approximately 45–60 m per minute looking for carcasses. While walking transects, searchers would scan both sides out to three m for fatalities within the plot. All areas within the plot were searched. To the extent possible, searches were rotated throughout the day so that plots were surveyed during all daylight periods (i.e., morning, midday, and afternoon).


**Figure 2. Schematic illustrating the cleared plot search area of the University of Minnesota Eolos Turbine at the Rosemount Research Station, Dakota County, Minnesota.**

Note: The cleared search plot was 120-meter radius circle centered on the search turbine.

All bird and bat carcasses found were recorded, photographed, mapped, and cause of death determined, when possible. Data recorded for all carcasses included:

- an identification code
- species, sex, age, and reproductive condition (when possible)
- date and time recorded
- Universal Transverse Mercator location
- measured distance from turbine
- azimuth from turbine
- estimated time of death
- condition:
    - intact – a carcass that was completely intact, was not badly decomposed, and showed no sign of being fed upon by a predator or scavenger
    - scavenged – an entire carcass that showed signs of scavenging or was heavily infested by insects, or portion(s) of a carcass in one location (e.g., wings)
    - dismembered – a carcass with missing limbs
    - feather spot – 10 or more feathers (or two or more primary feathers) at one location that indicated predation or scavenging
    - injured – a live bird or bat harmed, damaged, or impaired in some way
- any comments that indicated possible cause of death
- photograph of carcass as found
- location of carcass plotted on map
- primary ground cover

Bird carcasses that were found within the plot were photographed, left in place, and marked with spray paint to avoid double counting fatality events. Bat carcasses were collected under MNDNR Scientific Research – Salvage Permit (permit number 19024, held by WEST), placed in a plastic bag, and stored temporarily in a freezer on site. A freezer tag with a unique carcass identification number, turbine number, and date was maintained with the bat carcasses at all times. Staff wore leather and nitrile gloves when handling bat carcasses to minimizes the risk of injury or transmission of zoonotic disease to biologists. Any injured birds or bats were recorded and treated as a fatality but were left in place in the field.

Carcasses found outside of the plot or within a plot but not during scheduled searches, were also recorded following the above protocol. Carcasses found outside of plot were not included in the fatality estimates. Carcasses found within the plot but not during a scheduled search were included in the analysis under the assumption these carcasses would have been found during the next scheduled search. If any species of concern were found during carcass searches, they were recorded and immediately reported to the MNDNR or US Fish and Wildlife Service (USFWS).

*Searcher Efficiency Trials*

The objective of SEEF trials was to estimate the probability that an available bird or bat carcass was found by searchers. SEEF trials commenced with the start of carcass searches and were

conducted throughout the study period (i.e., year), eight trials in summer and seven trials in fall, in the same plot as carcass searches. SEEF trials were stratified by the size of carcass (large bird, medium bird, small bird, and bat). Estimates of SEEF were used to adjust the number of carcasses found for those missed by searchers, thereby accounting for detection bias. Searchers conducting carcass searches were unaware of when SEEF trials were being conducted or the locations where the trial carcasses were placed within the plot.

In total, 82 carcasses (11 large birds, 17 medium birds, 26 small birds, and 28 bats; Appendix B) were placed in plots for SEEF trials. Carcasses used in SEEF trials were primarily native birds, rock pigeons (*Columba livia*), and coturnix quail (*Coturnix coturnix*; used under USFWS Scientific Collecting Permit MB154929 to the University of Minnesota).

All SEEF trial carcasses were placed at random locations within the plot prior to that day's scheduled search. Each trial carcass was discreetly marked (e.g., zip tie on the leg of the carcass) prior to placement so that it could be identified as a trial carcass. Trial carcasses were dropped from waist-height or higher and allowed to land in a random posture. To avoid attracting scavengers, no more than four carcasses were placed in the plot during any SEEF trial. The location of trial carcasses found during the subsequent carcass search were recorded. The number of carcasses available for detection during each trial was determined immediately following the trial by the bias trial administrator.

*Carcass Persistence Trials*

The objective of CPTs was to estimate the average probability that a bird or bat carcass remained available to be found (i.e., were not removed by scavengers or through deterioration by other natural processes) during the search interval. CPTs were conducted throughout the study period to incorporate the effects of varying weather conditions and scavenger densities. Estimates of bird and bat carcass persistence were used to adjust the number of carcasses found, correcting for removal bias.

CPTs began when carcass search studies began. A total of 32 carcasses were placed within the plot throughout the duration of the study for CPT (eight large birds, eight medium birds, eight small birds, and eight bats; Appendix B). Bird and bat carcasses consisted of the same species as the SEEF trial species. Carcasses were placed on six dates throughout the study period to incorporate the effects of varying weather, climatic conditions, and scavenger densities.

All CPT carcasses were placed at random locations within the plot. Carcasses were dropped from waist-height or higher and allowed to land in a random posture. Global Positioning System coordinates marked each trial carcass so multiple personnel could track carcasses as needed.

Personnel conducting carcass searches monitored the trial birds and bats over a 30-day period according to the following schedule as closely as possible. Carcasses were placed and checked concurrently with the searches for the following schedule: days 1, 2, 4, 7, 9, 11, 14, 16, 18, 21, 23, 25, 28 and 30. This schedule varied depending on weather and coordination with the other

survey work. Carcasses were left at the location until the end of the CPT. At the end of the 30-day period, any evidence of the carcasses that remained was removed

## Data Management

### *Quality Assurance and Quality Control*

Quality assurance and quality control (QA/QC) measures were implemented at all stages of the study, including in the field, during data entry and analysis, and report writing. All WEST field staff were trained in proper survey techniques, and all data collected were recorded on a tablet data form. Following field surveys, searchers were responsible for inspecting data forms for completeness, accuracy, and legibility. If errors or anomalies were found, follow-up measures were implemented including discussions and review of field data with searchers and/or Project Managers.

### *Data Compilation and Storage*

WEST field staff were trained in proper data entry procedures. System controls were implemented to ensure correct data were entered; however, if any errors, omissions, or problems were identified in later stages of analysis, they were traced back to the raw tablet data entry where appropriate changes and measures were implemented. Data were incorporated into a Microsoft SQL Server database and were QA/QC'd throughout the course of the study. Statisticians provided an additional level of QA/QC to ensure proper protocols were followed and data collected were congruent with the objectives of the study.

## Statistical Analysis

### *Fatality Rate Estimation*

Carcasses included in the fatality rate estimation were found within the plot and had an estimated time of death within the study period. Fatality estimates were calculated for all categories (all birds, large birds, medium birds, small birds, and bats) using GenEst (a generalized estimator of fatality; Dalthorp et al. 2018, Simonis et al. 2018). Carcass searches were conducted from June 24 – November 9, 2022; however, the WT-Bird® system was operational from August 18 – November 3, 2022. Unless otherwise stated, this report (with Appendices C-D), focuses on data collected from the fall season (August 18 – November 3, 2022) when the WT-Bird® system was operational GenEst results for the entire study period are included in Appendices E–I. To obtain an overall estimate of fatality, each carcass included in the analysis was adjusted for SEEF, carcass persistence, a detection reduction factor (also referred to as "k"; see below), and a search area adjustment. Estimates and confidence intervals (CIs) were calculated using a parametric bootstrap (Dalthorp et al. 2018) for each individual category listed above, if five or more fatalities were detected. CIs were not calculated when the observed number of carcasses in a class was less than five because CIs from Horvitz-Thompson estimators can be unreliable when carcass counts are low (Korner-Nievergelt et al. 2011). A second GenEst analysis was performed, removing large bird feather spots found south of the turbine, near a MET tower guy wire, from the analysis. These feather spots may have been attributed to the collisions with the guy wire or with scent detection training conducted by other researchers in the area. As such, two analyses are

presented in the results section and additional details for the analysis without feather spots are included in Appendix I.

*Searcher Efficiency Estimation*

Data collected during SEEF trials were used to estimate the probability searchers detected bird and bat carcasses. Estimates of SEEF were used to adjust carcass counts for detection bias. SEEF estimated the probability of a searcher detecting a carcass given the carcass was available to be found. Estimates were obtained for each size class using a logit regression model (Dalthorp et al. 2018). Season was used as a potential explanatory variable (covariate) for the logit regression models. Models were selected using an information-theoretic approach known as AICc, or corrected Akaike Information Criterion (Burnham and Anderson 2002); models with lower AICc values are considered to have a better fit. The best model was selected as the most parsimonious model (the model with the fewest variables) within two AICc units of the model with the lowest AICc value was selected as the best model.

*Carcass Persistence Estimation*

Data collected during CPT were used to estimate the amount of time, in days, that carcasses remained available to be located by the searcher. Estimates of carcass persistence were used to adjust carcass counts for removal bias. The carcass persistence adjustment estimated the average probability a carcass persisted through the search interval (i.e., the time between scheduled searches). The persistence of a carcass was modeled using an interval-censored survival regression for each size class using exponential, loglogistic, lognormal, and Weibull distributions (Dalthorp et al. 2018, Kalbfleisch and Prentice 2002). Season was used as a potential covariate. The covariate was fit to each parameter of the distributions. The most parsimonious model within two AICc units of the model with the lowest AICc value was selected as the best model.

*Detection Reduction Factor*

The change in SEEF between successive searches was defined by a parameter called the detection reduction factor ($k$) that ranged from zero to one. When $k$ is zero it implies that a carcass is missed on the first search and that carcass would never be found. A $k$ of one implies SEEF remained constant no matter how many times a carcass is missed. The detection reduction factor was a required parameter for GenEst; however, data were not collected to estimate $k$. A value for $k$ of 0.67 has been estimated for bats (Huso et al. 2017) and this value was assumed in this study for birds and bats.

*Search Area Adjustment Estimate*

The search area adjustment accounted for unsearched areas beneath turbines and was calculated as a probability that ranged from zero to one. For example, an area adjustment of 0.75 meant that an estimated 75% of carcasses fell within the plot. Areas could be unsearchable due to shrub and tree cover, or there could be areas where carcasses fell outside the plot (e.g., a carcass landed 130 m from the turbine). The area adjustment was estimated as the product of the unsearched area around each turbine and a carcass-density distribution. The carcass-density

distribution predicts the likelihood that a carcass fell a given distance from the turbine base. Separate area adjustments were estimated for large birds, small birds, and bats.

A number of analysis methods exist to calculate the search area adjustment. The method employed was determined by the number of carcasses found during surveys. For this study, there were an insufficient number of large bird, small bird, or bat carcasses (one, five, and 14, respectively) found during searches, therefore the truncated weighted maximum likelihood method could not be used. Consequently, we used the Hull and Muir (2013) approach to calculate the maximum fall distance of large birds, small birds, and bats carcasses. The Hull and Muir (2013) approach uses a physics-based model for a given turbine height and rotor diameter to estimate the relative carcass-density distribution following a linear decrease from the turbine base out to the maximum predicted fall distance (Huso and Dalthorp 2014).

# RESULTS

A list of species found as fatalities within the Project during the study period can be found in Appendix B, and details of all carcasses found during the study period are presented in Appendix C. The number, species, location, and other characteristics of the bird and bat carcasses found during the study and included in the GenEst analysis, as well as the GenEst fatality estimates, are discussed below.

### Standardized Carcass Searches

Overall, 60 carcass searches were conducted from June 24 – November 9, 2022; a carcass clearing search preceded the first carcass search by one week. The average search interval was 2.37 days throughout the duration of the study. Over the course of the study, eight bird carcasses and 15 bat carcasses were found within the Project; however, only five bird carcasses and eight bat carcasses were included in the fatality estimate (Table 1; Appendix B-C).

Bird Carcasses

Four identifiable bird species were discovered during the study. Five bird fatalities were included in the analysis (Table 1; Appendices C and D). One bald eagle was found during carcass searches; however, no additional bird species of concern were found during the study. Four rock pigeon feather spots were removed from the second analysis because the cause of death was undetermined, and could have been a result of collisions with the guy wires from a nearby MET, or predation.

Five of the bird carcasses were found during the fall and the remaining three were found during the summer (Figure 3). The number of bird carcasses per turbine was highest on September 28, 2022, when two birds were found during a search (Figure 3). Due to the limited number of bird carcasses, spatial trends of bird carcasses were limited; however, all four rock pigeon feather spots found at the Project were southwest of the turbine, approximately 220 degrees, and between 80 m and 120 m from the turbine.

**Table 1. Number and percent (%) of carcasses by species included and excluded from analysis at the University of Minnesota Eolos Turbine at the Rosemount Research Station, Dakota County, Minnesota, from June 24 – November 9, 2022.**

| | Included in Fatality Estimate | | Found before WT-Bird® System was Active* | | Total | |
|---|---|---|---|---|---|---|
| **Species** | **Total** | **%** | **Total** | **%** | **Total** | **%** |
| **Bird** | | | | | | |
| rock pigeon** | 4 | 80.0 | 0 | 0 | 4 | 50.0 |
| bald eagle | 1 | 20.0 | 0 | 0 | 1 | 12.5 |
| horned lark | 0 | 0 | 1 | 33.3 | 1 | 12.5 |
| unidentified small bird | 0 | 0 | 1 | 33.3 | 1 | 12.5 |
| unidentified large bird | 0 | 0 | 1 | 33.3 | 1 | 12.5 |
| **Overall Birds** | **5** | **100** | **3** | **100** | **8** | **100** |
| **Bat** | | | | | | |
| hoary bat | 3 | 37.5 | 4 | 57.1 | 7 | 46.67 |
| silver-haired bat | 3 | 37.5 | 2 | 28.6 | 5 | 33.33 |
| eastern red bat | 2 | 25.0 | 0 | 0 | 2 | 13.33 |
| big brown bat | 0 | 0 | 1 | 14.3 | 1 | 6.67 |
| **Overall Bats** | **8** | **100** | **7** | **100** | **15** | **100** |

* Carcasses not included in analysis, found before August 18, 2022.

** Carcasses found as feather spots removed from second analysis.

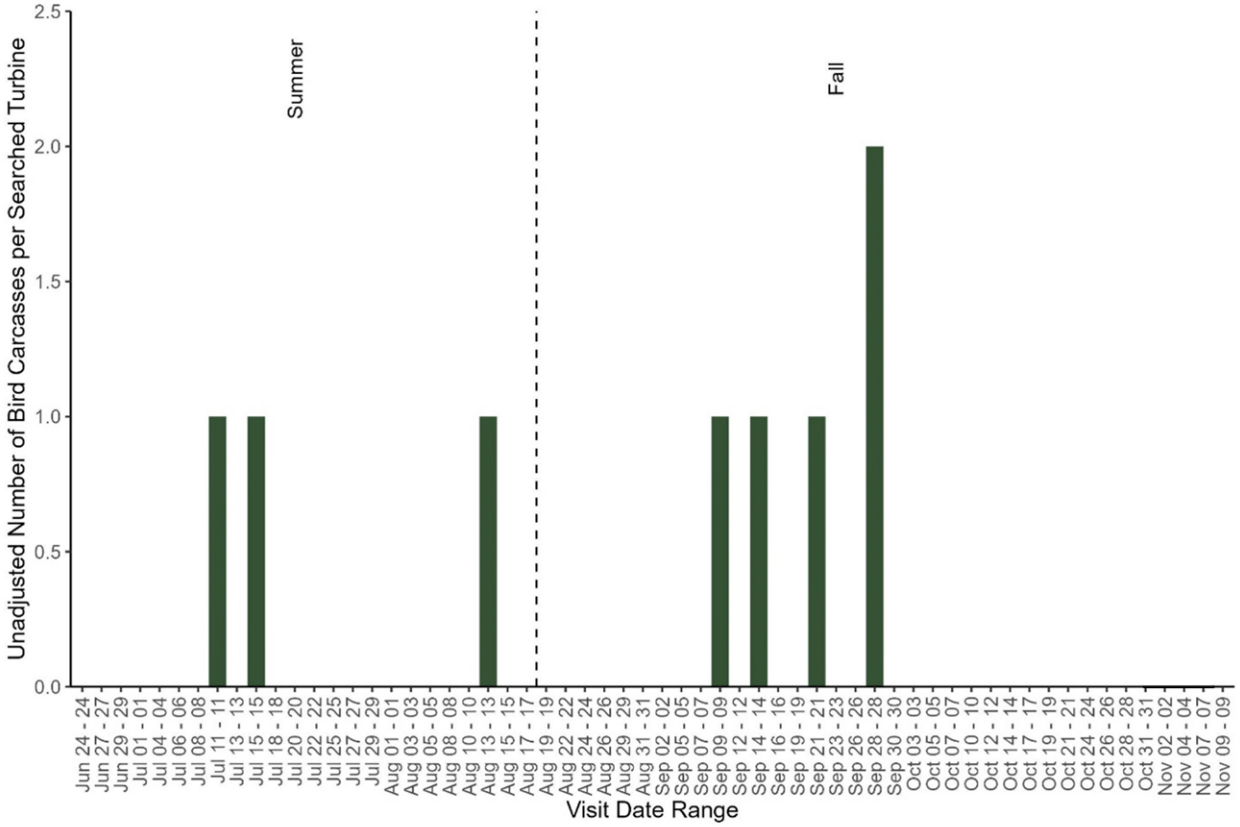


**Figure 3. Temporal distribution of bird carcasses found during scheduled searches at the University of Minnesota Eolos Turbine at the Rosemount Research Station, Dakota County, Minnesota from June 24 – November 9, 2022.**

Note: Searches were conducted three times per week in summer and fall.

Bat Carcasses

Four identifiable bat species were documented as fatalities, and eight fatalities were included in the analysis (Table 1; Appendices C and D). No bat species of concern were found. Big brown bat (*Eptesicus fuscus*), hoary bat (*Lasiurus cinereus*), and silver-haired bat (*Lasionycteris noctivagans*) species are designated as a Minnesota SGCN (MNDNR 2015).

The distribution of bat carcasses was split between the summer (seven carcasses) and fall (eight carcasses; Figure 4). The number of bat carcasses per turbine was highest on September 2, 2022, when four bat fatalities were found (Figure 4; Appendix D). There was no obvious spatial trend in bat carcasses found at the Project.

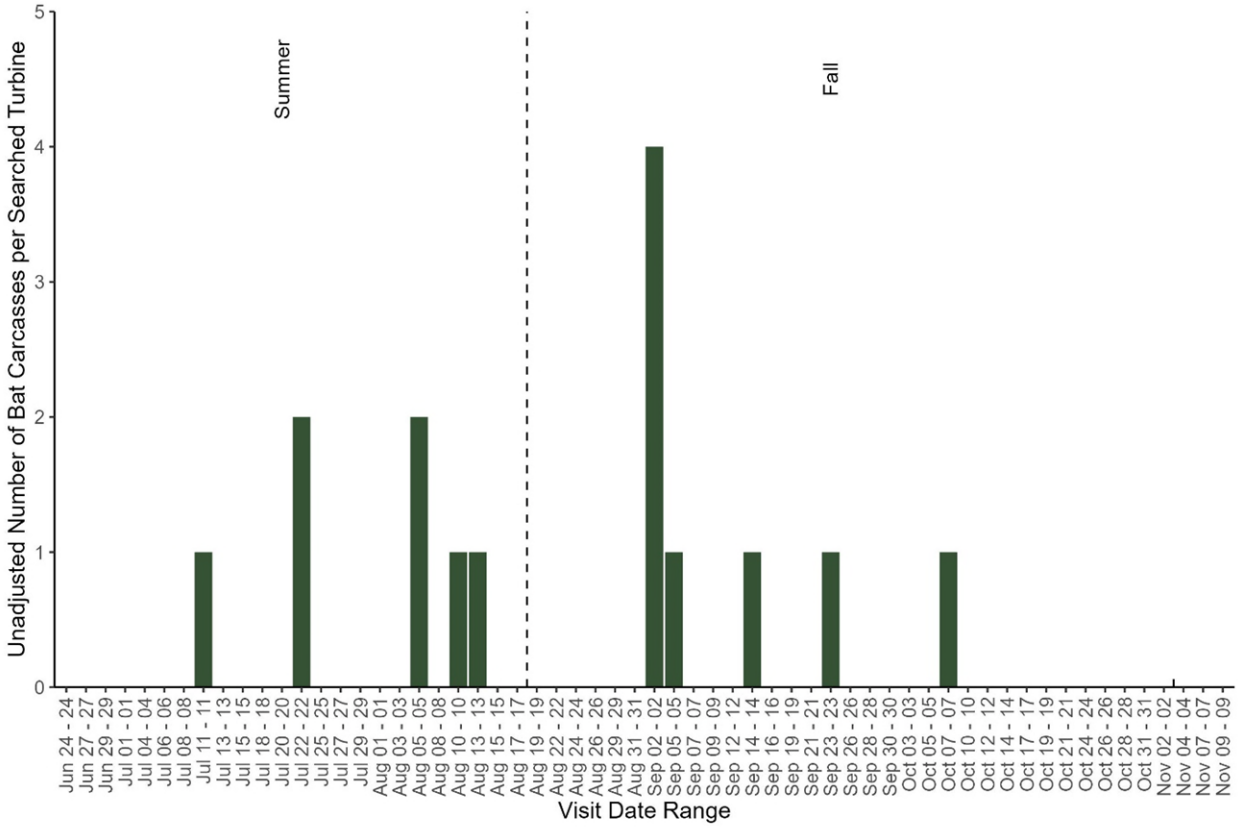


**Figure 4. Temporal distribution of bat carcasses found during scheduled searches at the University of Minnesota Eolos Turbine at the Rosemount Research Station, Dakota County, Minnesota, from June 24 – November 9, 2022.**

Note: Searches were three times per week in summer and fall.

## Searcher Efficiency

Overall, 82 carcasses composed of 11 large birds, 17 medium birds, 26 small birds, and 28 bats were placed for SEEF trials at the Project (Appendix D). Of these, 78 remained available for the searcher to find during scheduled searches (11 large birds, 17 medium birds, 23 small birds, and 27 bats). For large birds, 10 of the 11 carcasses were found for medium birds, 13 of the

17 carcasses were found, for small birds nine of the 23 carcasses were found, and for bats, 11 of the 27 carcasses were found (Table 2).

**Table 2. Searcher efficiency results for cleared search area at the University of Minnesota Eolos Turbine at the Rosemount Research Station, Dakota County, Minnesota, from June 24 – November 9, 2022, as a function of carcass size.**

| Size Class | # Placed | # Available | # Found | % Found |
|---|---|---|---|---|
| Large Bird | 11 | 11 | 10 | 90.91 |
| Medium Bird | 17 | 17 | 13 | 76.47 |
| Small Bird | 26 | 23 | 9 | 39.13 |
| Bat | 28 | 27 | 11 | 40.74 |

Models were fit for each size class to determine whether a seasonal covariate or an intercept-only model provided the best model for estimating SEEF based on corrected AICc values. Analysis of the study data for the Project resulted in the selection of the simplest intercept-only model for all size classes SEEF (Appendix E). As such, SEEF trials that occurred before WT-Bird® was active were included in the analysis for the estimate when WT-Bird® was active. Estimated annual SEEF rates were 0.91 (90% CI: 0.64–0.98) for large birds, 0.76 (90% CI: 0.56–0.89) for medium birds, 0.39 (90% CI: 0.24–0.56) for small birds, and 0.41 (90% CI: 0.27–0.57) for bats (Table 3).

### Carcass Persistence Rates

Thirty-two carcasses were placed at search plots throughout the duration of the study for CPTs (eight large birds, eight medium birds, eight small birds, and eight bats). The estimated percentages of carcasses remaining were generally similar to those seen at other Minnesota studies (Stucker et al. 2021a, 2021b).

For large birds, medium birds, small birds, and bats, an intercept-only exponential model was identified as the best model of carcass persistence, meaning there were not any significant differences between seasons for carcass persistence (Appendix F). Similarly to the SEEF data, CPT data for the entire study period were included in the analysis. The best-fitting model for each size class estimated that by day 2.37 (the search interval) approximately 97% of large bird, 84% of medium bird, 78% of small bird, and 87% of bat carcasses remained (Table 3, Figure 5). The median removal time was 26.4 days for large birds, 4.5 days for medium birds, 3.2 days for small birds, and 5.7 days for bats.

**Table 3. Estimated adjustment factors by season with 90% confidence intervals (CIs) during post-construction fatality monitoring at the University of Minnesota Eolos Turbine at the Rosemount Research Station, Dakota County, Minnesota, from June 24 – November 9, 2022, as a function of carcass size.**

| | Summer | | Fall | |
|---|---|---|---|---|
| | 1 turbine searched | | 1 turbine searched | |
| | Estimate | 90% CI | Estimate | 90% CI |
| **Searcher Efficiency** | | | | |
| Large Bird | 0.91 | 0.64–0.98 | 0.91 | 0.64–0.98 |
| Raptor | 0.91 | 0.64–0.98 | 0.91 | 0.64–0.98 |
| Medium Bird | 0.76 | 0.56–0.89 | 0.76 | 0.56–0.89 |
| Small Bird | 0.39 | 0.24–0.56 | 0.39 | 0.24–0.56 |

**Table 3. Estimated adjustment factors by season with 90% confidence intervals (CIs) during post-construction fatality monitoring at the University of Minnesota Eolos Turbine at the Rosemount Research Station, Dakota County, Minnesota, from June 24 – November 9, 2022, as a function of carcass size.**

| | Summer | | Fall | |
|---|---|---|---|---|
| | 1 turbine searched | | 1 turbine searched | |
| | Estimate | 90% CI | Estimate | 90% CI |
| Bat | 0.41 | 0.27–0.57 | 0.41 | 0.27–0.57 |
| **Average Probability of a Carcass Persisting Through the Search Interval*** | | | | |
| Large Bird | 0.97 | 0.93–0.99 | 0.97 | 0.93–0.99 |
| Raptor | 0.97 | 0.93–0.99 | 0.97 | 0.93–0.99 |
| Medium Bird | 0.84 | 0.73–0.90 | 0.84 | 0.72–0.91 |
| Small Bird | 0.78 | 0.65–0.87 | 0.78 | 0.66–0.87 |
| Bat | 0.87 | 0.78–0.93 | 0.87 | 0.77–0.93 |
| **Search Area Adjustment** | | | | |
| Large Bird | 0.85 | 0.85–0.85 | 0.89 | 0.89–0.89 |
| Raptor | 0.84 | 0.84–0.84 | 0.87 | 0.87–0.87 |
| Medium Bird | 0.95 | 0.95–0.95 | 0.95 | 0.95–0.95 |
| Small Bird | 0.95 | 0.95–0.95 | 0.95 | 0.95–0.95 |
| Bat | 0.98 | 0.98–0.98 | 0.98 | 0.98–0.98 |

* The search interval was 2.37 days.

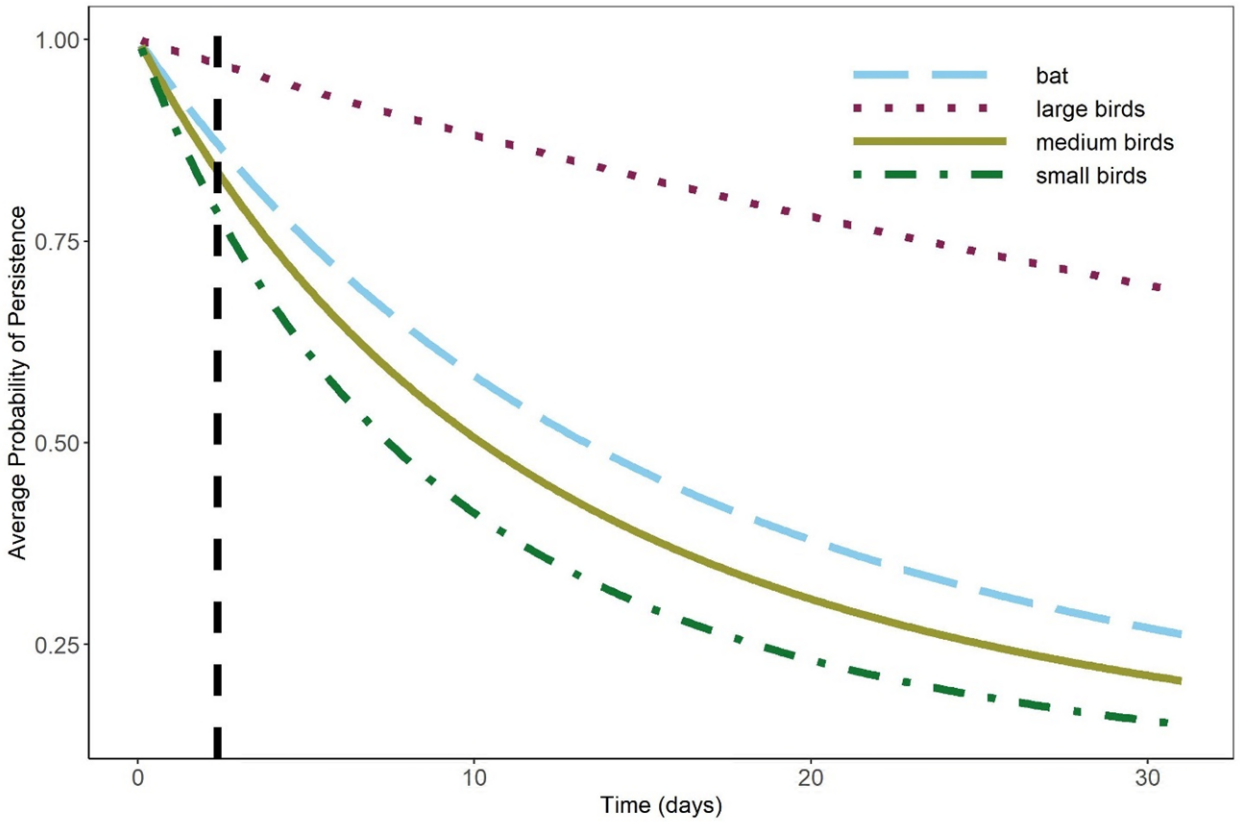


**Figure 5. Carcass persistence rates* for bat, large bird, medium bird, and small bird carcasses at the University of Minnesota Eolos Turbine at the Rosemount Research Station, Dakota County, Minnesota, from June 24 – November 9, 2022.**

Note: Vertical line indicates the 2.37-day search interval.

* Carcass persistence trials were conducted for a 30-day period for large birds, small birds, and bats.

### Search Area Adjustment

Searchable area within the search plot was expanded on August 18, 2022, following crop harvest to the south of the turbine, increasing the area adjustment for all size classes except medium and small birds (Table 3). For the purpose of this analysis, the larger plot size area adjustment was used as it encompassed the WT-Bird® period (fall). The modeled fall distances indicate approximately 85% of large bird carcasses, 95% of medium bird carcasses, and small bird carcasses, and 98% of bat carcasses fell within the plot (Table 3, Figure 6; Appendix G). The Hull and Muir (2013) method does not have a medium bird category, for this study the small bird distribution is also used for medium birds.

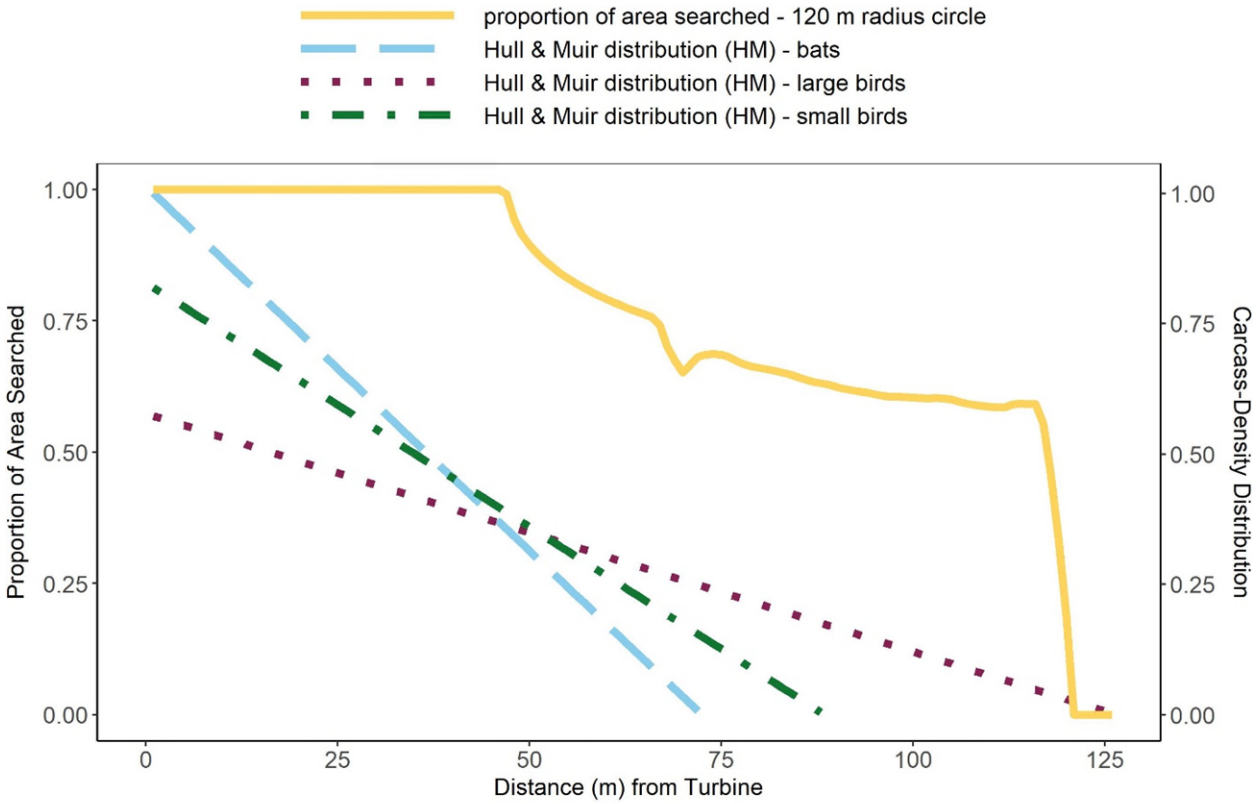


**Figure 6. Estimated bat, large bird, and small bird carcass-density distribution during the fall season for a proportion of area searched (yellow line) by distance from turbine using Hull and Muir (2013) model.**

Note: carcass-density distribution during the summer season is included in Appendix G.

### Adjusted Fatality Estimates

Adjusted fatality estimates and 90% CIs were calculated on a per-turbine and per-MW basis for all birds, large birds, medium birds, small birds, and bats using GenEst during the WT-Bird®

period (fall; Table 4). Fatality estimates were calculated based on search area adjustments, carcass persistence, and SEEF, which were used to calculate the probability an available carcass is detected (Appendix H). The average probability that a large bird or raptor carcass remained in the plot and was found by searchers was 0.95 for the Project (Appendix H). The average probability that a medium bird carcass remained in the plot and was found by searchers was 0.75 for the Project (Appendix H). The average probability a small bird carcass remained in the plot and was found by searchers was 0.44 for the Project (Appendix H). The average probability of a bat carcass remained in the plot and was found by searchers was 0.54 for the Project (Appendix H).

*Birds*

The estimated all bird fatality rate was 6.10 (90% CI: 4.33–7.55) bird fatalities/turbine and 2.44 (90% CI: 5.65–13.33) bird fatalities/MW during the fall season (Table 4). Only large bird carcasses were found during the fall, so the all bird fall fatality estimate is equal to the large bird fatality estimate. No GenEst estimate is available for small birds and medium birds because no carcasses of these size classes were found during the fall. Removing feather spots from the analysis adjusts the estimated all bird fatality rate to 1.41 (no CI; fewer than five fatalities) bird fatalities/turbine and 0.56 (no CI; fewer than five fatalities) bird fatalities/MW during the fall season (Appendix I).

*Bats*

The estimated bat fatality rate was 15.67 (90% CI: 8.68–26.36) bat fatalities/turbine and 6.27 (90% CI: 3.47–10.55) bat fatalities/MW during the fall season (Table 4).

*All Birds and Bats*

The estimated all bird and bat fatality rate was 21.70 (90% CI: 14.12–33.33) fatalities/turbine and 8.68 (90% CI: 5.65–13.33) fatalities/MW during the fall season (Table 4). When feather spots were removed from the analysis the estimated all bird and bat fatality rate was 16.88 (90% CI: 9.88–27.92) fatalities/turbine and 6.75 (90% CI: 3.95–11.17) fatalities/MW during the fall season (Appendix I).

**Table 4. Fatality rates per megawatt and per turbine at the University of Minnesota Eolos Turbine in Rosemount, Minnesota, from August 18 – November 3, 2022.**

| | Per Megawatt Estimates | | Per Turbine Estimates | |
|---|---|---|---|---|
| **Size Class** | **Estimate** | **90% CI*** | **Estimate** | **90% CI*** |
| All Bird and Bat | 8.68 | 5.65–13.33 | 21.70 | 14.12–33.33 |
| All Bird | 2.44 | 1.73–3.02 | 6.10 | 4.33–7.55 |
| Large Bird | 2.44 | 1.73–3.02 | 6.10 | 4.33–7.55 |
| Medium Bird | 0 | n/a* | 0 | n/a* |
| Small Bird | 0 | n/a* | 0 | n/a* |
| Bat | 6.27 | 3.47–10.55 | 15.67 | 8.68–26.36 |

* Confidence interval (CI) not calculated because the observed carcass count was less than five.

# REFERENCES

Bald and Golden Eagle Protection Act. 1940. 16 United States Code Sections (§§) 668-668d. Bald Eagle Protection Act of 1940, June 8, 1940, Chapter 278, § 2, 54 Statute (Stat.) 250; Expanded to include the related species of the golden eagle October 24, 1962, Public Law (PL) 87-884, 76 Stat. 1246. [As amended June 8, 1940, chapter (ch.) 278, §§ 1-5, 54 Stat. 250-251; PL 86-70, § 14, June 25, 1959, 73 Stat. 143; PL 87-884, October 24, 1962, 76 Stat. 1246; PL 90–578, title IV, § 402(b)(2), October 17, 1968, 82 Stat. 1118; PL 92–535, § 1-4, October 23, 1972, 86 Stat. 1064-1065; PL 95-616, § 9, November 8, 1979, 92 Stat. 3114; PL 101–650, title III, § 321, December 1, 1990, 104 Stat. 5117.].

Burnham, K. P. and D. R. Anderson. 2002. Model Selection and Multimodel Inference: A Practical Information-Theoretic Approach. Second Edition. Springer, New York, New York.

Dalthorp, D. H., L. Madsen, M. M. Huso, P. Rabie, R. Wolpert, J. Studyvin, J. Simonis, and J. M. Mintz. 2018. GenEst Statistical Models—a Generalized Estimator of Mortality. US Geological Survey Techniques and Methods, Volume 7, Chapter A2. 13 pp. doi: 10.3133/tm7A2. Available online: https://pubs.usgs.gov/tm/7a2/tm7a2.pdf

Endangered Species Act. 1973. 16 United States Code Sections (§§) 1531-1544. [As amended by Public Law (PL) 93-205, §2, December 28, 1973, 87 Statute (Stat.) 884; PL 96-159, §1, December 28, 1979, 93 Stat. 1225; PL 97-304, §9(a), October 13, 1982, 96 Stat. 1426; PL. 100-478, title I, §1013(a), October 7, 1988, 102 Stat. 2315.].

Esri. 2023, 2024. World Imagery and Aerial Photos (World Topo). ArcGIS Resource Center. Environmental Systems Research Institute (Esri), producers of ArcGIS software, Redlands, California. Accessed February 2023 and December 2024. Available online: https://www.arcgis.com/home/webmap/viewer.html?useExisting=1&layers=10df2279f9684e4a9f6a7f08febac2a9

Hull, C. L. and S. C. Muir. 2013. Behavior and Turbine Avoidance Rates of Eagles at Two Wind Farms in Tasmania, Australia. Wildlife Society Bulletin 37(1): 49-58. doi: 10.1002/wsb.254.

Huso, M., D. Dalthorp, and F. Korner-Nievergelt. 2017. Statistical Principles of Post-Construction Fatality Monitoring Design. Pp. *In*: M. Perrow, ed. Wildlife and Wind Farms, Conflicts and Solutions. Pelagic Publishing, Exeter, United Kingdom. Vol. 2, Onshore: Monitoring and Mitigation.

Huso, M. M. P. and D. Dalthorp. 2014. Accounting for Unsearched Areas in Estimating Wind Turbine-Caused Fatality. Journal of Wildlife Management 78(2): 347-358. doi: 10.1002/jwmg.663.

Kalbfleisch, J. D. and R. L. Prentice. 2002. The Statistical Analysis of Failure Time Data. John Wiley & Sons, Hoboken, New Jersey.

Korner-Nievergelt, F., P. Korner-Nievergelt, O. Behr, I. Niermann, R. Brinkmann, and B. Hellriegel. 2011. A New Method to Determine Bird and Bat Fatality at Wind Energy Turbines from Carcass Searches. Wildlife Biology 17: 350-363. doi: 10.2981/10-121.

Minnesota Administrative Rules Chapter 6134. Chapter 6134 - Endangered, Threatened and Special Concern Species; Parts 6134.0100 - 6134.0400. [Minnesota Statutes Section 84.0895; 8 SR 1921; L 1986 Chapter 386 Article 4 Section 9]. Available online: https://www.revisor.mn.gov/rules/?id=6134

Minnesota Department of Natural Resources (MNDNR). 2015. Minnesota's Wildlife Action Plan: 2015-2025. Division of Ecological and Water Resources, MDNR, Saint Paul, Minnesota. Available online: http://files.dnr.state.mn.us/assistance/nrplanning/bigpicture/mnwap/wildlife-action-plan-2015-2025.pdf

Simonis, J., D. H. Dalthorp, M. M. Huso, J. M. Mintz, L. Madsen, P. Rabie, and J. Studyvin. 2018. GenEst User Guide—Software for a Generalized Estimator of Mortality. US Geological Survey Techniques and Methods, Volume 7, Chapter C19, 72 pp. doi: 10.3133/tm7C19. Available online: https://pubs.usgs.gov/tm/7c19/tm7c19.pdf

Stucker, J., A. Suehring, and J. Bushey. 2021a. Post-Construction Bird and Bat Fatality Monitoring Study, Lake Benton II Wind Farm, Pipestone County, Minnesota. Final: March - November 2020. Prepared for Northern States Power, Minneapolis, Minnesota. Prepared by Western EcoSystems Technology, Inc. (WEST), Golden Valley, Minnesota. February 2021. 44 pp. + appendices.

Stucker, J., A. Suehring, and R. Clark. 2021b. Post-Construction Bird and Bat Fatality Monitoring Study. Blazing Star Wind Farm, Lincoln County, Minnesota. Final: March - November 2020. Prepared for Northern States Power, Minneapolis, Minnesota. Prepared by Western EcoSystems Technology, Inc. (WEST), Golden Valley, Minnesota. January 28, 2021.

Stucker, J, J. Bushey, and R. Good. 2022. Milestone. 2.3 Preliminary Report on Collision Testing of the WT-Bird® system for A Multi-Sensor Approach for Measuring Bird and Bat Collisions with Offshore Wind Turbines Report. Prepared for the US Department of Energy, Office of Energy Efficiency and Renewable Energy Wind Energy Technology Office Advanced Wind R&D to Reduce Costs and Environmental Impact (DE-FOA-0001924) DE-EE0008734. Prepared by Western EcoSystems Technology, Inc. (WEST), Golden Valley, Minnesota. April 2022. 14 pp.

Stucker, J., R. Knoedler, and T. Prebyl. 2024. A Multi-Sensor Approach for Measuring Bird and Bat Collisions with Offshore Wind Turbines. Task 4: Land-based validation trial results Minnesota June 2022 – November 2022. Prepared for the US Department of Energy, Office of Energy Efficiency and Renewable Energy Wind Energy Technology Office Advanced Wind R&D to Reduce Costs and Environmental Impact (DE-FOA-0001924) DE-EE0008734. Prepared by Western EcoSystems Technology, Inc. (WEST), Golden Valley, Minnesota. December 2024.

# Appendix A. Overview of Study Design and Search Methods for Post-construction Fatality Monitoring at the University of Minnesota Eolos Turbine at the Rosemount Research Station, Dakota County, Minnesota, from June 24 – November 9, 2022

**Appendix A. Overview of study design and search methods for post-construction fatality monitoring at the University of Minnesota Eolos Turbine in Rosemount, Minnesota, from June 24 – November 9, 2022.**

| Design Component | Sampling Unit |
|---|---|
| Plot Type | Cleared Plot |
| Number of Plots (% of all turbines) | 1 (100%) |
| Turbines Searched | T1 |
| Size/Shape | 120-m radius circle plot centered on the search turbine |
| Search Interval | 3x per week |
| Dog-assisted (Yes/No) | No |
| Search Period | June 24 – November 9, 2022 |
| Searcher efficiency – seasons | Summer, Fall |
| Searcher efficiency – carcass sizes | bat, small bird, medium bird, large bird |
| Carcass persistence trials – seasons | Summer, Fall |
| Carcass persistence trials – carcass sizes | bat, small bird, medium bird, large bird |
| **Turbine Specifications** | |
| Turbine Model | 2.5-MW Clipper Liberty (1 turbine) |
| Hub Height | 80 m |
| Rotor Diameter | 96 m |
| Curtailment | Unknown |
| Blade serrations (Yes/No) | No |

m = meters; MW = megawatt.

# Appendix B. Common and Scientific Names of Species Found during Fatality Monitoring at University of Minnesota Eolos Turbine at the Rosemount Research Station, Dakota County, Minnesota, from June 24 – November 9, 2022

**Appendix C. Species found during fatality searches at the University of Minnesota Eolos Turbine in Rosemount, Minnesota, from June 24 – November 9, 2022.**

| Common Name | Scientific Name |
|---|---|
| **Birds** | |
| bald eagle | *Haliaeetus leucocephalus* |
| horned lark | *Eremophila alpestris* |
| rock pigeon | *Columba livia* |
| **Bats** | |
| big brown bat | *Eptesicus fuscus* |
| eastern red bat | *Lasiurus borealis* |
| hoary bat | *Lasiurus cinereus* |
| silver-haired bat | *Lasionycteris noctivagans* |

# Appendix C. Bird and Bat Fatalities found at University of Minnesota Eolos Turbine at the Rosemount Research Station, Dakota County, Minnesota, from June 24 – November 9, 2022

**Appendix C. Complete listing of carcasses found at the University of Minnesota Eolos Turbine at the Rosemount Research Station, Dakota County, Minnesota, from June 24 – November 9, 2022.**

| Found Date | Common Name | Turbine | Search Type | Physical Condition |
|---|---|---|---|---|
| 07/11/2022 | hoary bat | 1 | carcass search | intact |
| 07/21/2022 | big brown bat | 1 | incidental | intact |
| 07/21/2022 | silver-haired bat | 1 | incidental | intact |
| 08/05/2022 | hoary bat | 1 | carcass search | scavenged |
| 08/05/2022 | hoary bat | 1 | carcass search | scavenged |
| 08/10/2022 | silver-haired bat | 1 | carcass search | scavenged |
| 08/13/2022 | hoary bat | 1 | carcass search | intact |
| 09/02/2022 | eastern red bat | 1 | carcass search | intact |
| 09/02/2022 | eastern red bat | 1 | carcass search | intact |
| 09/02/2022 | hoary bat | 1 | carcass search | dismembered |
| 09/02/2022 | silver-haired bat | 1 | carcass search | intact |
| 09/05/2022 | hoary bat | 1 | carcass search | intact |
| 09/14/2022 | silver-haired bat | 1 | carcass search | intact |
| 09/23/2022 | silver-haired bat | 1 | carcass search | injured |
| 10/07/2022 | hoary bat | 1 | carcass search | dismembered |
| 07/11/2022 | unidentified small bird | 1 | carcass search | scavenged |
| 07/15/2022 | unidentified large bird | 1 | carcass search | feather spot |
| 08/13/2022 | horned lark | 1 | carcass search | scavenged |
| 09/09/2022 | rock pigeon* | 1 | carcass search | feather spot |
| 09/14/2022 | rock pigeon* | 1 | carcass search | feather spot |
| 09/21/2022 | rock pigeon* | 1 | carcass search | feather spot |
| 09/28/2022 | bald eagle | 1 | carcass search | dismembered |
| 09/28/2022 | rock pigeon* | 1 | carcass search | feather spot |

# Appendix D. Carcass Persistence Trial and Searcher Efficiency Trial Information at the University of Minnesota Eolos Turbine at the Rosemount Research Station, Dakota County, Minnesota from June 24 – November 9, 2022

**Appendix D1. All carcasses placed for carcass persistence trials, by date, season, species, and turbine, at the University of Minnesota Eolos Turbine in Rosemount, Minnesota, from June 24 – November 9, 2022.**

| Date Placed | Season | Species | Scientific Name | Before Removal* | After Removal** |
|---|---|---|---|---|---|
| 08/01/2022 | summer | big brown bat | *Eptesicus fuscus* | 08/01/2022 | 08/02/2022 |
| 08/01/2022 | summer | brown creeper | *Certhia americana* | 08/01/2022 | 08/02/2022 |
| 08/01/2022 | summer | eastern red bat | *Lasiurus borealis* | 08/04/2022 | 08/08/2022 |
| 08/01/2022 | summer | horned lark | *Eremophila alpestris* | 08/09/2022 | 08/15/2022 |
| 08/01/2022 | summer | mallard | *Anas platyrhynchos* | 08/30/2022 | 08/30/2022 |
| 08/01/2022 | summer | mallard | *Anas platyrhynchos* | 08/13/2022 | 08/15/2022 |
| 08/15/2022 | summer | barn swallow | *Hirundo rustica* | 08/26/2022 | 08/29/2022 |
| 08/15/2022 | summer | hoary bat | *Lasiurus cinereus* | 08/15/2022 | 08/16/2022 |
| 08/15/2022 | summer | hoary bat | *Lasiurus cinereus* | 08/16/2022 | 08/19/2022 |
| 08/15/2022 | summer | horned lark | *Eremophila alpestris* | 08/17/2022 | 08/19/2022 |
| 08/15/2022 | summer | mallard | *Anas platyrhynchos* | 09/13/2022 | 09/13/2022 |
| 08/15/2022 | summer | sedge wren | *Cistothorus stellaris* | 08/19/2022 | 08/21/2022 |
| 08/29/2022 | summer | European starling | *Sturnus vulgaris* | 08/29/2022 | 08/31/2022 |
| 08/29/2022 | summer | European starling | *Sturnus vulgaris* | 08/31/2022 | 09/02/2022 |
| 08/29/2022 | summer | hoary bat | *Lasiurus cinereus* | 09/05/2022 | 09/07/2022 |
| 08/29/2022 | summer | mallard | *Anas platyrhynchos* | 09/28/2022 | 09/28/2022 |
| 08/29/2022 | summer | mourning dove | *Zenaida macroura* | 09/02/2022 | 09/05/2022 |
| 09/05/2022 | summer | coturnix quail | *Coturnix coturnix* | 09/29/2022 | 10/03/2022 |
| 09/05/2022 | summer | hoary bat | *Lasiurus cinereus* | 09/12/2022 | 09/13/2022 |
| 09/05/2022 | summer | Nashville warbler | *Leiothlypis ruficapilla* | 09/07/2022 | 09/09/2022 |
| 09/05/2022 | summer | ruby-crowned kinglet | *Corthylio calendula* | 09/05/2022 | 09/07/2022 |
| 09/05/2022 | summer | silver-haired bat | *Lasionycteris noctivagans* | 09/05/2022 | 09/05/2022 |
| 09/12/2022 | fall | coturnix quail | *Coturnix coturnix* | 09/22/2022 | 09/26/2022 |
| 09/12/2022 | fall | coturnix quail | *Coturnix coturnix* | 10/12/2022 | 10/12/2022 |
| 09/12/2022 | fall | eastern red bat | *Lasiurus borealis* | 10/12/2022 | 10/12/2022 |
| 09/12/2022 | fall | red-eyed vireo | *Vireo olivaceus* | 09/19/2022 | 09/21/2022 |
| 09/12/2022 | fall | ruby-crowned kinglet | *Corthylio calendula* | 09/14/2022 | 09/16/2022 |
| 09/19/2022 | fall | coturnix quail | *Coturnix coturnix* | 09/19/2022 | 09/19/2022 |
| 09/19/2022 | fall | coturnix quail | *Coturnix coturnix* | 09/19/2022 | 09/20/2022 |
| 09/19/2022 | fall | coturnix quail | *Coturnix coturnix* | 09/23/2022 | 09/26/2022 |
| 09/19/2022 | fall | horned lark | *Eremophila alpestris* | 09/19/2022 | 09/19/2022 |
| 09/19/2022 | fall | red-eyed vireo | *Vireo olivaceus* | 09/20/2022 | 09/22/2022 |

* Last date checked before removal.

** Date checked after removal.

**Appendix D2. All carcasses placed for searcher efficiency trials, by date, season, species, size class, and turbine, at the University of Minnesota Eolos Turbine in Rosemount, Minnesota, from June 24 – November 9, 2022.**

| Date Placed | Season | Species | Scientific Name | Size Class |
|---|---|---|---|---|
| 7/8/2022 | summer | blue jay | *Cyanocitta cristata* | medium bird |
| 7/8/2022 | summer | silver-haired bat | *Lasionycteris noctivagans* | bat |
| 7/8/2022 | summer | northern flicker | *Colaptes auratus* | large bird |
| 7/8/2022 | summer | silver-haired bat | *Lasionycteris noctivagans* | bat |
| 7/28/2022 | summer | unidentified wren | – | small bird |
| 7/28/2022 | summer | cliff swallow | *Petrochelidon pyrrhonota* | medium bird |
| 7/28/2022 | summer | cliff swallow | *Petrochelidon pyrrhonota* | medium bird |
| 7/28/2022 | summer | red-eyed vireo | *Vireo olivaceus* | small bird |
| 7/28/2022 | summer | silver-haired bat | *Lasionycteris noctivagans* | bat |

**Appendix D2. All carcasses placed for searcher efficiency trials, by date, season, species, size class, and turbine, at the University of Minnesota Eolos Turbine in Rosemount, Minnesota, from June 24 – November 9, 2022.**

| Date Placed | Season | Species | Scientific Name | Size Class |
|---|---|---|---|---|
| 8/4/2022 | summer | silver-haired bat | *Lasionycteris noctivagans* | bat |
| 8/4/2022 | summer | silver-haired bat | *Lasionycteris noctivagans* | bat |
| 8/4/2022 | summer | yellow warbler | *Setophaga petechia* | small bird |
| 8/4/2022 | summer | red-eyed vireo | *Vireo olivaceus* | small bird |
| 8/4/2022 | summer | horned lark | *Eremophila alpestris* | medium bird |
| 8/4/2022 | summer | red-eyed vireo | *Vireo olivaceus* | small bird |
| 8/10/2022 | summer | red-eyed vireo | *Vireo olivaceus* | small bird |
| 8/10/2022 | summer | silver-haired bat | *Lasionycteris noctivagans* | bat |
| 8/10/2022 | summer | mallard | *Anas platyrhynchos* | large bird |
| 8/10/2022 | summer | silver-haired bat | *Lasionycteris noctivagans* | bat |
| 8/10/2022 | summer | silver-haired bat | *Lasionycteris noctivagans* | bat |
| 8/10/2022 | summer | horned lark | *Eremophila alpestris* | medium bird |
| 8/17/2022 | summer | silver-haired bat | *Lasionycteris noctivagans* | bat |
| 8/17/2022 | summer | silver-haired bat | *Lasionycteris noctivagans* | bat |
| 8/17/2022 | summer | silver-haired bat | *Lasionycteris noctivagans* | bat |
| 8/17/2022 | summer | red-eyed vireo | *Vireo olivaceus* | small bird |
| 8/17/2022 | summer | tree swallow | *Tachycineta bicolor* | medium bird |
| 8/17/2022 | summer | rock pigeon | *Columba livia* | large bird |
| 8/25/2022 | summer | hoary bat | *Lasiurus cinereus* | bat |
| 8/25/2022 | summer | hoary bat | *Lasiurus cinereus* | bat |
| 8/25/2022 | summer | white-throated sparrow | *Zonotrichia albicollis* | medium bird |
| 8/25/2022 | summer | European starling | *Sturnus vulgaris* | medium bird |
| 8/25/2022 | summer | gray catbird | *Dumetella carolinensis* | large bird |
| 8/25/2022 | summer | rock pigeon | *Columba livia* | large bird |
| 9/2/2022 | summer | rock pigeon | *Columba livia* | large bird |
| 9/2/2022 | summer | white-throated sparrow | *Zonotrichia albicollis* | medium bird |
| 9/2/2022 | summer | coturnix quail | *Coturnix coturnix* | large bird |
| 9/2/2022 | summer | red-eyed vireo | *Vireo olivaceus* | small bird |
| 9/2/2022 | summer | eastern red bat | *Lasiurus borealis* | bat |
| 9/2/2022 | summer | hoary bat | *Lasiurus cinereus* | bat |
| 9/9/2022 | fall | golden-crowned kinglet | *Regulus satrapa* | small bird |
| 9/9/2022 | fall | eastern red bat | *Lasiurus borealis* | bat |
| 9/9/2022 | fall | cliff swallow | *Petrochelidon pyrrhonota* | medium bird |
| 9/9/2022 | fall | horned lark | *Eremophila alpestris* | medium bird |
| 9/9/2022 | fall | coturnix quail | *Coturnix coturnix* | large bird |
| 9/9/2022 | fall | eastern red bat | *Lasiurus borealis* | bat |
| 9/28/2022 | fall | red-eyed vireo | *Vireo olivaceus* | small bird |
| 9/28/2022 | fall | house wren | *Troglodytes aedon* | small bird |
| 9/28/2022 | fall | coturnix quail | *Coturnix coturnix* | medium bird |
| 9/28/2022 | fall | house wren | *Troglodytes aedon* | small bird |
| 9/28/2022 | fall | killdeer | *Charadrius vociferus* | small bird |
| 9/28/2022 | fall | grasshopper sparrow | *Ammodramus savannarum* | small bird |
| 9/30/2022 | fall | coturnix quail | *Coturnix coturnix* | medium bird |
| 9/30/2022 | fall | hoary bat | *Lasiurus cinereus* | bat |
| 9/30/2022 | fall | hoary bat | *Lasiurus cinereus* | bat |
| 9/30/2022 | fall | marsh wren | *Cistothorus palustris* | small bird |
| 9/30/2022 | fall | eastern red bat | *Lasiurus borealis* | bat |
| 9/30/2022 | fall | sedge wren | *Cistothorus stellaris* | small bird |
| 9/30/2022 | fall | coturnix quail | *Coturnix coturnix* | large bird |
| 10/5/2022 | fall | unidentified warbler | – | small bird |
| 10/5/2022 | fall | unidentified sparrow | – | small bird |

**Appendix D2. All carcasses placed for searcher efficiency trials, by date, season, species, size class, and turbine, at the University of Minnesota Eolos Turbine in Rosemount, Minnesota, from June 24 – November 9, 2022.**

| Date Placed | Season | Species | Scientific Name | Size Class |
|---|---|---|---|---|
| 10/5/2022 | fall | hoary bat | *Lasiurus cinereus* | bat |
| 10/5/2022 | fall | horned lark | *Eremophila alpestris* | medium bird |
| 10/5/2022 | fall | hoary bat | *Lasiurus cinereus* | bat |
| 10/7/2022 | fall | common yellowthroat | *Geothlypis trichas* | small bird |
| 10/7/2022 | fall | palm warbler | *Setophaga palmarum* | small bird |
| 10/7/2022 | fall | hoary bat | *Lasiurus cinereus* | bat |
| 10/7/2022 | fall | rock pigeon | *Columba livia* | large bird |
| 10/7/2022 | fall | eastern red bat | *Lasiurus borealis* | bat |
| 10/7/2022 | fall | marsh wren | *Cistothorus palustris* | small bird |
| 10/7/2022 | fall | coturnix quail | *Coturnix coturnix* | large bird |
| 10/14/2022 | fall | white-throated sparrow | *Zonotrichia albicollis* | medium bird |
| 10/14/2022 | fall | hoary bat | *Lasiurus cinereus* | bat |
| 10/14/2022 | fall | unidentified warbler | – | small bird |
| 10/14/2022 | fall | hoary bat | *Lasiurus cinereus* | bat |
| 10/21/2022 | fall | rock pigeon | *Columba livia* | large bird |
| 10/21/2022 | fall | marsh wren | *Cistothorus palustris* | small bird |
| 10/21/2022 | fall | house wren | *Troglodytes aedon* | small bird |
| 10/21/2022 | fall | unidentified flycatcher | – | small bird |
| 10/28/2022 | fall | hoary bat | *Lasiurus cinereus* | bat |
| 10/28/2022 | fall | tree swallow | *Tachycineta bicolor* | medium bird |
| 10/28/2022 | fall | eastern red bat | *Lasiurus borealis* | bat |
| 10/28/2022 | fall | palm warbler | *Setophaga palmarum* | small bird |

# Appendix E. Searcher Efficiency Model Results (GenEst and Shoenfeld) during Post-construction Fatality Monitoring at the University of Minnesota Eolos Turbine at the Rosemount Research Station, Dakota County, Minnesota, from June 24 – November 9, 2022

**Appendix E. Searcher efficiency models (GenEst and Shoenfeld) from the University of Minnesota Eolos Turbine in Rosemount, Minnesota, from June 24 – November 9, 2022 (n = 59 for large birds; n = 57 for small birds; n = 41 for bats).**

| Searcher Efficiency Covariates | Reduction Factor Covariates (k Value) for GenEst | AICc | Delta AICc |
|---|---|---|---|
| **Large Birds** | | | |
| No Covariates | k fixed at 0.67 | 9.15 | 0* |
| **Medium Birds** | | | |
| No Covariates | k fixed at 0.67 | 20.82 | 0* |
| **Small Birds** | | | |
| Season | k fixed at 0.67 | 32.98 | 0* |
| **Bats** | | | |
| No Covariates | k fixed at 0.67 | 38.66 | 0* |

* Selected model.

AICc = corrected Akaike Information Criterion; delta AICc = change from the minimum AICc.

# Appendix F. Carcass Persistence Model Results during Post-construction Fatality Monitoring at the University of Minnesota Eolos Turbine at the Rosemount Research Station, Dakota County, Minnesota, from June 24 – November 9, 2022

**Appendix F1. GenEst carcass persistence models with covariates and distributions for large birds at the University of Minnesota Eolos Turbine in Rosemount, Minnesota, from June 24 – November 9, 2022 (n = 8 trials).**

| Location Covariates | Scale Covariates | Distribution | AICc | Delta AICc |
|---|---|---|---|---|
| No Covariates | – | exponential | 34.01 | 0* |
| No Covariates | No Covariates | lognormal | 36.70 | 2.69 |
| No Covariates | No Covariates | loglogistic | 36.97 | 2.96 |
| No Covariates | No Covariates | Weibull | 37.35 | 3.34 |

* Selected model.

AICc = corrected Akaike Information Criterion; delta AICc = change from the minimum AICc.

**Appendix F2. GenEst carcass persistence models with covariates and distributions for medium birds at the University of Minnesota Eolos Turbine in Rosemount, Minnesota, from June 24 – November 9, 2022 (n = 8 trials).**

| Location Covariates | Scale Covariates | Distribution | AICc | Delta AICc |
|---|---|---|---|---|
| No Covariates | – | exponential | 37.99 | 0* |
| No Covariates | No Covariates | Weibull | 40.41 | 2.42 |
| No Covariates | No Covariates | lognormal | 40.64 | 2.65 |
| No Covariates | No Covariates | loglogistic | 40.88 | 2.89 |

* Selected model.

AICc = corrected Akaike Information Criterion; delta AICc = change from the minimum AICc.

**Appendix F3. GenEst carcass persistence models with covariates and distributions for small birds at the University of Minnesota Eolos Turbine in Rosemount, Minnesota, from June 24 – November 9, 2022 (n = 8 trials).**

| Location Covariates | Scale Covariates | Distribution | AICc | Delta AICc |
|---|---|---|---|---|
| No Covariates | – | exponential | 33.13 | 0* |
| No Covariates | No Covariates | lognormal | 34.34 | 1.21 |
| No Covariates | No Covariates | loglogistic | 34.90 | 1.77 |
| No Covariates | No Covariates | Weibull | 35.47 | 2.34 |

* Selected model.

AICc = corrected Akaike Information Criterion; delta AICc = change from the minimum AICc.

**Appendix F4. GenEst carcass persistence models with covariates and distributions for bats at the University of Minnesota Eolos Turbine in Rosemount, Minnesota, from June 24 – November 9, 2022 (n = 8 trials).**

| Location Covariates | Scale Covariates | Distribution | AICc | Delta AICc |
|---|---|---|---|---|
| No Covariates | – | exponential | 39.63 | 0* |
| No Covariates | No Covariates | loglogistic | 40.40 | 0.77 |
| No Covariates | No Covariates | lognormal | 40.60 | 0.97 |
| No Covariates | No Covariates | Weibull | 41.91 | 2.28 |

* Selected model.

AICc = corrected Akaike Information Criterion; delta AICc = change from the minimum AICc.

# Appendix G. Search Area Adjustment Models and Estimates for the University of Minnesota Eolos Turbine at the Rosemount Research Station, Dakota County, Minnesota, from June 24 – November 9, 2022

**Appendix G1. Area adjustment estimates for the University of Minnesota Eolos Turbine at the Rosemount Research Station, Dakota County, Minnesota, from June 24 – November 9, 2022.**

| Size Class | Search Area Type | Area Adjustment |
|---|---|---|
| Large Bird | area1 | 0.85 |
| | area2 | 0.89 |
| Raptor | area1 | 0.84 |
| | area2 | 0.87 |
| Small Bird | area1 | 0.95 |
| | area2 | 0.95 |
| Bat | area1 | 0.98 |
| | area2 | 0.98 |

Note: Estimates were calculated using the maximum fall distance of carcasses for a given turbine height (80 meters [m]) and rotor diameter (96 m) estimated using a physics-based model (Hull and Muir 2013). The relative carcass-density distribution was assumed to follow a linear decrease from the turbine base out to the maximum predicted fall distance (Huso and Dalthorp 2014). The search area was expanded during the fall season, thus area adjustments were different during the summer (area1) compared to fall (area2).

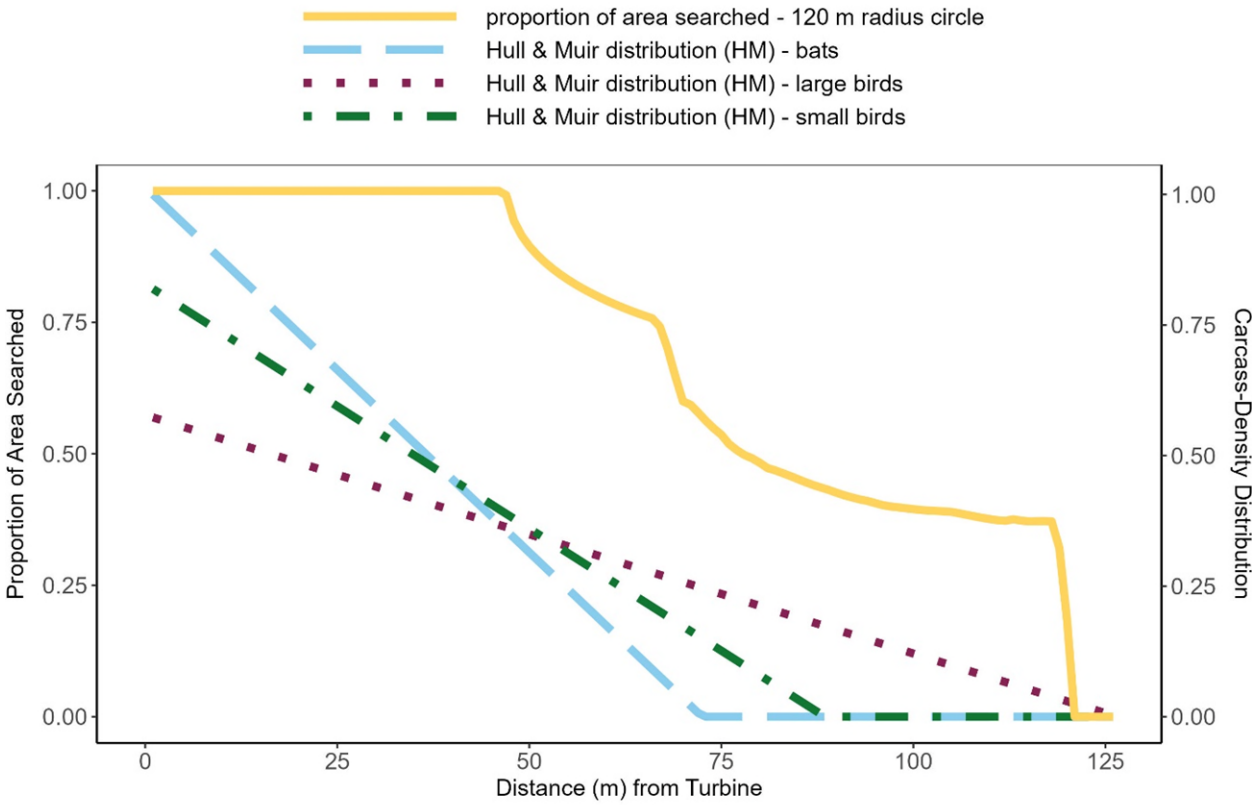


**Appendix G2. Estimated bat, large bird, and small bird carcass-density distribution for a proportion of area searched (yellow line) during the summer season by distance from turbine using the Hull and Muir (2013) model.**

# Appendix H. Probability an Available Carcass was Detected at the University of Minnesota Eolos Turbine at the Rosemount Research Station, Dakota County, Minnesota, from June 24 – November 9, 2022

**Appendix H. GenEst probability an available carcass was detected with 90% confidence intervals (CI) at the plot during the study conducted at the University of Minnesota Rosemount Research Station, Dakota County, Minnesota, from June 24 – November 9, 2022.**

| | Summer* | | Fall* | |
|---|---|---|---|---|
| | 10 turbines searched | | 10 turbines searched | |
| | Estimate | 90% CI | Estimate | 90% CI |
| **Probability of Available and Detected** | | | | |
| Large Bird | 0.95 | 0.84–0.98 | 0.95 | 0.84–0.98 |
| Raptor | 0.95 | 0.84–0.98 | 0.95 | 0.84–0.98 |
| Medium Bird | 0.75 | 0.59–0.86 | 0.75 | 0.59–0.86 |
| Small Bird | 0.44 | 0.27–0.62 | 0.44 | 0.27–0.62 |
| Bat | 0.54 | 0.36–0.70 | 0.54 | 0.36–0.70 |

* Summer = June 24 – August 17; fall = August 18 – November 9.

# Appendix I. Seasonal and Overall Estimated Fatality Rates for the University of Minnesota Eolos Turbine at the Rosemount Research Station, Dakota County, Minnesota, from June 24 – November 9, 2022

**Appendix I1. GenEst estimated seasonal fatality rates with 90% confidence intervals at the University of Minnesota Rosemount Research Station, Dakota County, Minnesota, from June 24 – November 9, 2022.**

| | Summer | | Fall | |
|---|---|---|---|---|
| | 1 turbine searched | | 1 turbine searched | |
| | Estimate | 90% CI | Estimate | 90% CI |
| **Estimated Fatality Rates (Fatalities/Turbine/Season)** | | | | |
| All Bird and Bat | 19.17 | 11.79–31.04 | 21.70 | 14.12–33.33 |
| All Bird | 5.48 | n/a* | 6.10 | 4.33–7.55 |
| Large Bird | 1.44 | n/a* | 6.10 | 4.33–7.55 |
| Large Bird Non-raptor | 1.44 | n/a* | 5.17 | n/a* |
| Raptor | 0 | n/a* | 1.41 | n/a* |
| Medium Bird | 1.64 | n/a* | 0 | n/a* |
| Small Bird | 2.67 | n/a* | 0 | n/a* |
| Bat | 13.62 | 7.28–23.79 | 15.67 | 8.68–26.36 |
| **Estimated Fatality Rates (Fatalities/Megawatt/Season)** | | | | |
| All Bird and Bat | 7.67 | 4.71–12.41 | 8.68 | 5.65–13.33 |
| All Bird | 2.19 | n/a* | 2.44 | 1.73–3.02 |
| Large Bird | 0.58 | n/a* | 2.44 | 1.73–3.02 |
| Large Bird Non-raptor | 0.58 | n/a* | 2.07 | n/a* |
| Raptor | 0 | n/a* | 0.56 | n/a* |
| Medium Bird | 0.66 | n/a* | 0 | n/a* |
| Small Bird | 1.07 | n/a* | 0 | n/a* |
| Bat | 5.45 | 2.91–9.52 | 6.27 | 3.47–10.55 |

* Confidence interval (CI) not calculated because the observed carcass count is less than five.

**Appendix I2. GenEst estimated seasonal fatality rates, after feather spots were removed, with 90% confidence intervals at the University of Minnesota Rosemount Research Station, Dakota County, Minnesota, from June 24 – November 9, 2022.**

| | Summer | | Fall | |
|---|---|---|---|---|
| | 1 turbine searched | | 1 turbine searched | |
| | Estimate | 90% CI | Estimate | 90% CI |
| **Estimated Fatality Rates (Fatalities/Turbine/Season)** | | | | |
| All Bird and Bat | 17.92 | 10.47–30.17 | 16.88 | 9.88–27.92 |
| All Bird | 4.24 | n/a* | 1.41 | n/a* |
| Large Bird | 0 | n/a* | 1.41 | n/a* |
| Large Bird Non-raptor | 0 | n/a* | 0 | n/a* |
| Raptor | 0 | n/a* | 1.41 | n/a* |
| Medium Bird | 1.64 | n/a* | 0 | n/a* |
| Small Bird | 2.67 | n/a* | 0 | n/a* |
| Bat | 13.62 | 7.28–23.79 | 15.67 | 8.68–26.36 |
| **Estimated Fatality Rates (Fatalities/Megawatt/Season)** | | | | |
| All Bird and Bat | 7.17 | 4.19–12.07 | 6.75 | 3.95–11.17 |
| All Bird | 1.70 | n/a* | 0.56 | n/a* |
| Large Bird | 0 | n/a* | 0.56 | n/a* |
| Large Bird Non-raptor | 0 | n/a* | 0 | n/a* |
| Raptor | 0 | n/a* | 0.56 | n/a* |
| Medium Bird | 0.66 | n/a* | 0 | n/a* |
| Small Bird | 1.07 | n/a* | 0 | n/a* |
| Bat | 5.45 | 2.91–9.52 | 6.27 | 3.47–10.55 |

* Confidence interval (CI) not calculated because the observed carcass count is less than five.

# Appendix B. Training Procedure and Performance of the Computer Vision Model Methods

## ANNOTATION

To determine which 5-minute videos were suitable for frame-by-frame object detection annotation, we generated single-image video composites to summarize movement and tracks within the images. The image composites were created using the Opencv python package with the following method:

1. Apply a binary threshold to the frame at a pixel value of 170.
2. Use the findContours function to delineate individual white objects in the frame.
3. Retain contoured objects with an area greater than 100 pixels (i.e., larger than the size of birds, bats, and insects) to generate a binary mask.
4. Add the inverse of the mask to the thresholded frame, such that only pixels that are white in both the frame and the mask stay white in the resulting image.
5. Add the masked frame to an ongoing composite image, such that any pixels that are white in either the ongoing composite or the subsequent masked frame are white.

The resulting images from this method range in clarity depending on background conditions. On clear nights, the video has minimal visual noise and it is easy to distinguish between noise from the turbine being incorrectly contoured and animal flight tracks. Videos dominated by atmospheric clouds result in too much visual noise in the composite image to conclusively determine if annotatable tracks are present in the video. We classified these images into four categories: Tracks, No Tracks, Possible Tracks, and Indeterminate (Appendices B1a-d).

From these classifications, we selected 5-minute videos for further frame-by-frame annotation. Although videos classified as having tracks based on the composite images were prioritized, we also reviewed and annotated videos from each category of Possible Tracks, No Tracks, and Indeterminate to avoid biasing the training set to clear conditions and slow-moving turbines.

Annotators used Computer Vision Annotation Tool (CVAT) to draw bounding boxes around flying objects and categorize them as either bats, small birds, medium birds, large birds, insects, airplanes, or unidentified flying objects (UFOs) and assign a confidence score of low, medium, or high to their classification. Each unique object was also given an object identification (ID) that remained constant across each frame it appeared in. Annotators further marked if the object was occluded in a detection and if the object collided with the turbine at any point in the video.



**NOT FOR DISTRIBUTION**

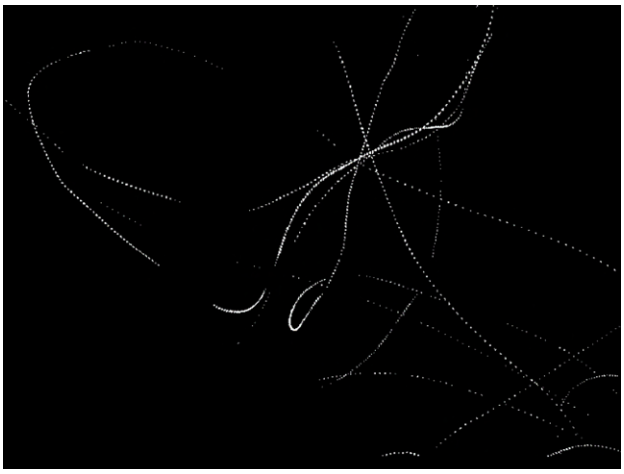

**Appendix B1a. A composite image classified as 'Tracks'. The white tracks in the image follow the flight patterns of a potential bat, insect or bird.**

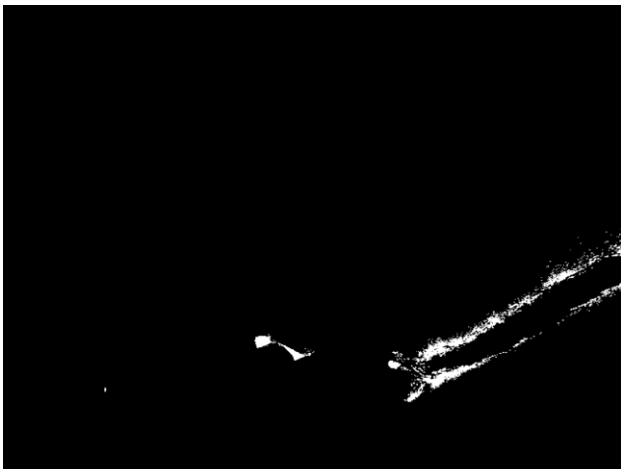

**Appendix B1b. A composite image classified as 'No Tracks.' The white patches in the image are an example of incomplete capture by contouring of the turbine blade, rather than animal passes.**

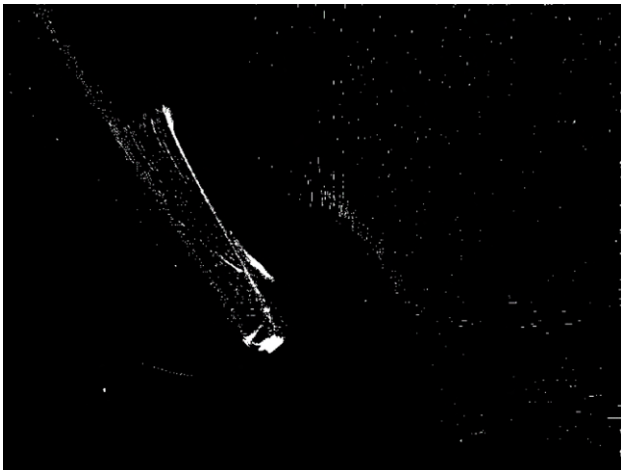

**Appendix B1c. A composite image classified as 'Possible Tracks'. Some of the white patches are clearly artifacts of turbine movement and clouds, but the string of dots in the bottom left indicate a potential animal track.**

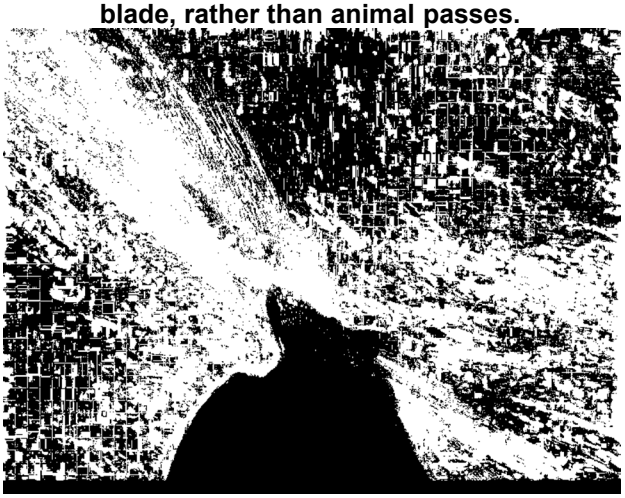

**Appendix B1d. A composite image classified as 'Indeterminate.' The noise from clouds and blade movement make it impossible to determine the presence or absence of animal tracks.**

To diversify the background conditions in the training set, the 5-minute thermal videos were split into 1-minute sections. Annotators watched and annotated these sections sequentially, but they only reviewed or annotated subsequent 1-minute sections if no annotations were generated in the previous minutes. In the latter portion of the annotation effort, insects, airplanes, and UFOs were not annotated to generate a more balanced sample of the bird and bat categories. Only frames that were annotated or definitively empty were used for model training, validation, and testing.



**NOT FOR DISTRIBUTION**

## MODEL DEVELOPMENT

The annotated data were divided into three independent categories: training, validation, and testing. These sets were stratified by the object ID of the annotated flying objects so that frames containing different detections of the same object were all within one group. We used the training and validation set to train a single-class YOLOv7 neural network to detect flying objects on a frame-by-frame basis in the videos. In 2022, we used a modified YOLOv7 training scheme (Hughes 2024). Our final model deployed on the 2022 thermal data was trained for 80 epochs, with a batch size of 16 samples, an initial learning rate of 0.001, momentum of 0.9, a base weight decay of 0.0005, and an SGD (Stochastic Gradient Descent) optimizer. This model was used based on its fast performance and relatively high recall on a per detection basis for the primary categories of interest in the testing set (i.e., birds and bats). In the final deployment of the model, we accepted detections with confidence exceeding 0.2 to balance between recall and precision. The model had the lowest recall on bats at 72% and the highest recall on large birds at 100%. Out of 2,062 predictions made on the testing set, 1,501 were true positives and 561 were false positives, for an overall precision of 0.73. As the model was not trained to distinguish among object classes, we could not classify the false positives and provide a class-wise estimate of precision. The model was unable to distinguish between object classes due to the relatively small sample size of the annotation set, despite the intensive efforts put towards annotation. This was, in part, due to the difficulty annotators had in distinguishing between different classes with high confidence.

**Appendix B2. Model performance on a class-wise basis for 2022 trials based on image frames.**

| Size Class | True Positives | False Negatives (What Was Missed) | Recall |
|---|---|---|---|
| Bat | 209 | 80 | 72% |
| Small bird | 307 | 22 | 93% |
| Medium bird | 105 | 5 | 95% |
| Large bird | 170 | 0 | 100% |
| Airplane | 195 | 9 | 96% |
| Insect | 264 | 35 | 88% |
| UFO | 251 | 44 | 85% |
| **Overall** | **1,501** | **195** | **89%** |

For the real-time deployment, we used the same training dataset as in 2022 to train the base YOLOv7 neural network provided by Ultralytics, as this version of the model could be transformed into a NVIDIA TensorRT model for even faster deployment. NVIDIA TensorRT increases performance speed by reduced floating point precision in model weights, but this can lead to some compromises in model accuracy (Appendix B3). The NVIDIA TensorRT model had lower performance than the previous model version across most classes. However, in some cases, even though frame-wise detection performed worse, overall object detection (across frames) was improved, as not every frame of a flying object had to be detected for a portion of the track to be detected and saved.



NOT FOR DISTRIBUTION

**Appendix B3. Model performance on a class-wise basis for 2023 edge deployment based on image frames.**

| Size Class | True Positives | False Negatives | Recall |
|---|---|---|---|
| Bat | 162 | 127 | 56% |
| Small bird | 299 | 25 | 92% |
| Medium bird | 97 | 13 | 88% |
| Large bird | 169 | 1 | 99% |
| Airplane | 199 | 5 | 98% |
| Insect | 207 | 92 | 69% |
| UFO | 226 | 69 | 77% |
| **Overall** | **1,359** | **332** | **80%** |

## OBJECT TRACKING

We used a custom centroid tracker algorithm to associate detections across frames into object tracks. This algorithm assumed that detections belonged to the same flying object based on distance from the most recent detections in subsequent frames. Various parameters dictated whether detections were considered new tracks or part of existing tracks, such as maximum distance, which capped the amount of pixel distance between adjacent detections, and maximum missed, which limited the number of frames allowed between detections to account for instances like an object flying behind a turbine blade. The algorithm also incorporated parameters to remove some false positive detections from the final track outputs, such as requiring a minimum number of detections to be accepted, and standard movement deviation, which required a track's detections have a minimum standard deviation in detection coordinates to minimize false positive tracks associated with stationary objects like lens scratches. We tested a range of parameters to optimize the overall number of flying objects in the testing set for which at least a portion of the annotated track was detected and associated together into a predicted track. The parameter set deployed on the 2022 data utilized a maximum missed threshold of 32, maximum distance threshold of 59, minimum hit threshold of six, and a standard deviation minimum of 10. Although these parameters led to high recall outputs for the size classes of interest, it also accepted a high number of false positive tracks (tracks made up of only false positive detections), with only 44% of output tracks being associated with true flying object instances (Appendix B4).

**Appendix B4. Percent of individual birds and bats for which a portion of the overall flight track was output by the centroid tracking algorithm on both 2022 and 2023 model versions.**

| Size Class | Group | n | Recall (2022) | Recall (2023) |
|---|---|---|---|---|
| Bat | Training | 23 | 83% | 87% |
| | Validation | 8 | 100% | 100% |
| | **Testing** | **4** | **75%** | **75%** |
| | **Overall** | **35** | **86%** | **89%** |
| Small bird | Training | 51 | 90% | 82% |
| | Validation | 32 | 81% | 72% |
| | **Testing** | **6** | **67%** | **67%** |
| | **Overall** | **89** | **85%** | **78%** |
| Medium bird | Training | 19 | 58% | 32% |
| | Validation | 11 | 72% | 27% |
| | **Testing** | **3** | **100%** | **57%** |



NOT FOR DISTRIBUTION

**Appendix B4. Percent of individual birds and bats for which a portion of the overall flight track was output by the centroid tracking algorithm on both 2022 and 2023 model versions.**

| Size Class | Group | n | Recall (2022) | Recall (2023) |
|---|---|---|---|---|
| | **Overall** | **33** | **67%** | **33%** |
| Large bird | Training | 15 | 100% | 100% |
| | Validation | 4 | 100% | 100% |
| | **Testing** | **2** | **100%** | **100%** |
| | **Overall** | **21** | **100%** | **100%** |

## SEGMENTATION MODEL

Appendix B5 shows a predicted segmentation mask in pink over the original image. We selected a sample of 100 images of turbines from a random sample of 100 deployment videos based on a rating of their uniqueness given by the software FiftyOne. We annotated the segmentation masks in LabelBox and used 60 for training, 40 for validation, and 20 for testing.

## COLLISION CLASSIFIER

The collision classifier made use of the bounding boxes from the object detections and the turbine segmentations to track each object's trajectory and position relative to the turbine.

The collision classifier excluded videos according to several criteria:

- Object never approached the turbine within 10 pixels
- Object never went further than 15 pixels from the turbine (to reduce the prevalence of false positive detections of turbine blades)
- Object approached the turbine but did not exhibit a significant change in velocity upon retreating from the turbine (i.e., airplanes flying straight through the field of view)



NOT FOR DISTRIBUTION

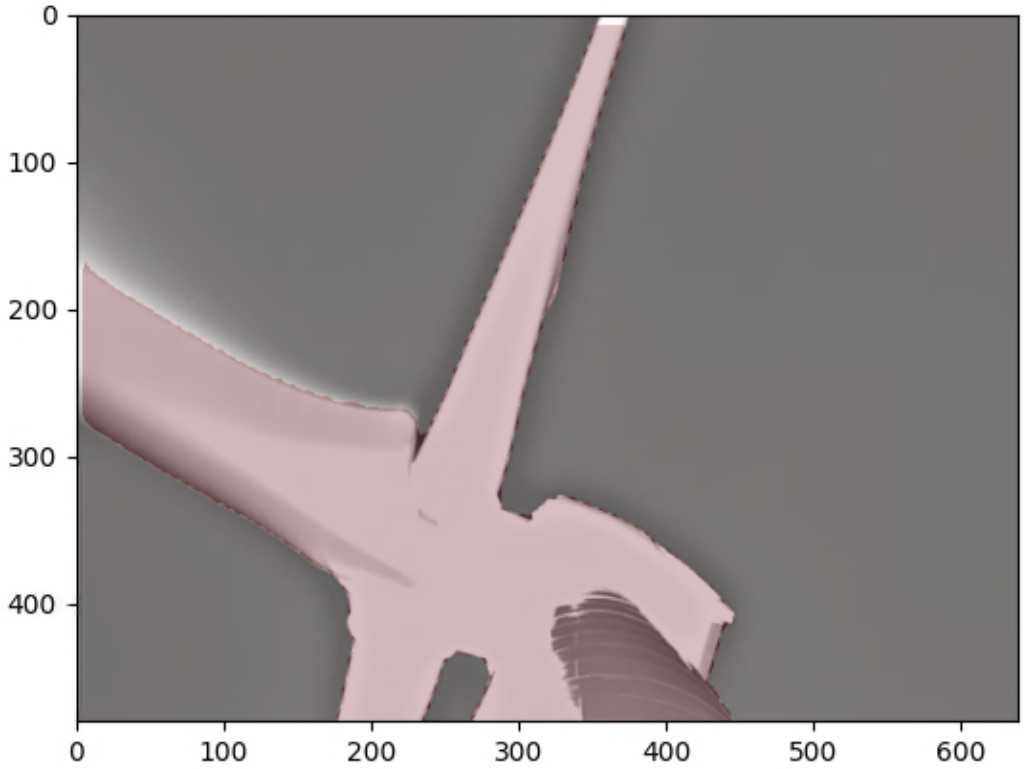


**Appendix B5. The predicted segmentation mask of the turbine shown in pink.**

The collision classifier flagged videos for review if:

- Object demonstrated a significant change in velocity after approaching the turbine
- Object disappeared after approaching the turbine (velocity or change in position could not be measured)

The second flagging criteria was conservative and added many more videos for review. However, one of the collisions we found was flagged under this criterion, as the collision occurred very close to the edge of the frame and the object's flight path prior to collision was not found by the object detector.

## REVIEW METHODOLOGY

We processed the videos associated with nine vibration sensor detection events taking place between August 21 – September 21, 2022. We were not able to process additional thermal videos taken prior to October 10, 2022, due to data losses. For each 4-hour period across three possible days, we randomly selected a 5-minute interval to process, comprised of one video from each of the three axis cameras for a total of three videos per time period. The random sample was 15 video hours, or five monitoring hours, out of the 1,536 hours in the study period. The random sample of videos and the videos from the detection events were processed by the YOLOv7 object detection model described above. Reviewers watched these clips to search for collision events



NOT FOR DISTRIBUTION

and potential collisions were then reviewed again by experts in order to classify the flying object as a bat, insect, small bird, medium bird, large bird, or other object and to confirm whether or not a collision occurred in the clip.

In the camera-only deployment, we reviewed videos from the time periods preceding the estimated time of death from carcasses found on the ground. We reviewed videos that were flagged as a potential collision by the collision detector algorithm (Appendix B6).

**Appendix B6. Percent of videos reviewed during the camera only deployment at the University of Minnesota Eolos Turbine in Rosemount, Minnesota, 2023.**

| Date | Number of Videos | Total Duration (hours) | Number Reviewed | Review Duration (hours) | Percent Reviewed |
|---|---|---|---|---|---|
| 2023/04/24 | 1,710 | 4.76 | 307 | 0.85 | 17.95% |
| 2023/04/25 | 2,110 | 5.87 | 395 | 1.09 | 18.72% |
| 2023/04/26 | 4,642 | 12.87 | 454 | 1.26 | 9.78% |
| 2023/04/27 | 3,326 | 9.24 | 243 | 0.67 | 7.31% |
| 2023/04/28 | 2,341 | 6.62 | 58 | 0.16 | 2.48% |
| 2023/04/29 | 1,275 | 3.67 | 20 | 0.06 | 1.57% |
| 2023/04/30 | 831 | 2.28 | 6 | 0.02 | 0.72% |
| 2023/05/01 | 436 | 1.20 | 17 | 0.05 | 3.90% |
| 2023/05/02 | 601 | 1.66 | 62 | 0.17 | 10.32% |
| 2023/06/02 | 1,648 | 4.57 | 166 | 0.46 | 10.07% |
| 2023/06/03 | 2,094 | 5.80 | 260 | 0.72 | 12.42% |
| 2023/06/04 | 4,392 | 12.18 | 425 | 1.18 | 9.68% |
| 2023/06/05 | 2,844 | 7.89 | 141 | 0.39 | 4.96% |
| 2023/06/06 | 2,460 | 6.82 | 578 | 1.60 | 23.50% |
| 2023/06/07 | 1,565 | 4.34 | 410 | 1.14 | 26.20% |
| 2023/06/08 | 2,653 | 7.34 | 940 | 2.60 | 35.43% |
| **Total** | **34,928** | **97.12** | **4,482** | **12.40** | **12.83%** |

Of the five known fatalities during this deployment, four were located in thermal video (Appendix B7).

**Appendix B7. Fatalities observed during systematic ground-based carcass searches at the University of Minnesota Eolos Turbine in Rosemount, Minnesota during spring deployment 2023.**

| Date Found (ground search) | Species | Collision video timestamp (UTC) | Local time (CST) | Camera |
|---|---|---|---|---|
| 05/01/2023 | golden-crowned kinglet | 2023/04/29 09:41:01 | 2023/04/29 04:41:01 | Axis 2 |
| 06/05/2023 | silver-haired bat | 2023/06/03 07:29:24 | 2023/06/03 02:29:24 | Axis 3 |
| 06/05/2023 | red-tailed hawk | 2023/06/02 15:12:54 | 2023/06/02 10:12:54 | Axis 3 |
| 06/08/2023 | silver-haired bat | 2023/06/07 03:41:43 | 2023/06/06 22:41:43 | Axis 1 |
| 06/08/2023 | horned lark | NA | NA | NA |

UTC = Coordinated Universal Time; CST = Central Standard Time; NA = not applicable.

## REFERENCES

Hughes, C. 2024. Yolov7-Training. GitHub. Available online: https://github.com/Chris-hughes10/Yolov7-training



NOT FOR DISTRIBUTION

# Appendix C. A Simulation Analysis to Investigate the Influence of Sample Size on the Accuracy of Estimated Fatality Rates Obtained Using the Double-Observer Methodology



**NOT FOR DISTRIBUTION**

To evaluate the influence of sample size of fatality rates, we created a large, simulated dataset that includes randomly generated timestamps that indicate a single actual collision (Appendix C1). Each assumed collision fatality at a specified turbine includes a vibration that is either recorded or fails to record, a video record that occurs or fails to show the collision, and indicator for whether either or both "observers" are not functioning (down time).

**Appendix C1. Example simulated data with a viable row indicator.**

| Random Time Stamp | Vibration | Video | Viable Row |
|---|---|---|---|
| 2/13/2023 7:53 | 0 | 0 | 0 |
| 4/5/2023 5:31 | 1 | 0 | 1 |
| 4/3/2023 22:15 | 1 | 0 | 1 |
| 4/5/2023 8:06 | 1 | 0 | 1 |
| 4/29/2023 2:11 | 1 | 0 | 1 |
| 4/7/2023 0:44 | 1 | 0 | 1 |
| 2/2/2023 21:47 | 1 | 0 | 1 |
| 2/25/2023 5:07 | 1 | 0 | 0 |
| 4/9/2023 14:36 | 0 | 0 | 1 |
| 3/25/2023 10:12 | 0 | 0 | 0 |

This example data is filtered to only those collisions for which both observers are functioning to for double-observer study. We assume (for now) that collisions missed during down time occur at the same rate as when both observers are functioning. The collisions that occurred on April 9 above were a viable row, but both observers failed to detect the fatality. First, we test the above formulas on a larger simulated data set. We assume the vibration detection probability is 0.70 and that video detection probability is 0.50. We start with 100 fatalities. For these made-up data, the uptime of both observers is 0.75. Filtering out all downtime, we have 74 rows for which both detection methods were functioning. An additional filter to include at least a detection from either source provides 63 collisions would be detected of the actual 100.

Substituting these 63 rows of data into the above equations, we have the following estimates (Appendix C2).

**Appendix C2. Simulated data results from a sample size of 100.**

| | | | 90% CI | |
|---|---|---|---|---|
| **Observer** | **Detection Probability** | **Detection SE** | **Lower** | **Upper** |
| Vibration | 0.6840 | 0.0754 | 0.5600 | 0.8080 |
| Video | 0.5090 | 0.0700 | 0.3939 | 0.6242 |
| **Overall** | **0.8450** | **0.0500** | **0.7628** | **0.9273** |

SE = standard error; CI = confidence interval.

We see that the individual detection probability estimates are near the truth provided in the assumptions. We can also see the relative degree of uncertainty when supposing the total number of collisions as well as the uptime of both detection methods at these detection rates.



**NOT FOR DISTRIBUTION**

## SMALLER DATASET OF 20 COLLISIONS

When considering a more realistic dataset for a single wind turbine over the course of a couple of seasons, we can compare the relative differences in confidence interval (CI) for smaller fatality counts. Here we have the same initial assumptions, but use a smaller dataset. Below is an example of those data (Appendix C3). Note, in this example there are rows where neither observer detected the collision; thus, these rows would be excluded from the overall detection estimate.

**Appendix C3. Example simulated data with a viable row indicator.**

| Random Time Stamp | Vibration | Video | Viable Row |
|---|---|---|---|
| 5/10/2023 16:42 | 1 | 0 | 1 |
| 3/11/2023 8:23 | 1 | 0 | 1 |
| 4/19/2023 3:36 | 1 | 1 | 1 |
| 4/25/2023 5:58 | 1 | 1 | 1 |
| 3/31/2023 8:30 | 1 | 0 | 1 |
| 4/12/2023 3:23 | 1 | 0 | 1 |
| 3/12/2023 21:44 | NA | NA | 0 |
| 3/20/2023 21:28 | 1 | 1 | 1 |
| 3/28/2023 7:56 | NA | NA | 0 |
| 5/5/2023 11:44 | 0 | 1 | 1 |
| 2/15/2023 20:06 | 0 | 0 | 1 |
| 4/13/2023 4:46 | 1 | 1 | 1 |
| 2/18/2023 4:15 | 1 | 0 | 1 |
| 4/2/2023 22:20 | NA | NA | 0 |
| 3/24/2023 14:29 | 0 | 0 | 1 |
| 5/3/2023 4:44 | 1 | 1 | 1 |
| 3/14/2023 1:12 | 1 | 0 | 1 |
| 2/5/2023 1:16 | 0 | 0 | 1 |
| 2/9/2023 2:15 | 1 | 1 | 1 |
| 3/20/2023 19:57 | 1 | 0 | 1 |
| **Total** | **13** | **7** | **14** |

NA = not applicable.

Below is a similar table of results with the smaller dataset of 20 collisions (Appendix C4).

**Appendix C4. Simulated fatality data results based on from a sample size of 20 collisions.**

| | | | 90% CI | |
|---|---|---|---|---|
| **Observer** | **Detection Probability** | **Detection SE** | **Lower** | **Upper** |
| Vibration | 0.8570 | 0.1323 | 0.6394 | 1.0000 |
| Video | 0.4615 | 0.1383 | 0.2340 | 0.6890 |
| **Overall** | **0.9231** | **0.0790** | **0.7931** | **1.0000** |

SE = standard error; CI = confidence interval.

The actual detection rates are once again captured in the 90% CIs, though the interval size is much larger compared to the dataset of 100 collisions. To calculate a fatality estimate with the vibration detection estimate over the observation period, we divide the point estimate by 0.857. There were 13 vibrations detected, implying an estimate of 13/0.857 = 15.17 total fatalities (Appendix C5). Assuming there was a 25% downtime of either or both observers,



NOT FOR DISTRIBUTION

15.17 represents an undercount of fatalities. With a uniform fatality rate over time, we estimated 15.17/0.75 = 20.22 fatalities during the study period from vibration detections (Appendix C5).

**Appendix C5. Simulated fatality data results based on a sample size of 100 collisions but with and without adjustment to the fatality rate based on operational uptime.**

| | Unadjusted | Unadjusted 90% CI | | Uptime Adjusted | Uptime Adjusted 90% CI | |
|---|---|---|---|---|---|---|
| **Observer** | **Fatality Estimate** | **Lower** | **Upper** | **Estimate** | **Lower** | **Upper** |
| Vibration | 15.17 | 13.00 | 20.33 | 20.23 | 17.33 | 27.11 |
| Video | 15.17 | 10.16 | 29.91 | 20.22 | 13.55 | 39.89 |
| **Overall** | **15.17** | **14.00** | **17.65** | **20.22** | **18.67** | **23.53** |

CI = confidence interval.



NOT FOR DISTRIBUTION

# Appendix B. Test results of TNO WTBird® trial at the University of Minnesota TNO 2023 R10376, 12 April 2023

# Test results of TNO WT-Bird® trial at the University of Minnesota

TNO Public ⟩ TNO 2025 R11067
21 May 2025

Energy & Materials Transition
www.tno.nl
+31 88 866 50 65
info@tno.nl

TNO 2025 R11067 – 21 May 2025

# Test results of TNO WT-Bird® trial at the University of Minnesota

| | |
|---|---|
| Author(s) | F.A. Kaandorp |
| Classification report | TNO Public |
| Report text | TNO Public |
| Number of pages | 33 (excl. front and back cover) |
| Number of appendices | 0 |
| Sponsor | United States Department of Energy |
| Project name | DOE WT-Bird |
| Project number | 060.36431 |

**All rights reserved**
No part of this publication may be reproduced and/or published by print, photoprint, microfilm or any other means without the previous written consent of TNO.

© 2025 TNO

# Contents

# 1 Introduction

The instrumentation of the WT-Bird® system installed at the Clipper turbine at the University of Minnesota is described in detail in report TNO 2022 R10697, “WT-Bird installation plan at University of Minnesota”[1] and TNO 2022 R11392, “WT-Bird installation report University of Minnesota “ [2]. This report aims at the results of the trial period from 2022-07-21 until 2022-11-03. The period of interest is limited from 2022-08-13 until 2022-11-03 due to start up issues with the existing network in the turbine and wear of the pitch gears. The latter resulted in a loud noise twice a rotation per blade which affected the WT-Bird system and was solved by applying an offset of 5 degrees to the pitch system. The issues with the network were solved by replacing and reconfiguring network equipment.

Chapter 2 describes the summary of the detected collisions in the period from 2022-08-13 until 2022-11-03, Chapter 3 describes every detected collision in detail and chapter 4 contains the conclusion and recommendations.

# 2 Summary of results

In the trial period the WT-Bird® system detected 15 bird collisions, however not all could be confirmed visually, mainly because 13 of the 15 collisions occurred during dusk or night, 4 are visually confirmed, 2 “likely” (meaning that only bird/bat activity or falling items/bodies were spotted) and the remaining have no visual confirmation. The day cameras supported by IR illuminators did not have sufficient light sensitivity to visualize the collision events. Fortunately, there is (limited) thermal camera data available to confirm some of the collisions. The thermal cameras however could not cover the full rotor area. Table 2.1 shows the list of detected collisions.

Table 2.1: List of collisions

| No. | Date and time (UTC) | Day / Night | Visual confirmation |
|---|---|---|---|
| 1 | 21-08-2022 082935 | Night | Yes |
| 2 | 25-08-2022 055931 | Night | Yes |
| 3 | 25-08-2022 094643 | Night | Yes |
| 4 | 26-08-2022 013928 | Dusk | No |
| 5 | 26-08-2022 084520 | Night | Likely |
| 6 | 31-08-2022 053655 | Night | Likely |
| 7 | 02-09-2022 012053 | Dusk | No |
| 8 | 02-09-2022 020458 | Dusk | No |
| 9 | 11-09-2022 010714 | Dusk | No |
| 10 | 21-09-2022 072328 | Night | No |
| 11 | 21-09-2022 174207 | Day | No |
| 12 | 23-09-2022 055742 | Night | No |
| 13 | 27-09-2022 232436 | Day | Yes |
| 14 | 06-10-2022 034605 | Night | No |
| 15 | 22-10-2022 034740 | Night | No |

All Collisions occurred during turbine operation.

# 3 Collision results in detail

The following paragraphs show each collision in detail.

## 3.1 Collision 21-08-2022 082935

Figure 3.1 and Figure 3.2 show the data measured during Collision “21-08-2022 082935”, the WT-Bird® software takes the raw data (Top left in Figure 3.1) and first applies a band pass filter to eliminated the DC and rotor rotation component, resulting in the graph down left in Figure 3.1 The next step is a RMS calculation displayed in the top right graph in Figure 3.1 When a certain threshold limit is crossed the WT-Bird system reports a trigger, the data of all blades and sensors are compared after the trigger detection to determine a confidence level of the trigger. The data is visualized in Figure 3.1 is collected with Sensor 3 of blade 1.

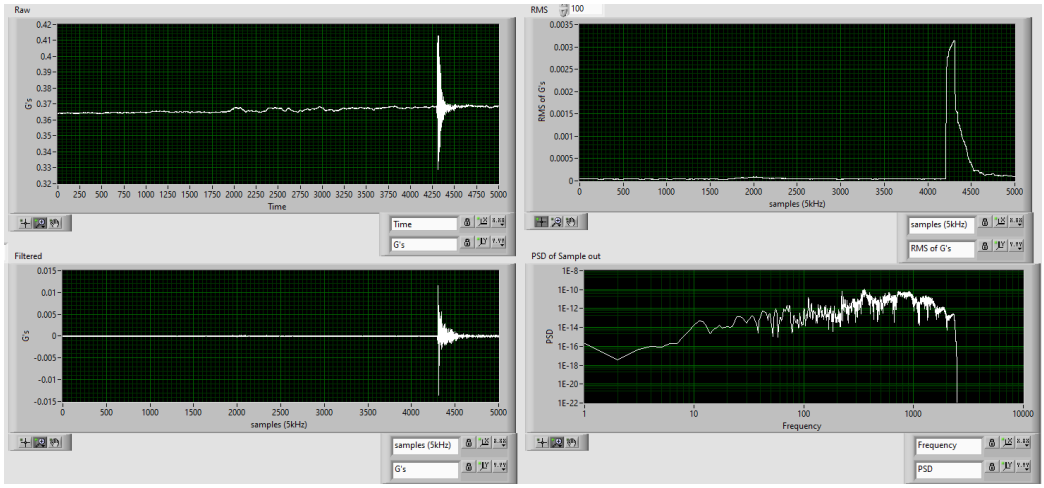


Figure 3.1: Data of Collision 21-08-2022 082935, step by step filtering

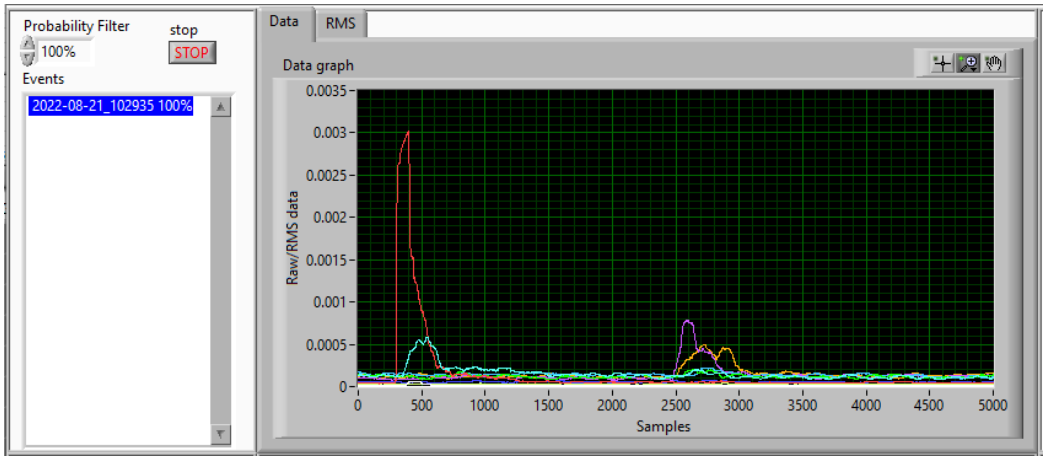


Figure 3.2: Data of Collision 21-08-2022 082935, WT-Bird output

Collision “21-08-2022 082935” did not have a visual confirmation on the Sony day cameras, the thermal camera data is analyzed as well and we have detected the presence of a bird during the time of the collision, it is however not visible on the thermal cameras that the bird actually hit the blade. This is however very likely. Figure 3.3 shows an image of the thermal camera during the collision.

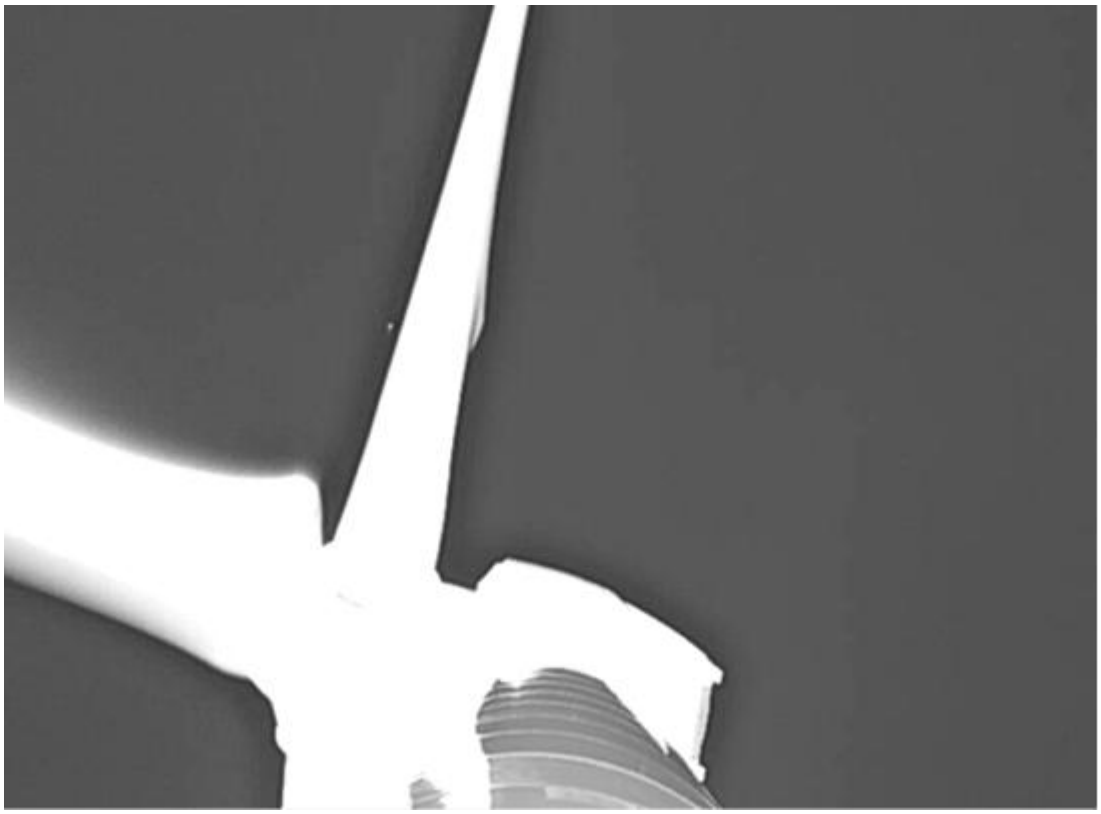

Figure 3.3: Image of the thermal camera during collision 21-08-2022 082935

## 3.2 Collision 25-08-2022 055931

Figure 3.4 shows the actual output of the WT-Bird® system when a trigger occurs, the output is data container with measured (filtered) data, calculated RMS data and pictures taken during the collision. In Figure 3.4 one can see a larger RMS signal on sensor 2 of blade 2 depicted as the blue line. Note that the RMS values of the remaining 8 sensors are also depicted in Figure 3.4, however these values are much lower.

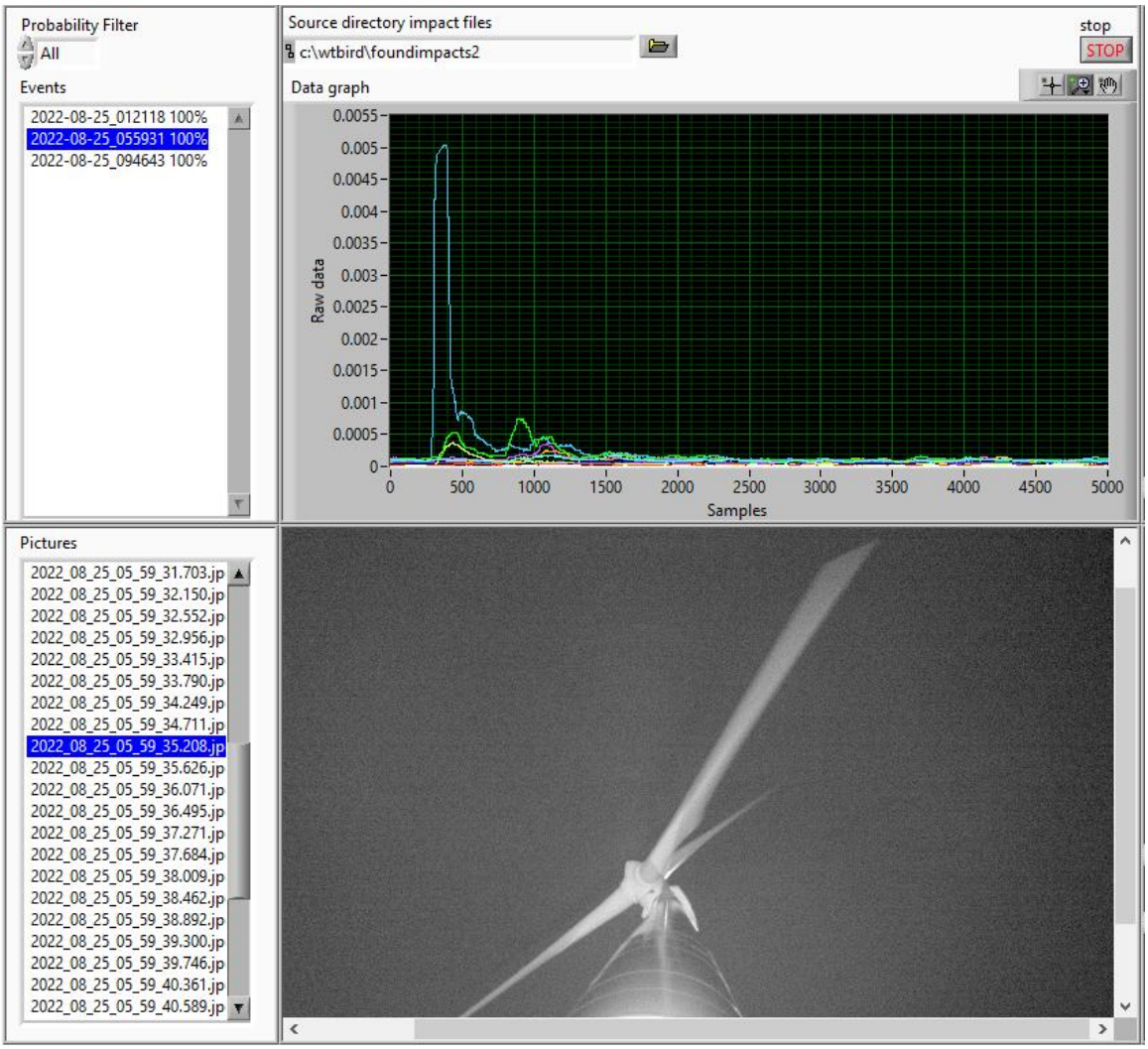


Figure 3.4: Collision 25-08-2022 055931

Collision “25-08-2022 055931” does not have a visual confirmation on the day cameras however it was recorded by the thermal cameras. A clear bounce is visible where the bird changes direction quite fast, depicted in Figure 3.5 and Figure 3.6

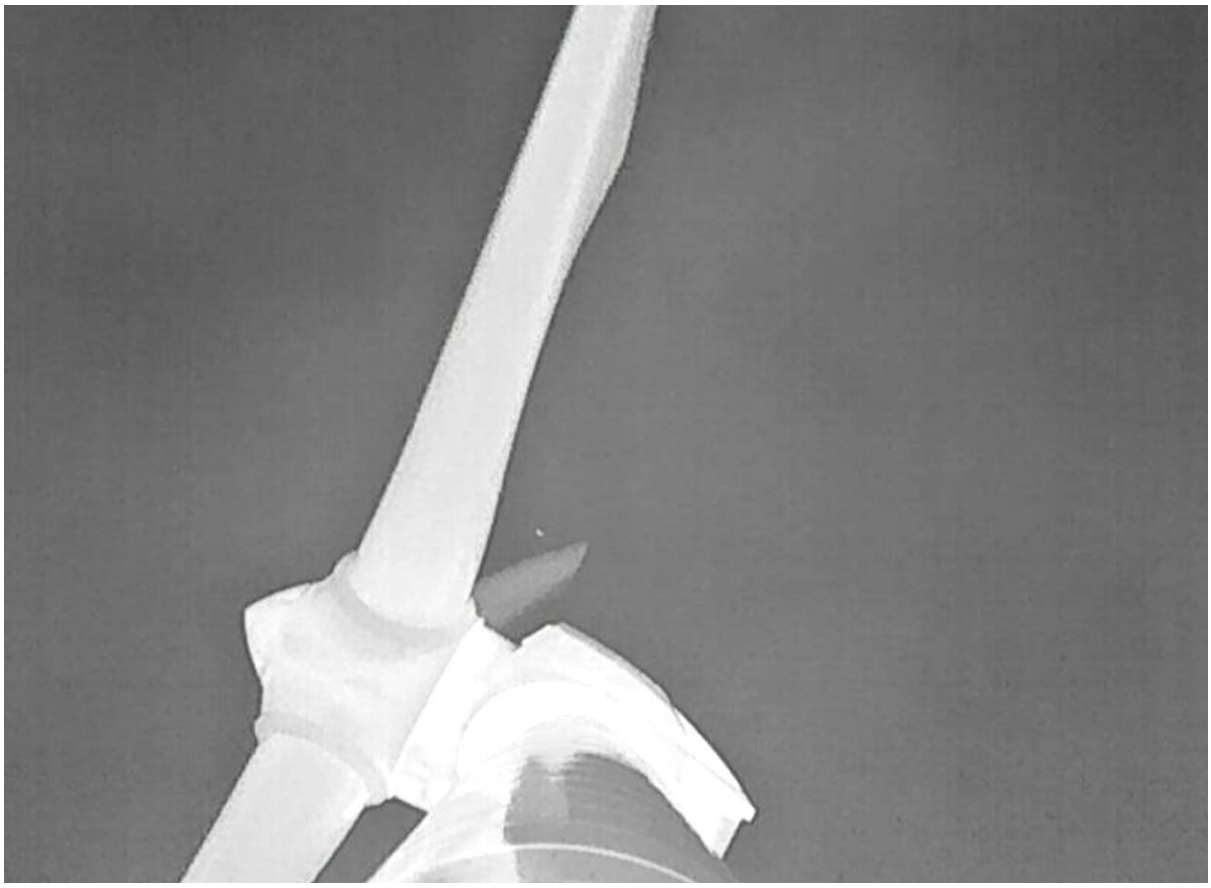

Figure 3.5: Thermal camera image before impact, collision 25-08-2022 055931

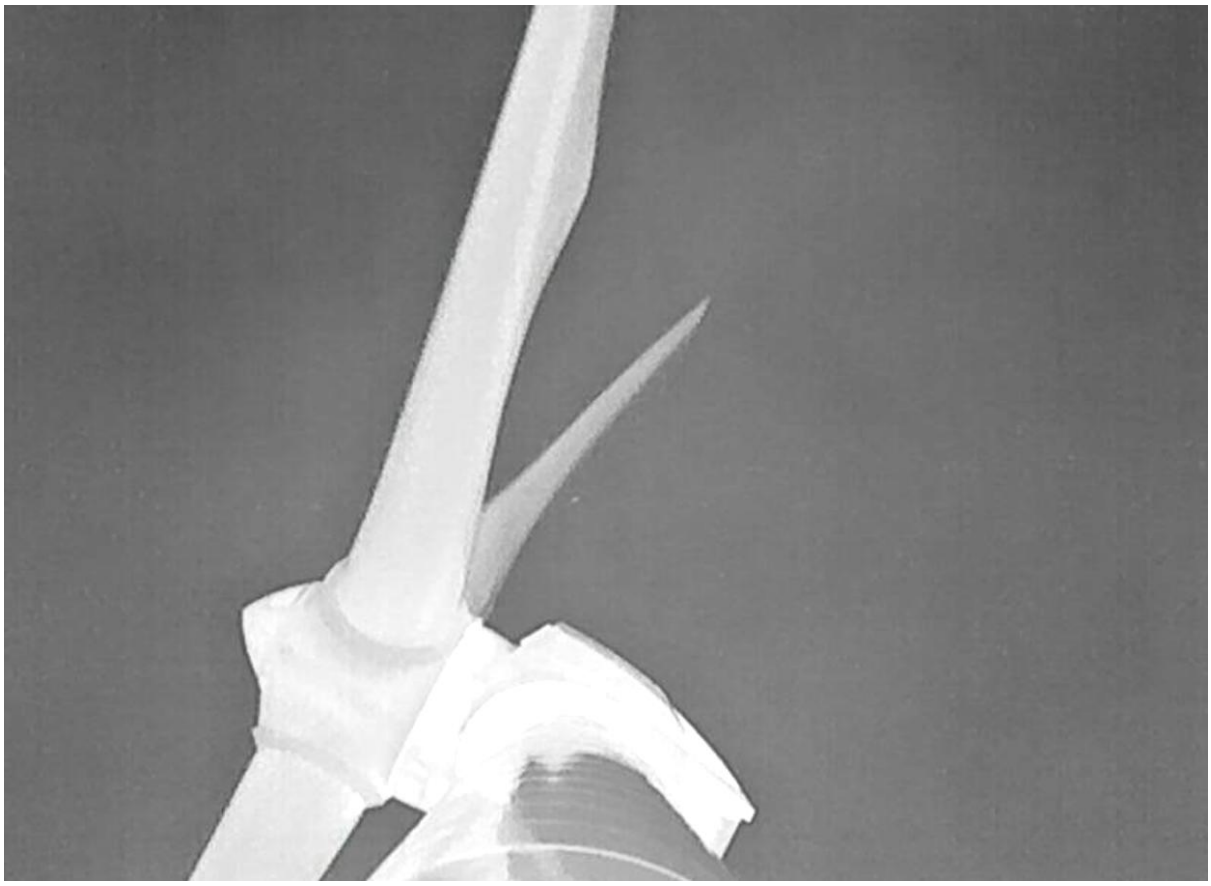

Figure 3.6: Thermal image after impact, collision 25-08-2022 055931

# 3.3 Collision 25-08-2022 094643

Collision “25-08-2022 094643” was detected by sensor 2 of blade 3. As the previous collision one of the RMS values is much larger than the other two, indicating this is a likely collision, especially when the collision is detected at sensor 2 or 3 and not at sensor 1 which is close to the root.

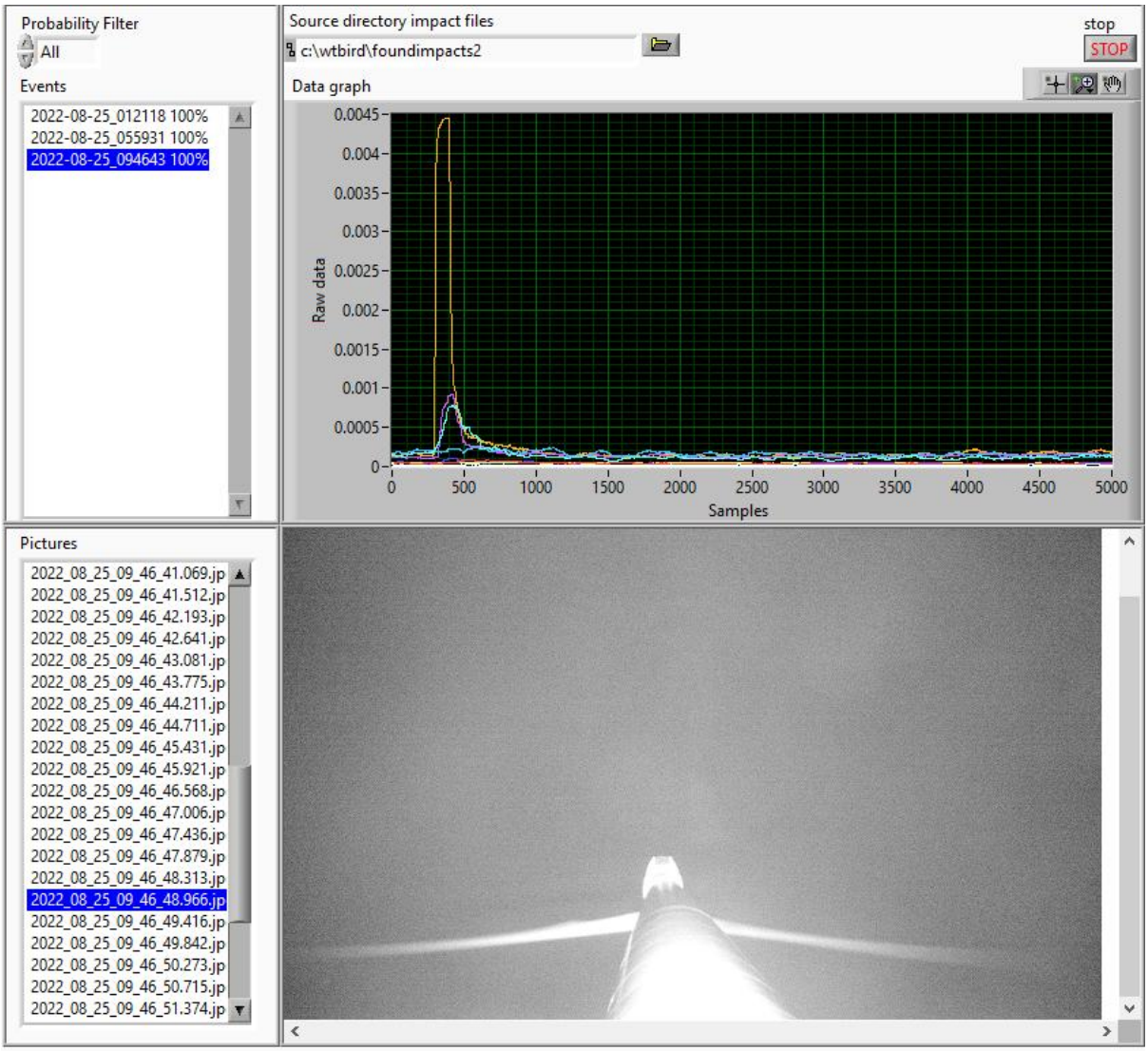


Figure 3.7: Collision 25-08-2022 094643

Collision “25-08-2022 094643” has a visual confirmation on the day cameras however it is very faint, Figure 3.8 shows the zoomed version of the bottom left corner of Figure 3.7, below the blade an object is noticed what likely is the bird which hit the blade. On the thermal cameras the collision was clearly visible depicted in Figure 3.9 and Figure 3.10.

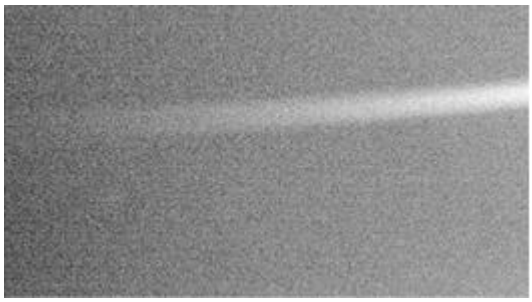

Figure 3.8: Zoom in on “Collision 25-08-2022 094643”

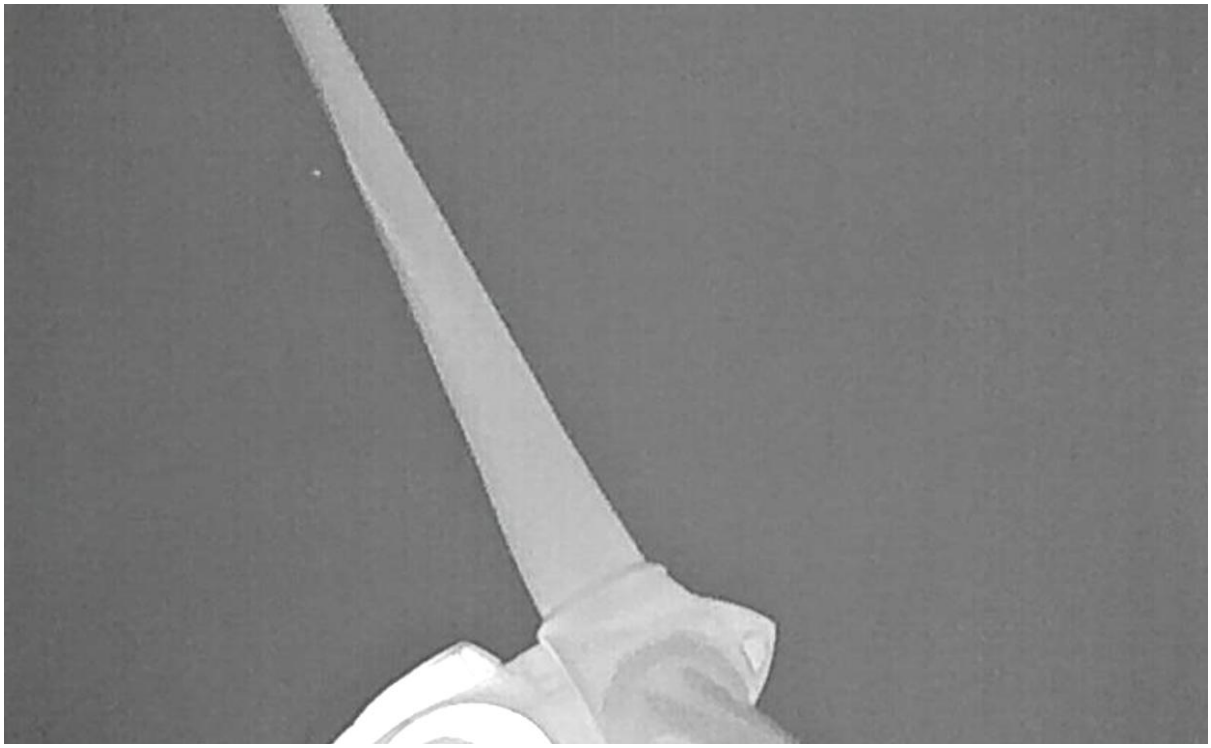

Figure 3.9: Thermal image before impact, Collision 25-08-2022 094643

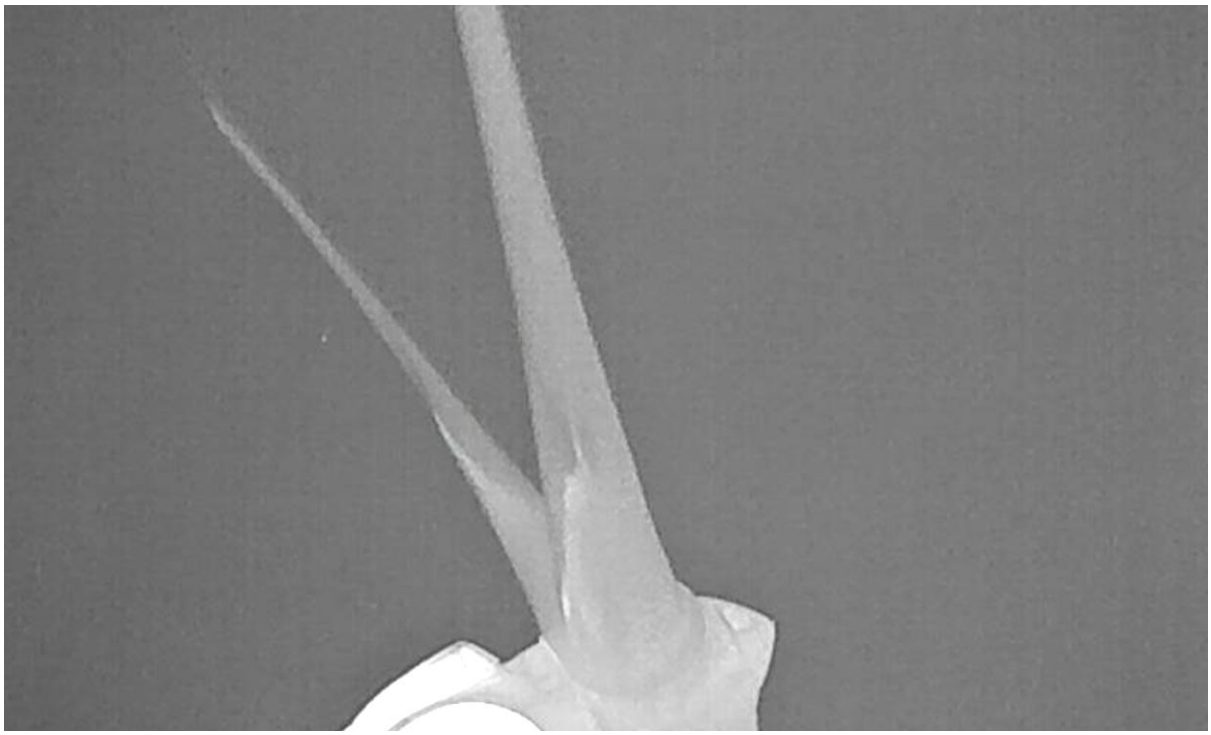

Figure 3.10: Thermal image after impact, Collision 25-08-2022

# 3.4 Collision 26-08-2022 013928

Figure 3.11 shows collision “26-08-2022 013928”. The collision was detected on sensor 2 of blade 2

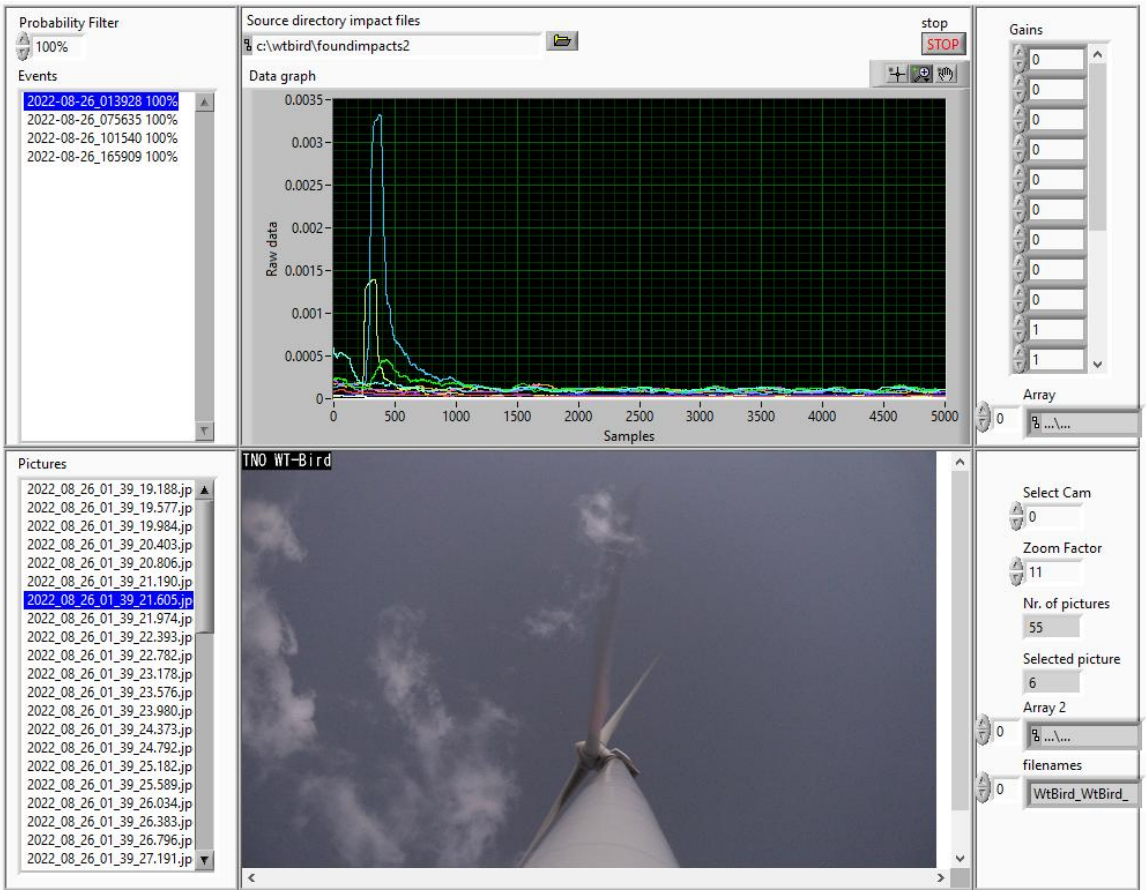


Figure 3.11: Collision 26-08-2022 013928

Collision “26-08-2022 013928” does not have a visual confirmation.

# 3.5 Collision 26-08-2022 084520

Figure 3.12 shows collision 26-08-2022 084520, detected on sensor 2 of blade 2. The reading is a bit stronger in comparison to the previous collisions.

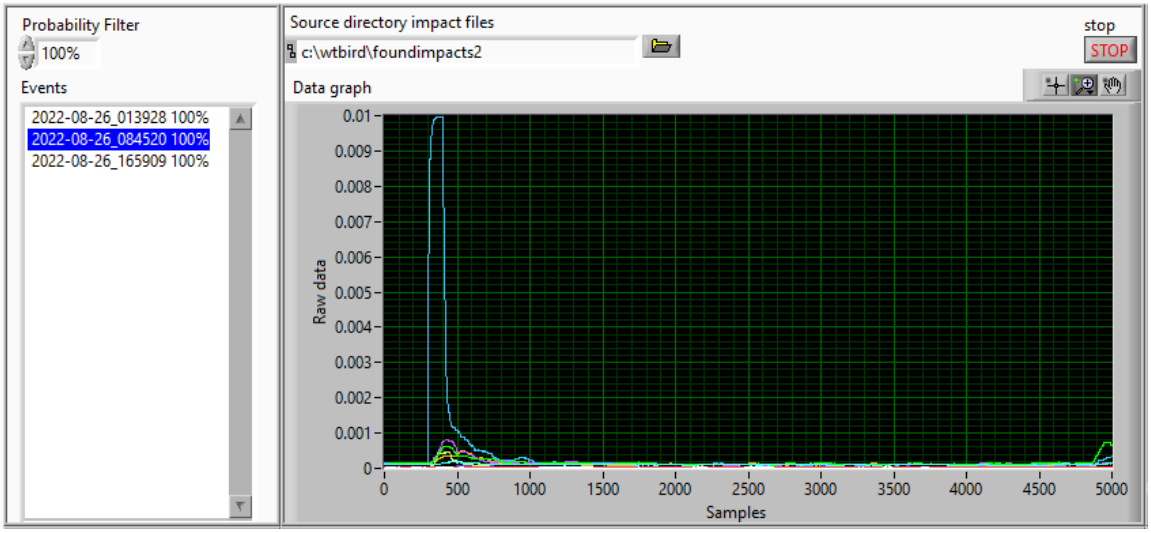


Figure 3.12: Collision 26-08-2022 084520

Right after the collision something is falling down from hub height, depicted in Figure 3.13. This is recorded by the day cameras.

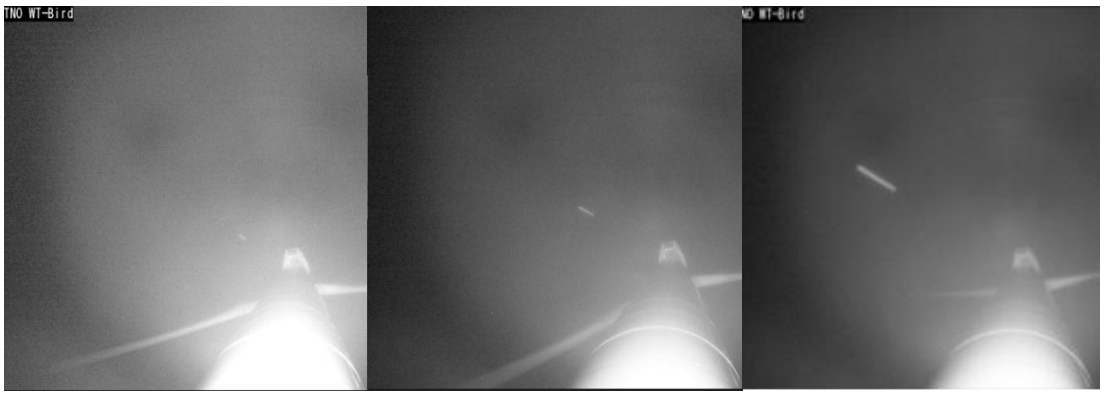


Figure 3.13: Pictures of collision 26-08-2022 084520

Figure 3.14 shows an image of the thermal cameras, there is no impact visible on the day or thermal cameras however there is bird activity in the air.

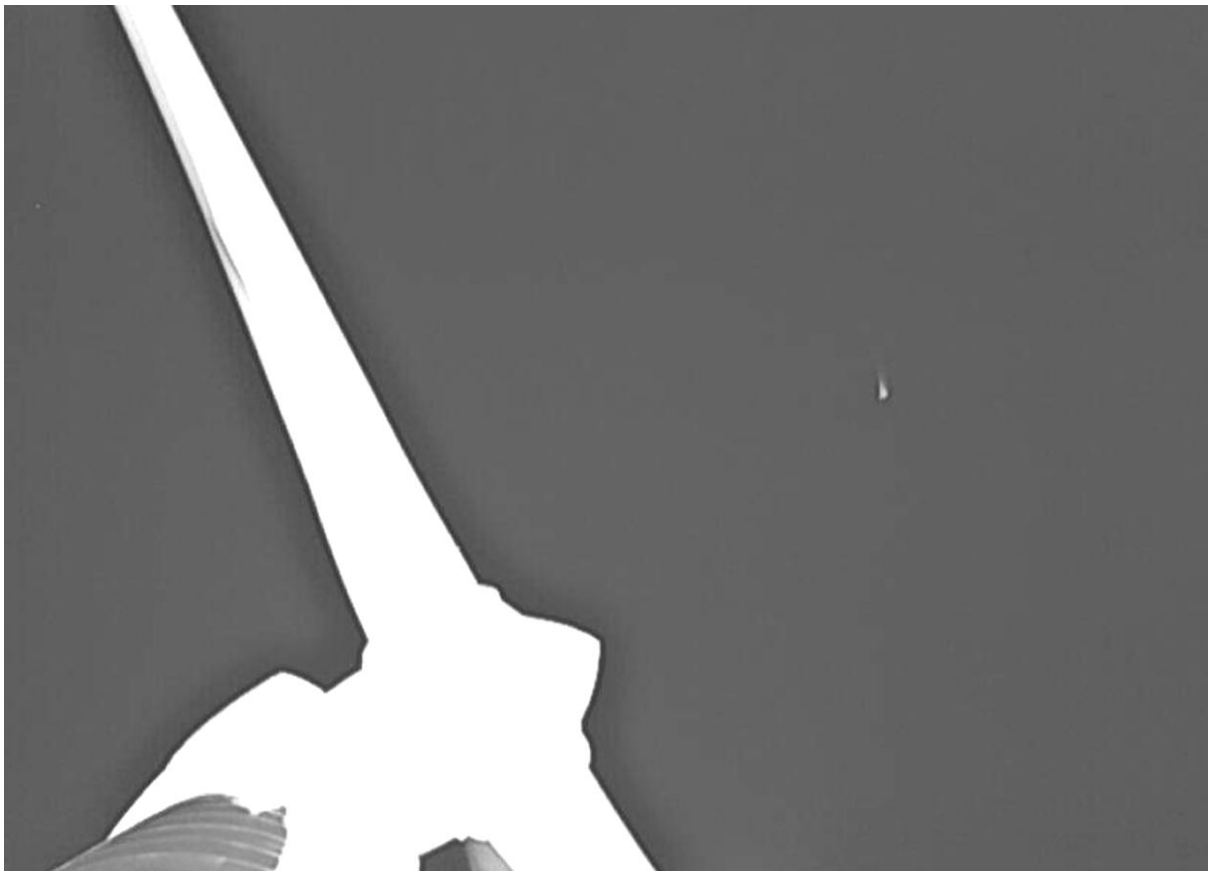

Figure 3.14: Passing bird on thermal camera during collision 26-08-2022 084520

# 3.6 Collision 31-08-2022 053655

Collision 31-08-2022 053655 was detected on sensor 2 of blade 3, Figure 3.15 shows the sensor data as output by the WT-Bird® system.

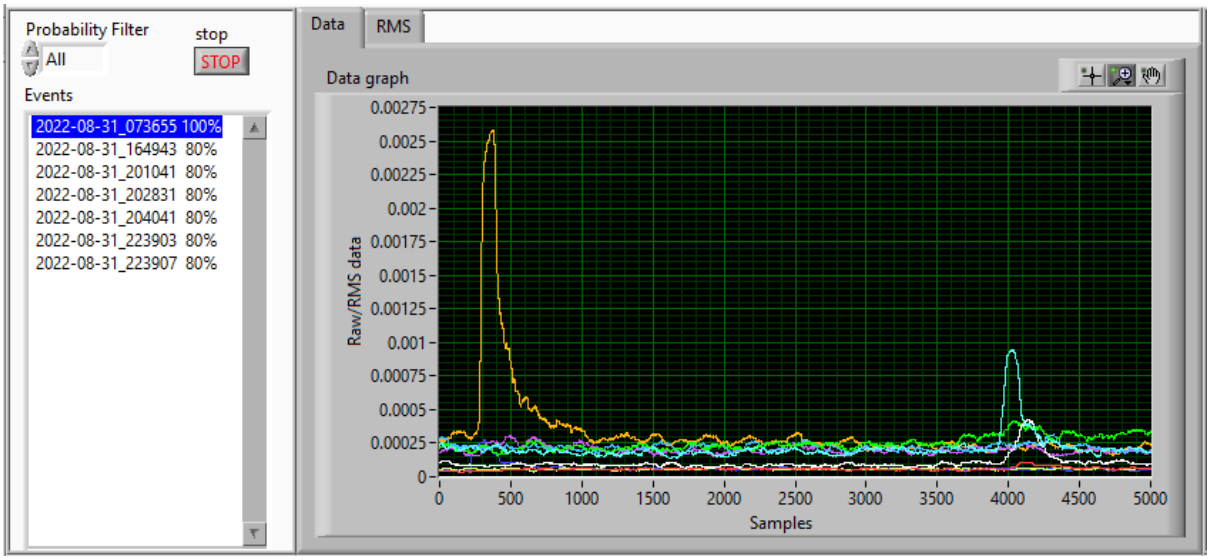


Figure 3.15: Collision 31-08-2022 053655

Figure 3.16 shows to our interpretation, the object that touched the blade. It is difficult to see during night time.

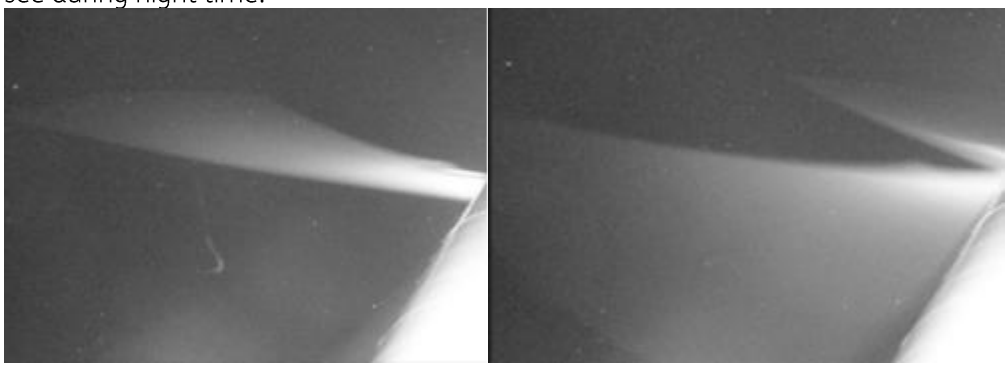

Figure 3.16: Picture of collision 31-08-2022 053655

Figure 3.17 shows a bird falling / passing the turbine in the upper right corner, it is unclear if the bird was able to continue its flight path.

Figure 3.17: Thermal image during collision 31-08-2022 053655

# 3.7 Collision 02-09-2022 012053

Figure 3.18 shows the WT-Bird® output of collision 02-09-2022 012053, a clear impact at blade 2 sensor 2 was measured.

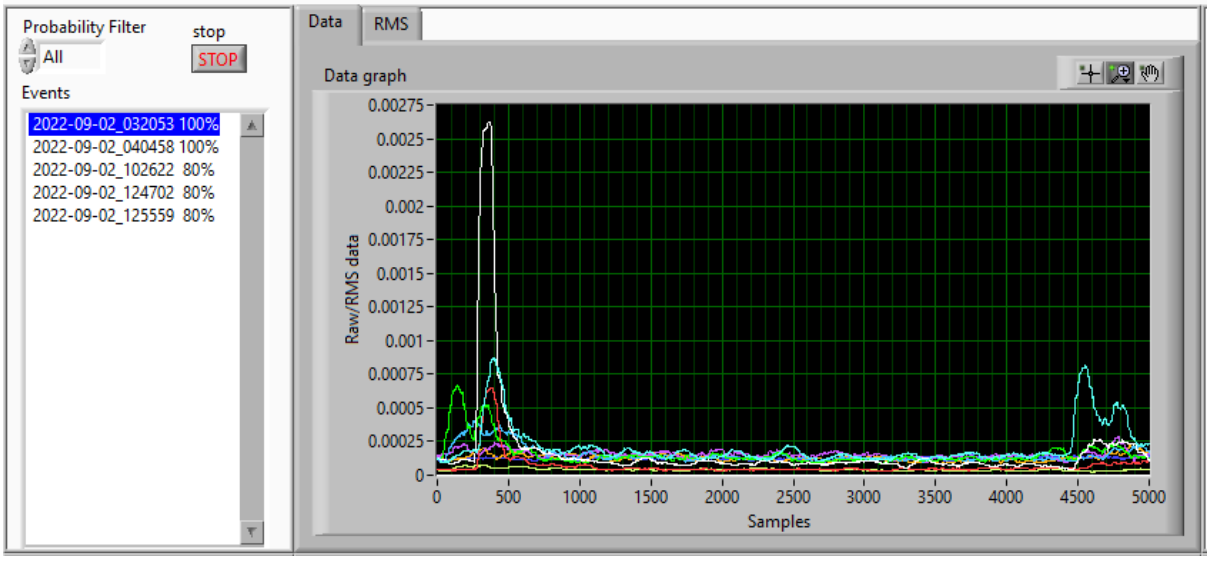


Figure 3.18: Collision 02-09-2022 012053

The day cameras did not show anything during the collision, the thermal cameras however recorded the bird impact. Figure 3.19 shows a bird close to the blade before the collision. Figure 3.20 shows the same bird just after the collision. When the full thermal fragment is analysed one can see that the bird survived and continued its way.

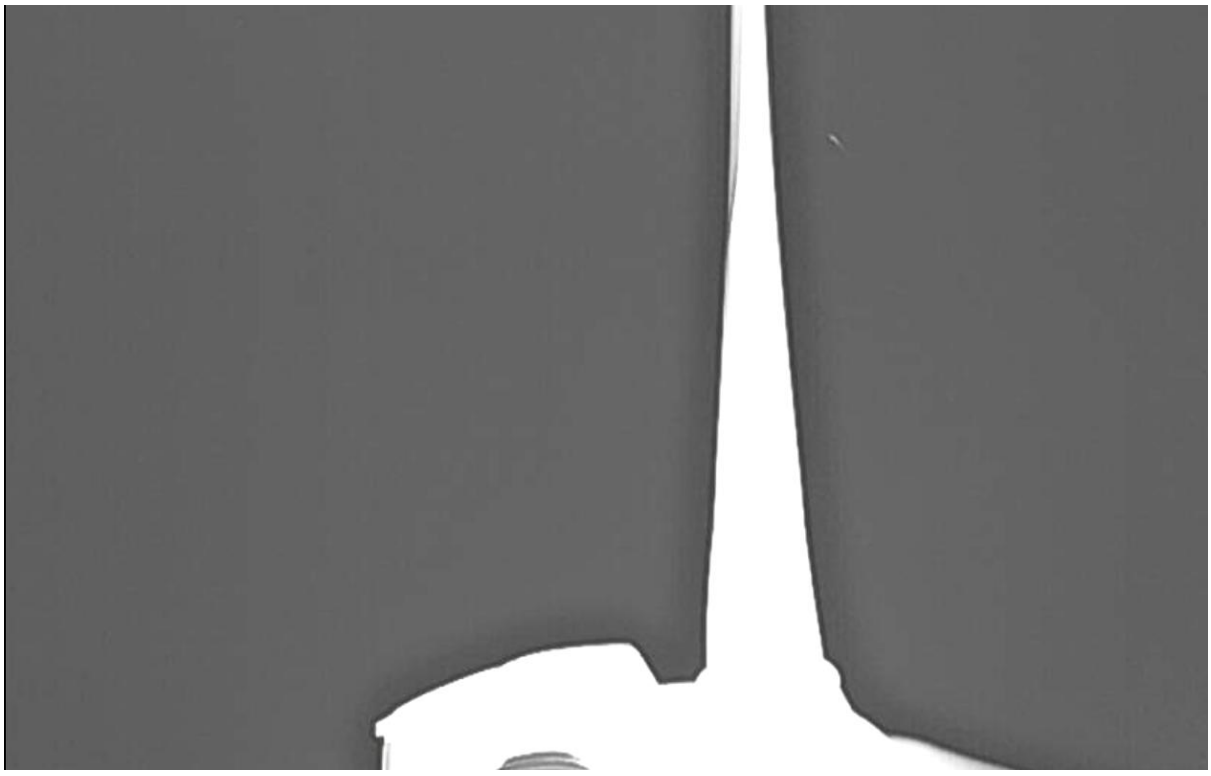

Figure 3.19: Thermal image before collision 02-09-2022 012053

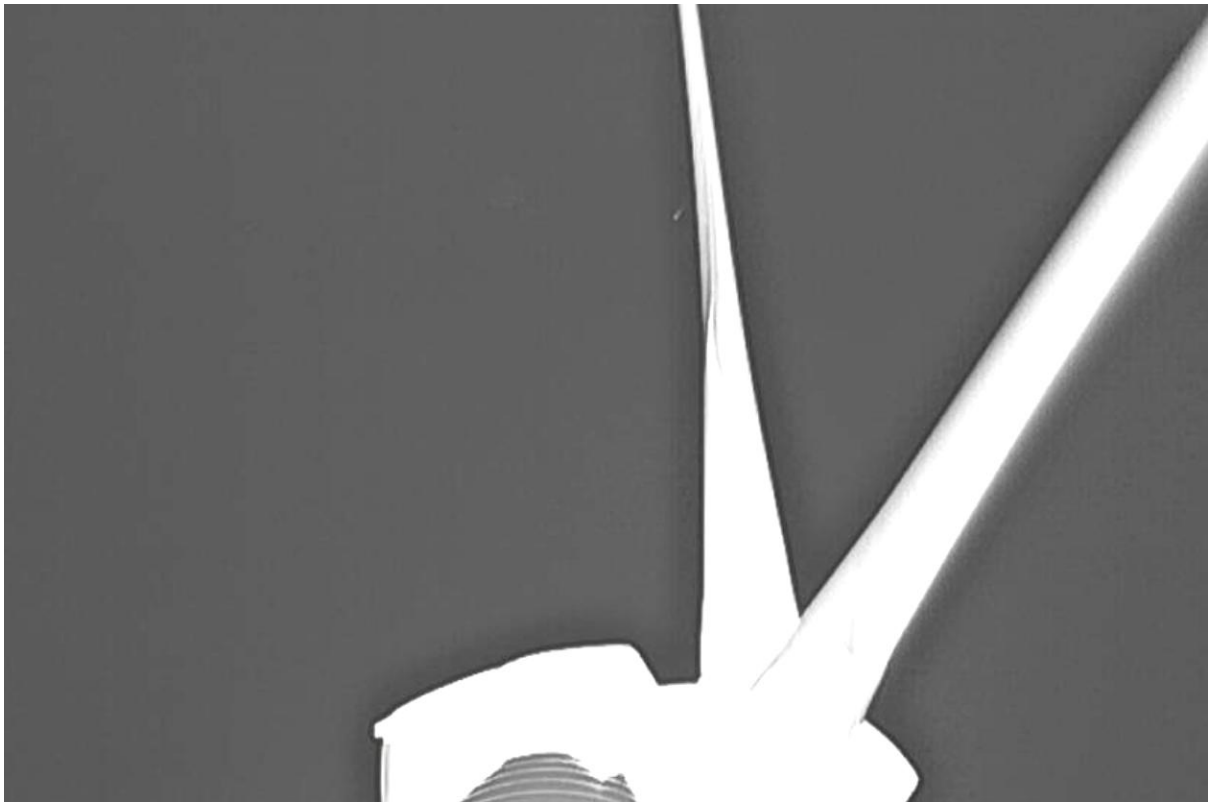

Figure 3.20: Thermal image after collision 02-09-2022 012053

# 3.8 Collision 02-09-2022 020458

Below the WT-Bird® output of collision 02-09-2022 020458 is depicted, the collision was detected on sensor 2 of blade 1 and also sensor 1 of blade 1 showed an impact (the lower peak touching 0.001).

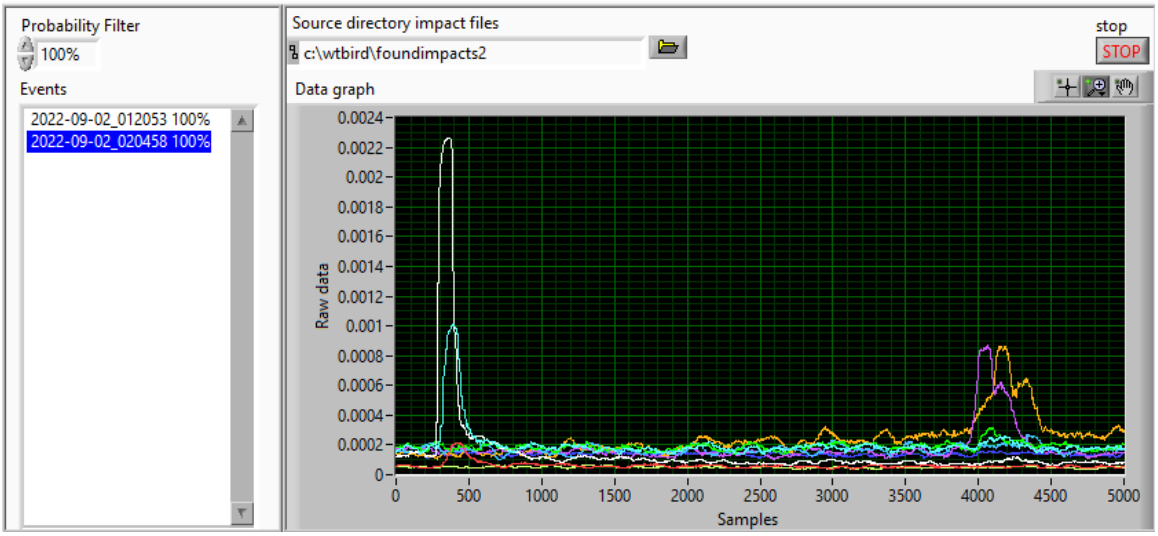


Figure 3.21: Collision 02-09-2022 020458

The day cameras did not show any bird activity, the Collision 02-09-2022 020458 was however captured by the thermal cameras, Figure 3.22 and Figure 3.23 show the thermal images before and after the collision.

Figure 3.22: Thermal image before collision 02-09-2022 020458

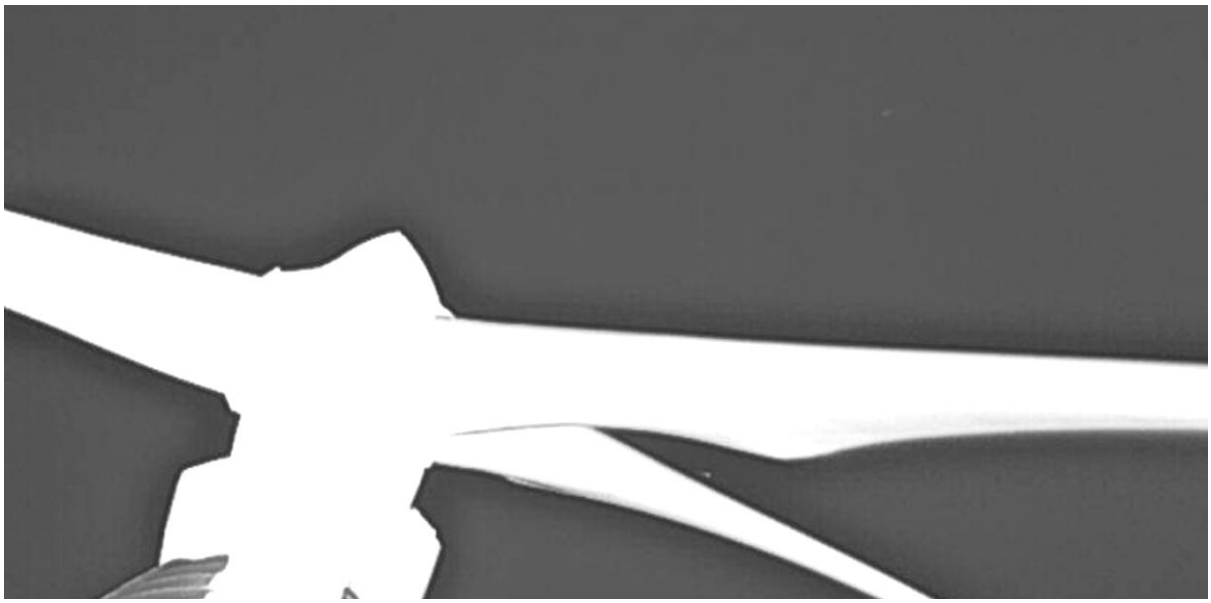

Figure 3.23: Thermal image after collision 02-09-2022 020458

# 3.9 Collision 11-09-2022 010714

Figure 3.24 shows the WT-Bird® output of collision 11-09-2022 010714, it was detected on blade 2, sensor 2.

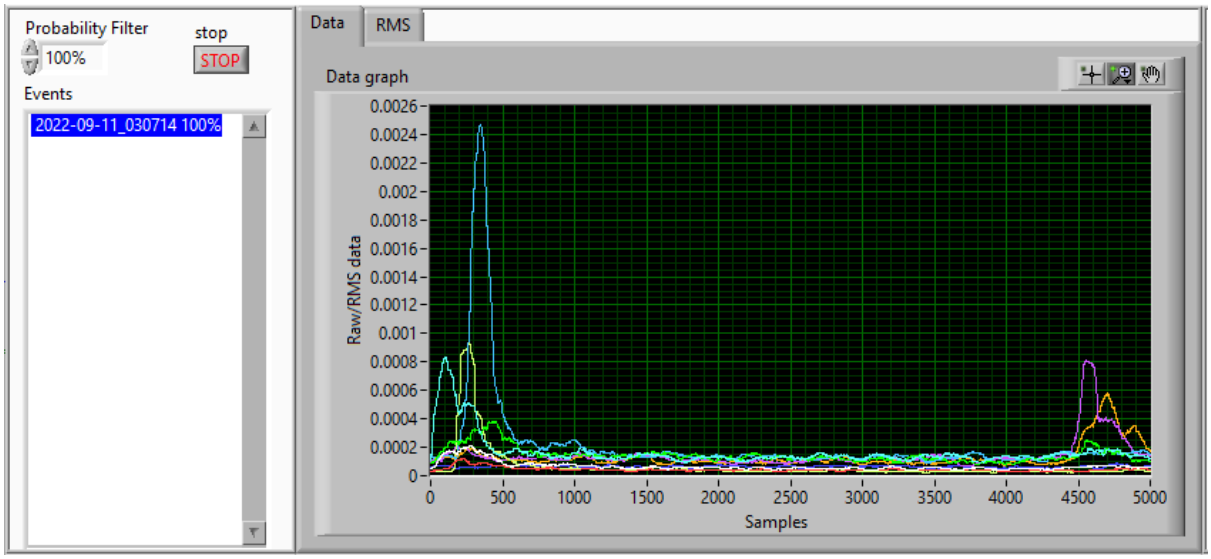


Figure 3.24: Collision 11-09-2022 010714

There is no visual confirmation on the day cameras, thermal camera data is not available.

# 3.10 Collision 21-09-2022 072328

Figure 3.25 shows the collision 21-09-2022 072328, the collision was detected at sensor 2 of blade 2.

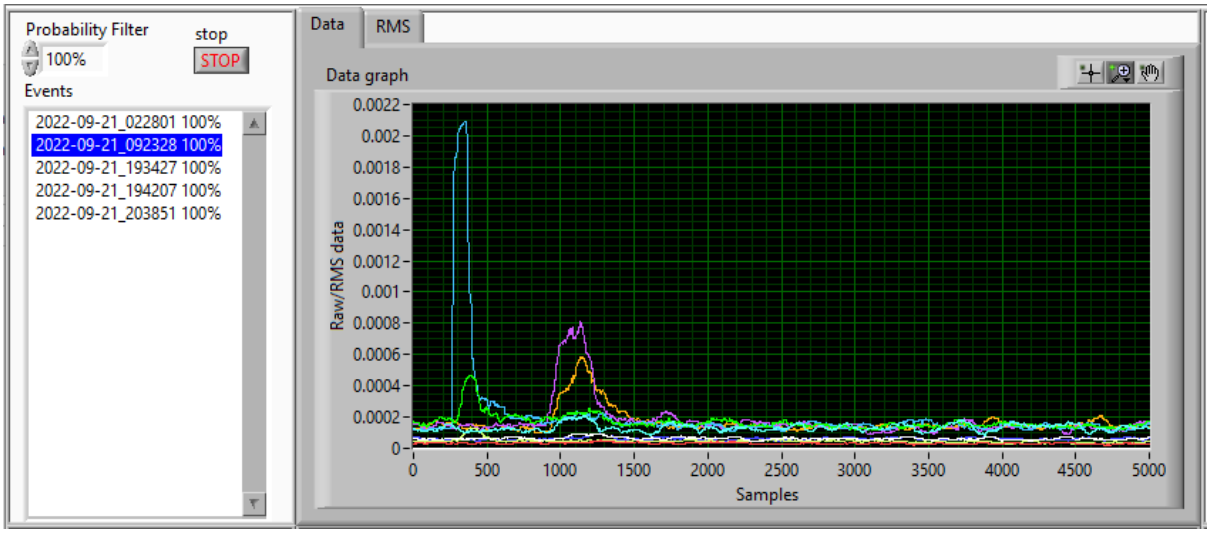


Figure 3.25: Collision 21-09-2022 072328

At night time there was no visual confirmation on the day cameras, there is no thermal camera data available in this period.

# 3.11 Collision 21-09-2022 174207

Figure 3.26 shows collision 21-09-2022 174207, the collision was detected on blade 3 sensor 2.

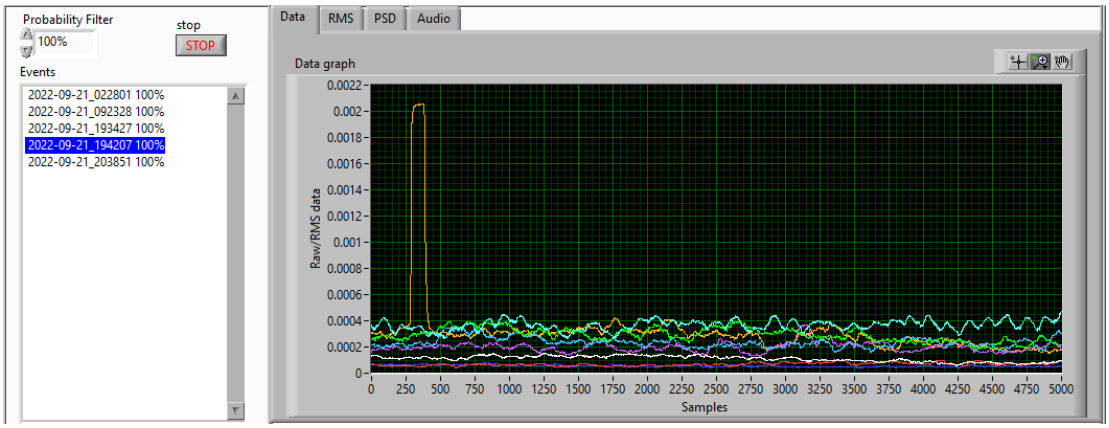


Figure 3.26: Collision 21-09-2022 174207

There is no visual confirmation.

# 3.12 Collision 23-9-2022 055742

Figure 3.27 shows collision 23-9-2022 055742, this collision was detected on blade 3 sensor 2. There is no visual confirmation. The shape of the impact, which is similar to the collision in the next section, suggests this collision occurred further away from the sensor towards the tip. It also shows that the sensor setup in the box beam (sensor 3) is not very effective.

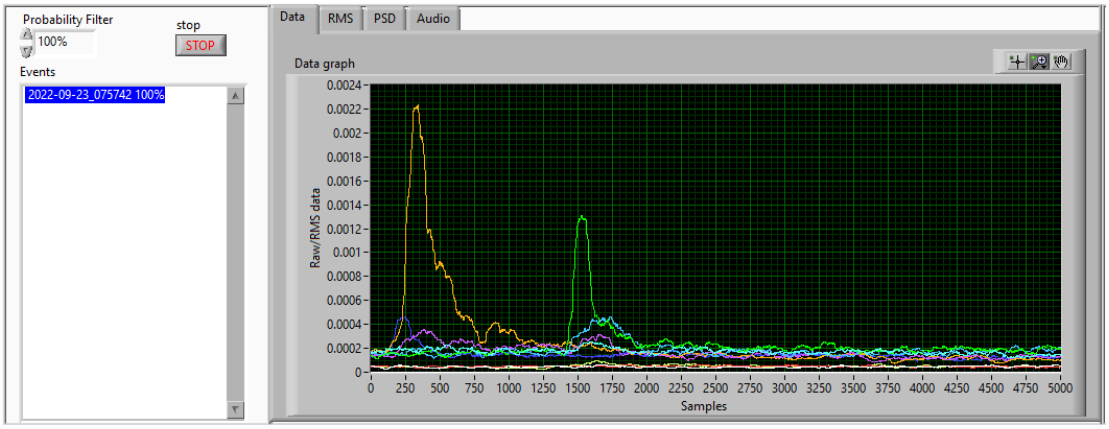


Figure 3.27: Collision 23-9-2022 055742

# 3.13 Collision 27-09-2022 232436

The collision detected on the 27th of September was the only collision detected during day time, this collision is tragic from an ecologic point view and at the same time very interesting from the technical point view because the bird which collided was a bald eagle (Haliaeetus leucocephalus and this is the National Bird of the United States of America) and it hit very close to the tip.

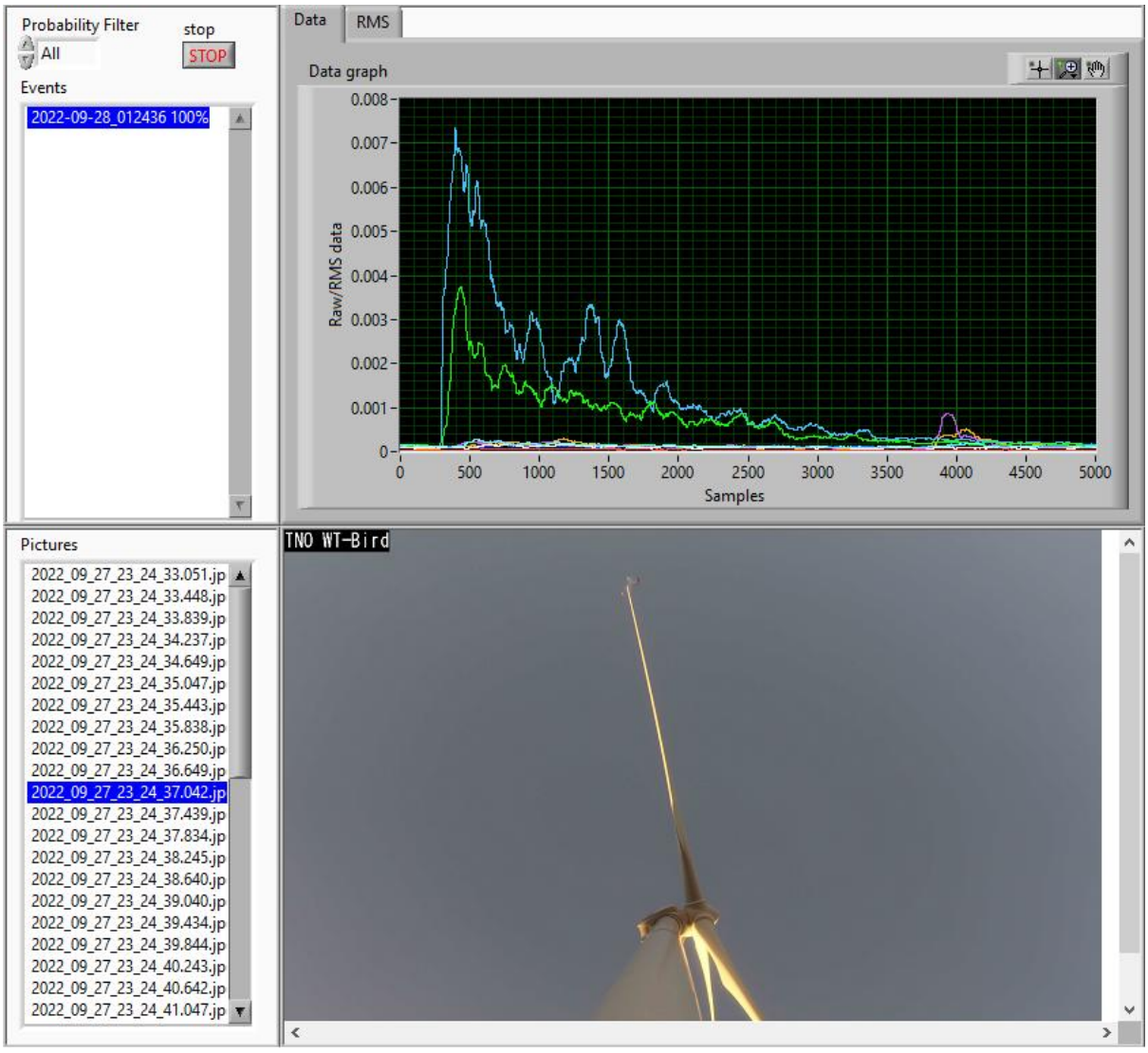


Figure 3.28: Collision 27-09-2022 232436

Figure 3.29: Zoom of collision 27-09-2022 232436

# 3.14 Collision 06-10-2022 034605

Figure 3.30 shows collision 06-10-2022 034605 was detected on blade 3 sensor 2.

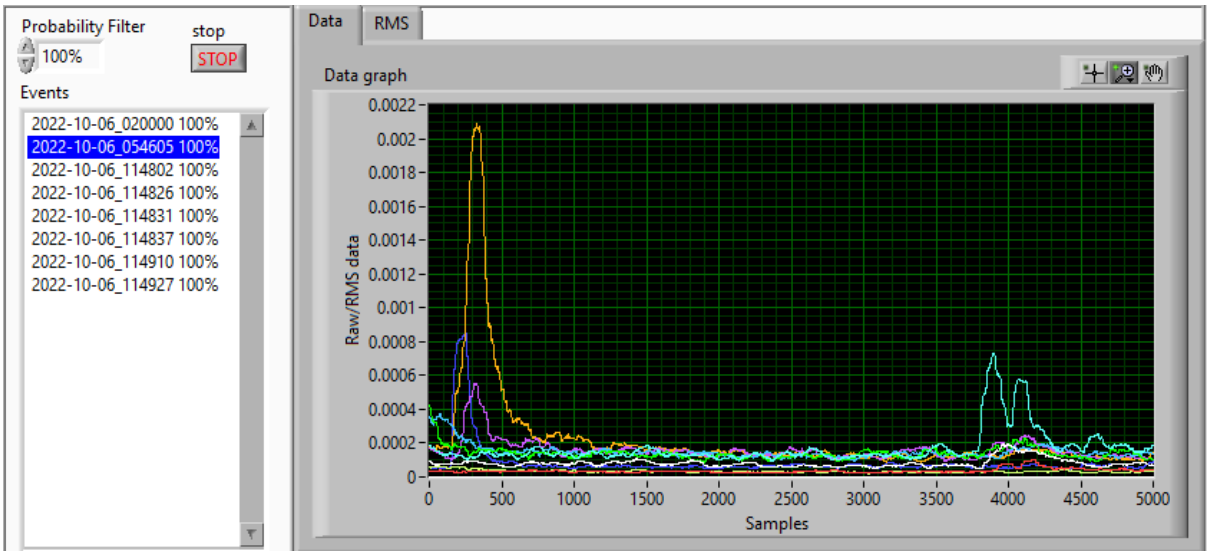


Figure 3.30: Collision 06-10-2022 034605

No visual confirmation for this collision, the day cameras did not show anything and no thermal data is available.

# 3.15 Collision 22-10-2022 034740

Figure 3.31 shows collision 22-10-2022 034740, it was detected on blade 2 sensor 2. There is no visual confirmation of collision 22-10-2022 034740.

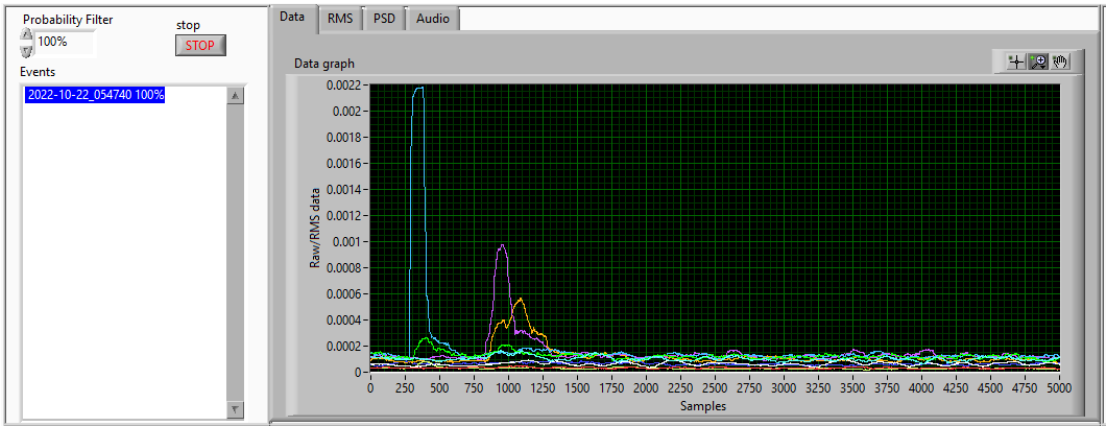


Figure 3.31: Collision 22-10-2022 034740

# 4 Conclusion and recommendation

In total 15 collisions are detected in a period of 3 months (2022-08-13 until 2022-11-03). 4 of the collisions are visually confirmed, 2 of the collisions are “likely” confirmed (meaning that only bird/bat activity or falling items/bodies were spotted) and the remaining have no visual confirmation. Most of the collisions occurred during night or dusk where unfortunately the Sony day cameras with 100W IR illumination support did not have enough light sensitivity to capture the bird movements. Fortunately, Western EcoSystems Technology, Inc. (WEST) had installed thermal cameras which made it possible to visually confirm a number of detected collisions.

The “Trigger and confidence” algorithms are improving as we gain experience throughout the project, currently most of the turbine sound can be filtered out by lowering the confidence level when the system suspects the source of the vibration is not in the blade but in the hub or nacelle. Still, one must pay attention not to set the thresholds too low because you could “blind” the system when there is too much vibration orientated in the hub. An example is the pitch gear wear at the Clipper turbine, 6 times per full turbine revolution a strong impact sound was picked up by the sensors. Due to these impacts, other bat/bird impacts at the same time occurrence could not have been detected by the system. Another point of attention is the precipitation, this can generate a lot of vibration/sound and therefore can result in false positives. It is recommended to add meteorological sensors to the WT-Bird® system.

The sensor setup in the Clipper turbine learnt us that a sensor installed in the box beam area (sensor 3), see [2], is not very effective. For this reason most of the collisions were detected on sensor 2 installed at 16 meter from the blade root.

# 5 References

[1] TNO 2022 R10697 rev4, WT-Bird installation plan at University of Minnesota, F.A. Kaandorp
[2] TNO 2022 R11392 rev1, WT-Bird installation report University of Minnesota, F.A. Kaandorp

Energy & Materials Transition

Westerduinweg 3
1755 LE  Petten
www.tno.nl

TNO innovation for life

1162-FTR202510-EE0008734